UDK 62

MACHINERY & ENERGETICS

Publisher:
National University of Life and Environmental Sciences of Ukraine

Year of foundation: 2010
Frequency of issue: Four times per year

Recommended for printing and distribution
via the Internet by the Academic Council
of National University of Life and Environmental Sciences of Ukraine
(Minutes No. 2 of September 23, 2025)

State Registration:
Media identifier R30-02298.
Decision of the National Council
of Television and Radio Broadcasting of Ukraine
No. 1795, Minutes No. 31, dated 21.12.2023.

The journal is included in the list of Professional Scientific Publications of Ukraine
Category "A". Branch of sciences – Technical.
Specialties: 0715 – Mechanics and Metal Trades, 0716 – Motor Vehicles, Ships and Aircraft,
0713 – Electricity and Energy, 0714 – Electronics and Automation
(Order of the Ministry of Education and Science of Ukraine of June 26, 2024, No. 920)

The journal is presented international scientometric databases, repositories and scientific systems:
Google Scholar, Professional Publications of Ukraine, Vernadsky National Library of Ukraine,
BASE, J-Gate, Dimensions, Cambridge University Library, Leipzig University Library,
European University Institute, SOLO - Search Oxford Libraries Online, University of Hull Library,
University of Oslo Library, EBSCO, UCSB Library, Ulrichsweb Global Serials Directory,
OUCI (Open Ukrainian Citation Index), WorldCat, Litmaps

Editors office address:
National University of Life and Environmental Sciences of Ukraine
03041, 15 Heroiv Oborony, Kyiv, Ukraine
Tel.: +38(044)-258-42-63
E-mail: info@technicalscience.com.ua
https://technicalscience.com.ua/en

УДК 62

ТЕХНІКА ТА ЕНЕРГЕТИКА

Видавець:
Національний університет біоресурсів і природокористування України

Рік заснування: 2010
Періодичність випуску: 4 рази на рік

Рекомендовано до друку та поширення
через мережу Інтернет Вченою радою
Національного університету біоресурсів і природокористування України
(протокол № 2 від 23 вересня 2025 р.)

Державна реєстрація:
Ідентифікатор медіа R30-02298.
Рішення Національної ради України
з питань телебачення і радіомовлення
№ 1795, протокол № 31 від 21.12.2023 р.

Журнал входить до переліку наукових фахових видань України

Категорія «А». Галузь наук – Технічні.
Спеціальності: 131 – «Прикладна механіка», 133 – «Галузеве машинобудування»,
141 – «Електроенергетика, електротехніка та електромеханіка»,
174 – «Автоматизація, комп'ютерно-інтегровані технології та робототехніка»
(Наказ Міністерства освіти і науки України від 26 червня 2024 року № 920)

Журнал представлено у міжнародних наукометричних базах даних,
репозитаріях та пошукових системах:
Google Scholar, Фахові видання України, Національна бібліотека України імені
В. І. Вернадського, BASE, J-Gate, Dimensions, Cambridge University Library,
Leipzig University Library, European University Institute, SOLO - Search Oxford Libraries Online,
University of Hull Library, University of Oslo Library, EBSCO, UCSB Library, Ulrichsweb Global
Serials Directory, OUCI (Open Ukrainian Citation Index), WorldCat, Litmaps

Адреса редакції:
Національний університет біоресурсів і природокористування України
03041, вул. Героїв Оборони, 15, м. Київ, Україна
Тел.: +38(044)-258-42-63
E-mail: info@technicalscience.com.ua
https://technicalscience.com.ua/uk

Редакційна колегія

CONTENTS

ЗМІСТ

Machinery & Energetics
Vol. 16, No. 3. 2025

Journal homepage:
https://technicalscience.com.ua/en

UDC 631.312:514.18
DOI: 10.31548/machinery/3.2025.09

Andrii Nesvidomin
PhD in Technical Sciences, Associate Professor
National University of Life and Environmental Sciences of Ukraine
03041, 15 Heroiv Oborony Str., Kyiv, Ukraine
https://orcid.org/0000-0002-9227-4652

Serhii Pylypaka
Doctor of Technical Sciences, Professor
National University of Life and Environmental Sciences of Ukraine
03041, 15 Heroiv Oborony Str., Kyiv, Ukraine
https://orcid.org/0000-0002-1496-4615

Tetiana Volina*
Doctor of Technical Sciences, Associate Professor
National University of Life and Environmental Sciences of Ukraine
03041, 15 Heroiv Oborony Str., Kyiv, Ukraine
https://orcid.org/0000-0001-8610-2208

Mykola Lokhonia
PhD
Sumy State Pedagogical University named after A.S. Makarenko
40002, 87 Romenska Str., Sumy, Ukraine
https://orcid.org/0000-0003-0778-252X

Yana Borodai
Senior Lecturer
Sumy National Agrarian University
40021, 160 Herasim Kondratiev Str., Sumy, Ukraine
https://orcid.org/0000-0003-0048-815X

Forming helical blades from flat blanks with minimal deformation

Abstract. Helical blades are increasingly used in the designs of forage harvesting equipment. They demonstrate better cutting characteristics compared to traditional flat ones, but their manufacture is complicated by the non-developable surface of the surface. The problem of creating an accurate flat workpiece for such knives necessitates the need for a mathematical description of their geometry. The purpose of this study was to determine an analytical method for constructing a flat workpiece for a helical knife, considering the minimum resistance during plastic deformation of the workpiece. To achieve this goal, differential geometry methods were used, in particular, vector analysis of helical surfaces, construction of a Frenet trihedron, and analysis of the first quadratic form of the surface. It was established that the working surface of the knife is a straight open helicoid, which can be bent into a surface of revolution without changing the first quadratic form. Parametric equations of bending of the knife surface using a variable parameter describing the process of transforming the helicoid into a one-sheeted hyperboloid of revolution were constructed. It was proven that the latter is approximated with high accuracy by a truncated cone, the sweep of which is determined by the design parameters of the

Article's History: Received: 03.06.2025; Revised: 01.09.2025; Accepted: 23.09.2025.

Suggested Citation:
Nesvidomin, A., Pylypaka, S., Volina, T., Lokhonia, M., & Borodai, Ya. (2025). Forming helical blades from flat blanks with minimal deformation. *Machinery & Energetics,* 16(3), 9-19. doi: 10.31548/machinery/3.2025.09.

*Corresponding author

knife. Formulas for calculating the geometric dimensions of the sweep from the known parameters of the knife, in particular the radii of the bases and the height of the truncated cone, were obtained. It was shown that the length of the blade arc and the central angle that outlines the workpiece enable precise determination of its shape. The practical value of the study consists in the creation of an effective method for constructing the most accurate flat workpiece for the manufacture of a helical knife, which allows minimising the resistance during forming, reducing the labor intensity, and increasing the accuracy of manufacturing parts of grinding drums

Keywords: Frenet formulas; curvature; torsion; vector equation of a surface; first quadratic form

INTRODUCTION

Helical blades are widely used in various industries due to their unique shape and ability to process materials efficiently. In particular, they are used in the food industry for grinding and mixing raw materials, in agriculture for processing feed, and in the woodworking and processing industries for grinding wood and secondary raw materials. The main purpose of using such blades is to ensure uniform cutting, improve equipment productivity, and reduce energy costs due to the optimised blade shape.

Helical surfaces find their application in a wide range of technical fields. V. Bulgakov *et al.* (2024) theoretically investigated the traction resistance of harrows with screw working bodies. The authors analysed the factors affecting the efficiency of such harrows, in particular their resistance when performing soil cultivation, which is important for improving agrotechnical characteristics and reducing energy costs in agriculture. The research of S. Liu *et al.* (2023) focuses on optimising the surface texture of screw pairs in screw hydraulic rotary actuator using surrogate methods. The authors used an approach based on surrogate modelling to improve surface parameters, which is important for increasing the efficiency and durability of such systems. M. Mushtruk *et al.* (2020) considered mathematical modelling of the oil extrusion process with pre-grinding of raw materials in a twin-screw extruder. The authors analysed various aspects of the process, in particular in food processing, to optimise the technological process to increase oil yield and reduce energy costs during raw material processing.

Scientists J.C.P. Ortiz *et al.* (2024) focused on optimising the Gorlov screw turbine for hydrokinetic applications using surface response methodology and experimental tests. This contributes to improving the turbine's performance when used in hydroelectric systems, optimising its characteristics for maximum performance and minimum energy consumption. J. Zhao *et al.* (2024) investigated the change in the morphology of tooth surfaces and tribological properties of helical gears during lubricated sliding wear. This made it possible to improve the operational characteristics of helical gears by studying their behaviour under different lubrication and wear conditions, which is important for increasing their durability. The article of H. Liu (2024) was devoted to the theory of formation and computer modelling of rotary cutting tools with helical teeth. The research is aimed at improving the production technologies of such tools, increasing their accuracy and efficiency in material processing processes. J. Chen *et al.* (2024) considered a general coupling model and dynamic analysis of a helical gear pair with tooth surface deviations. This made it possible to evaluate the effect of tooth deformations on the operation of helical gears and their dynamics to improve the accuracy and reliability of such systems in mechanical devices. A. Rucins *et al.* (2024) investigated the energy parameters of a screw conveyor with a bladed working body for transporting agricultural materials to improve efficiency and reduce energy costs when using such systems for moving grain and other agricultural cargo.

As a result of reviewing the sources on the selected topic, it was found that the issue of finding an approximate knife sweep in the form of a flat workpiece, which would be the most accurate and would present the least resistance when forming it into the surface of a helical knife, is relevant. In this regard, the problem of mathematical description of the bending of the helical surface of the knife arises (Filimonov & Bacherikov, 2022). This will make it possible to find a flat workpiece for its manufacture based on a scientific approach.

The article aimed to build an analytical model of the bending of the helical surface of the knife of the grinding drum, with the subsequent determination of an accurate flat workpiece that provides minimal resistance to plastic deformation during forming.

The scientific novelty of the research lies in the use of methods of differential geometry, namely the theory of bending of surfaces based on their internal geometry. Since the surface of a straight open helicoid is non-developable, the study of the bending process can contribute to the improvement of its manufacturing technology.

MATERIALS AND METHODS

The study used symbolic mathematics of the software product "Mathematica", as well as the MatLab software environment for visualisation of the obtained results. To achieve the goal, approaches based on the methodology of differential geometry were used.

One family of coordinate lines of the helical surface was adopted, as helical lines were taken to be helical lines. The helical surface was bent by gradually decreasing its pitch. In this case, the length of the helical lines did not change, as a result of which the radius of the cylinder on which they were located increased. When the pitch of the helical lines became zero, the helical surface was transformed into a surface of revolution. The spatial curve was characterised by two differential parameters – the curvature k and the torsion σ. For a helical line, these parameters were constant and were determined from the following expressions:

$$k = \frac{a}{a^2+b^2};\ \sigma = \frac{b}{a^2+b^2}, \tag{1}$$

where a is the radius of the cylinder on which the helix was located; b is the helix parameter, through which the pitch H was determined $(H=2\pi b)$. The helix had a pitch angle β, the tangent of which was the coefficient of proportionality between twist and curvature, and which was determined through a and b: $tg\beta = b/a$. Based on this, another expression was written to determine curvature and twist:

$$k = \frac{cos^2\beta}{a};\ \sigma = \frac{sin\,\beta\, cos\,\beta}{a}. \tag{2}$$

Having solved (1) for the constants a and b, we obtained expressions for finding them from the known curvature k and the torsion σ:

$$a = \frac{k}{k^2+\sigma^2};\ b = \frac{\sigma}{k^2+\sigma^2}. \tag{3}$$

The parametric equations of a helix as a function of the length s of its arc had the form:

$$x = a\,cos\frac{s}{\sqrt{a^2+b^2}};\ y = a\,sin\frac{s}{\sqrt{a^2+b^2}};\ z = \frac{bs}{\sqrt{a^2+b^2}}. \tag{4}$$

The helical line (4) was taken as the guiding curve through which the helical surface passes. For bending the surface, its vector equation in the accompanying Frenet trihedron of the curve (4) was used. In addition, the first quadratic form of the surface was used, with the help of which the length of the line on the surface was determined. Since the lengths of the lines did not change during bending, the first quadratic form of the surface remained unchanged during its bending. The achievement of such a result indicated that the analytical description of the process of bending the surface was correct.

It is necessary to analyse the shape of the helical knife of the chopping drum of a forage harvester. Figure 1a shows the chopping drum of the New Holland with knives fixed on it, and in Figure 1b – a separate knife with structural dimensions and cross-section. The blade of the knife is a helical line located on a cylinder of radius R with a lift angle β_R=$90°$-τ. The cross-section of the knife, the thickness of which is conventionally taken as zero, is a segment perpendicular to the axis of the helical line, and which makes an angle φ to the radial direction (Fig. 1c). The surface is formed by the helical movement of this segment at a constant value of the angle φ, therefore the formed surface is a straight open helicoid.

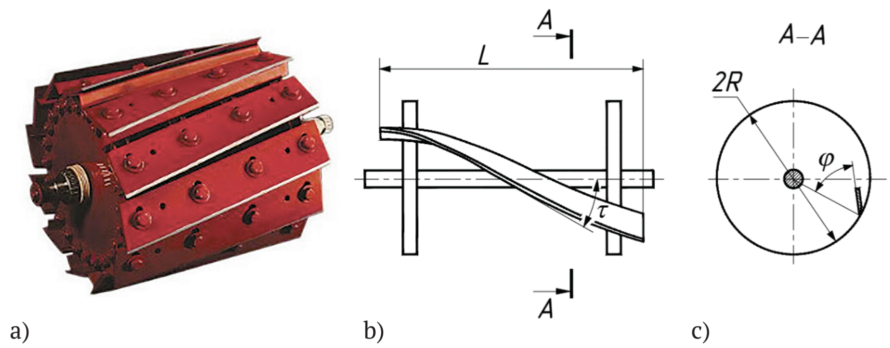

Figure 1. Grinding drum
and design parameters of a separate knife

Note: a) shredding drum with knives; b) separate knife on the drum; c) knife cross-section: L – knife length; τ – angle between the drum axis and the knife blade; $2R$ – drum diameter; φ – angle between the knife cross-section line and the radial direction

Source: a) Pull-type forage harvesters and flail harvester (n.d.); b), c) S. Pylypaka *et al.* (2017)

The guiding curve for forming the surface is taken to be a helix located on a cylinder of radius r and with an elevation angle β. At point A, a Frenet trihedron can be constructed, in which the orthogonal plane $\bar{\tau}$ is tangent to the helix, the orthogonal plane $\bar{n}$ is the main normal of the helix, and the orthogonal plane $\bar{b}$ is the binormal.

RESULTS

Figure 2a shows a frontal projection of a helix with a vertical axis, so the orthogonal plane of the principal normal $\bar{n}$ is projected to a point. The straight-line generators of a straight open helicoid intersect the helix, are parallel to the horizontal plane, therefore, are perpendicular to the axis of the helix, but are transverse to it. This condition is met by the straight-line generator u, which is located in the direct plane of the trihedron parallel to the horizontal plane (Fig. 2a). The direction vector $\bar{w}$ of the straight-line generator in the trihedron system has the coordinates:

$$\bar{w}:\{cos\beta;\ 0;\ -sin\beta\}. \tag{5}$$

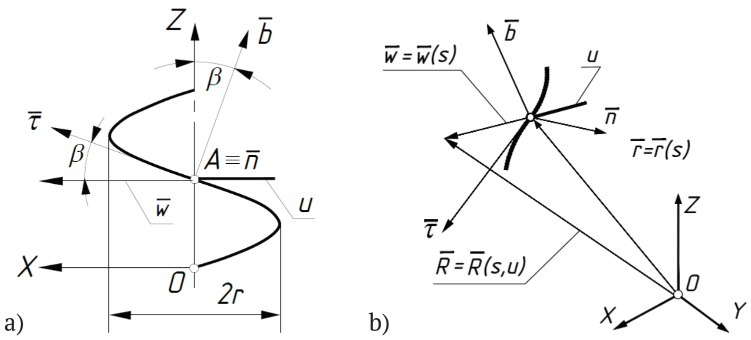

Figure 2. Graphical illustrations for constructing the vector equation of the surface of a straight open helicoid in the Frenet trihedron system of the helical line

Note: a) position of the rectilinear generator u of the surface in the direct plane of the trihedron; b) fragment of the helix and the Frenet trihedron on it with the rectilinear generator: *OX*, *OY*, *OZ* – coordinate axes, units of measurement – linear units; $\bar{\tau}$, $\bar{n}$, $\bar{b}$ – orts of the Frenet trihedron; $\bar{r} = \bar{r}(s)$ – vector equation of the helix $\bar{R} = \bar{R}(s,u)$ – vector equation of a straight open helicoid; $\bar{w} = \bar{w}(s)$ – direction vector of the rectilinear generator, u – rectilinear generator; β – angle of elevation of the helix, designated in the Frenet trihedron system concerning its orts; r – radius of the cylinder on which the helix is located

Source: developed by the authors based on research conducted

According to Figure 2b, any point on the surface of a straight open helicoid can be expressed as the vector sum of the distance $\bar{r}$ to the vertex of the trihedron and the distance u along the direction vector $\bar{w}$:

$$R(s,u) = \bar{r}(s) + \bar{\tau} u \cos\beta - \bar{b} u \sin\beta. \qquad (6)$$

It is known from differential geometry that when a surface is bent, its first quadratic form does not change. It is found through the partial derivatives of the surface (6), taking into account the fact that the angle $\beta = const$:

$$\frac{\partial \bar{R}}{\partial u} = \bar{\tau} \cos\beta - \bar{b} \sin\beta\,; \frac{\partial \bar{R}}{\partial s} = \frac{d\bar{r}}{ds} + \frac{d\bar{\tau}}{ds} u \cos\beta - \frac{d\bar{b}}{ds} u \sin\beta. \quad (7)$$

The vector $(d\bar{r})/ds = \bar{\tau}$, the derivatives of the vectors $\bar{\tau}$ and $\bar{b}$ are written in projections onto the vectors of the trihedron according to the Frenet formulas:

$$\bar{\tau}' = \bar{n}k;\ \ \bar{n}' = -\bar{\tau}k + \bar{b}\sigma;\ \ \bar{b}' = -\bar{n}\sigma. \qquad (8)$$

After substituting (8) into the partial derivative (7) of the surface along the arc s and grouping by vectors can be obtained:

$$\frac{\partial \bar{R}}{\partial s} = \bar{\tau} + \bar{n}u(k \cos\beta + \sigma \sin\beta). \qquad (9)$$

The coefficients of the first quadratic form will be written:

$$E = \left(\frac{\partial \bar{R}}{\partial u}\right)^2 = \cos^2\beta + \sin^2\beta = 1;\ F = \frac{\partial \bar{R}}{\partial u} \cdot \frac{\partial \bar{R}}{\partial s} = \cos\beta\,;$$
$$G = \left(\frac{\partial \bar{R}}{\partial s}\right)^2 = 1 + u^2(k \cos\beta + \sigma \sin\beta)^2. \qquad (10)$$

When bending the surface, it is necessary to maintain the condition under which the value of the coefficients (10) should not change. The coefficients E and F are constant values. The coefficient G includes the curvature k and the torsion σ. They can be changed so that the expression in parentheses of the coefficient G does not change in general. The angle β remains unchanged, since it is included in the coefficient F, which also should not change. After bending the surface, the curvature and torsion of the helical base curve will change their value. They can be denoted by k_b and σ_b, respectively. From the condition of invariance of the expression in parentheses of the coefficient G, it can be written:

$$k\cos\beta + \sigma\sin\beta = k_b\cos\beta + \sigma_b\sin\beta. \qquad (11)$$

In equation (11) we can change the curvature k_b or the twist σ_b. The twist σ_b will be changed by multiplying the initial twist σ by the factor p: $\sigma_b = p \cdot \sigma$. Substituting into (11) $\sigma_b = p \cdot \sigma$ and solving for k_b will give the result:

$$k_b = k + (1 - p)\sigma \cdot \mathrm{tg}\beta. \qquad (12)$$

Let the initial helix with the angle of rise β on a cylinder of radius r be given. Then its curvature and twist are determined according to expressions (2), in which instead of a, it is necessary to take r. The obtained values of curvature and twist should be substituted into the expressions $\sigma_b = p \cdot \sigma$ and (12) instead of k and σ. After simplifications, we can obtain new values of curvature and twist of the helix:

$$k_b = \frac{1}{r}(1 - p)\sin^2\beta\,; \sigma_b = \frac{1}{r} p \sin\beta \cos\beta. \qquad (13)$$

By giving different values of the coefficient p, the curvature and torsion of the helix will change, and the pitch angle β will remain constant. At $p = 1$, the initial helix will be obtained. To construct a directional helix according to parametric equations (4), it is necessary to find expressions for the constants a and b. Substituting the expressions for curvature and torsion (13) into formulas (3) gives the result:

$$a = r\frac{(1-p)\sin^2\beta + \cos^2\beta}{1 - 2p\sin^2\beta + p^2\sin^2\beta}\,; b = r\frac{p \sin\beta \cos\beta}{1 - 2p\sin^2\beta + p^2\sin^2\beta}. \quad (14)$$

At $p = 1$ from (14) we can obtain $a = r$, $b = r \cdot tg\beta$, i.e. the parameters of the initial helix. A straight-line generator passes through the helix (4), the direction of which is given by the unit vector (5) in the accompanying trihedron system. Therefore, it is necessary to pass from the trihedron system to the fixed coordinate system in which the helix is located. This can be done using the known transition formulas. After that, it is necessary to pass a straight-line generator of the surface through the helix (4) in the found direction. The parametric equations of the surface take the form:

$$X = a\cos\frac{s}{\sqrt{a^2+b^2}} - \frac{u(a\cos\beta + b\sin\beta)}{\sqrt{a^2+b^2}}\sin\frac{s}{\sqrt{a^2+b^2}};$$
$$Y = a\sin\frac{s}{\sqrt{a^2+b^2}} + \frac{u(a\cos\beta + b\sin\beta)}{\sqrt{a^2+b^2}}\cos\frac{s}{\sqrt{a^2+b^2}};$$
$$Z = \frac{bs}{\sqrt{a^2+b^2}} + \frac{u(b\cos\beta - a\sin\beta)}{\sqrt{a^2+b^2}}, \qquad (15)$$

where u is the second independent variable – the length of the straight-line generator, the count of which starts from the point on the helix. The coefficients of the first quadratic form of the surface (15) take the form:

$$E = \left(\frac{\partial X}{\partial u}\right)^2 + \left(\frac{\partial Y}{\partial u}\right)^2 + \left(\frac{\partial Z}{\partial u}\right)^2 = 1;$$
$$F = \frac{\partial X}{\partial u}\cdot\frac{\partial X}{\partial s} + \frac{\partial Y}{\partial u}\cdot\frac{\partial Y}{\partial s} + \frac{\partial Z}{\partial u}\cdot\frac{\partial Z}{\partial s} = \cos\beta;$$
$$G = \left(\frac{\partial X}{\partial s}\right)^2 + \left(\frac{\partial Y}{\partial s}\right)^2 + \left(\frac{\partial Z}{\partial s}\right)^2 =$$
$$= 1 + \frac{u^2}{2(a^2+b^2)}\left(1 + \frac{(a^2-b^2)\cos 2\beta + 2ab\sin 2\beta}{(a^2+b^2)}\right). \qquad (16)$$

The coefficients E and F coincide with the same coefficients (10). In equations (15), the constants a and b, which are included in the coefficient G, will change during bending according to (14). It is necessary to substitute the expressions a and b from (14) into the expression for the coefficient G (16):

$$G = 1 + \frac{u^2\cos^2\beta}{r^2}. \qquad (17)$$

Thus, none of the coefficients E, F, G includes the parameter p. This indicates that equation (15), where the constants a and b are given in (14), describe a one-parameter set of bendings of a straight open helicoid. If the curvature of the initial helical line from (3) is substituted into the coefficient G (10) at $a = r$, an expression similar to expression (17) will be obtained. This indicates that equation (15), when substituting expressions a and b from (14) into it, describes the process of bending of a straight open helicoid. The parameter p, which is included in the expressions a and b, that is, in the equations of the surface (15), affects the shape of the surface, but does not affect its first quadratic form.

It is advisable to consider the obtained result on the bending of a surface in which the initial helix has a lift angle $\beta = 45°$ and is located on a cylinder $r = 5$ linear units. In Figure 3, intermediate positions of the surface (frontal projections) are constructed for certain values of the parameter p. The guide helix is thickened. The length of the straight generator is 10 linear units (separate figures are made at different scales for clarity, therefore, the length of the generators on them is not proportional). When bending a straight open helicoid by reducing the torsion of the guide helix, it turns into an oblique open helicoid (Fig. 2b) and with further bending – into a single-cavity hyperboloid of rotation with a torsion equal to zero (Fig. 2c). The reduction of the pitch of the surface turn occurs by reducing the parameter p, that is, by reducing the twist of the guide helix.

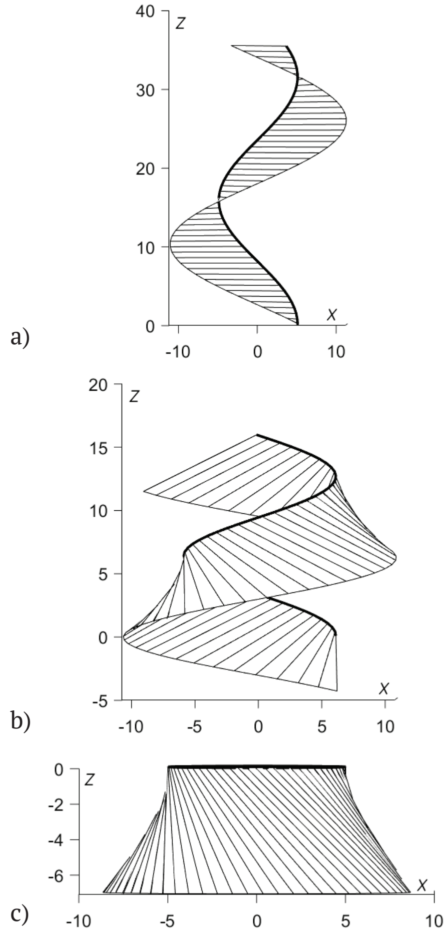

Figure 3. Individual intermediate positions of an open helicoid during its bending

Note: a) $p = 1$; b) $p = 0.5$; c) $p = 0$: X, Z are coordinate axes, units of measurement are linear units

Source: developed by the authors based on research conducted

The task is to find the necessary constants and variable parameters to describe the surface of the knife using equations (15). To do this, we need to find the radius r and the angle β of the helix. The straight-line generator of the surface on the cross-section of the knife is tangent to a circle of radius r (Fig. 4a). The length of the cross-section of the knife u_0 is part of the straight-line generator. From the right triangle, it was found the radius r:

$$r = R\sin\varphi. \qquad (18)$$

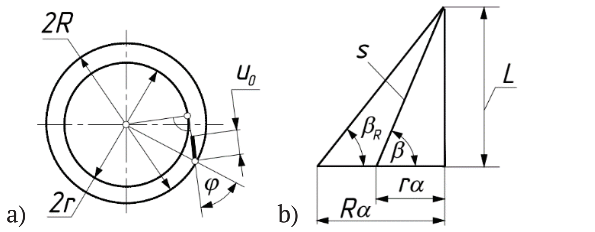

Figure 4. Graphical illustrations for finding the necessary input data for constructing the surface of a helical knife

Note: a) the relationship between the radius of the cylinders on which the helical lines are located; b) the relationship between the angles of elevation of the helical lines: r – radius of the cylinder on which the guiding helix is located; R – radius of the cylinder on which the outer helix of the knife (blade) is located; u_o – width of the knife; φ – angle between the radial direction and the cross-section of the knife; L – length of the knife; s – length of the guiding helix; β – the angle of elevation of the guide helix; β_R – the angle of elevation of the knife blade; r_α – the value of the leg of the triangle on the sweep of the guiding helical line, where α is the angle of rotation of the point during its movement along the guiding helical line, as well as along the blade line within its length; R_α – the value of the leg of the triangle on the sweep of the helical line – the blade of the knife

Source: developed by the authors based on research conducted

From the same triangle, we find the length of the straight line generator to the point on the blade and the limits of change of the parameter u, which correspond to the width of the knife u_o:

$$u = R\cos\varphi - u_0 \ldots R\cos\varphi. \tag{19}$$

Figure 4b shows helical lines on the sweeps of their cylinders. Through the length of the drum L and the length of the corresponding arc of the circle on the sweep, which are the legs of right-angled triangles, it is possible to determine the tangents of the angles of elevation β and β_R of the helical lines. The angles of rotation α of the ends of the straight generatrix around the axis when moving this generatrix along the helical lines within the distance L are the same. The expressions for the tangents of the angles are written:

$$\mathrm{tg}\beta = \frac{L}{r\alpha};\;\; \mathrm{tg}\beta_R = \frac{L}{R\alpha}. \tag{20}$$

β and β_R can be found taking into account (18):

$$\beta = \mathrm{Arctg}\left(\frac{R}{r}\mathrm{tg}\beta_R\right) = \mathrm{Arctg}\left(\frac{\mathrm{tg}\beta_R}{\sin\varphi}\right). \tag{21}$$

It was needed to find the length s of the arc of the helix on the cylinder of radius r. It can be found from the right triangle through the length L and the angle β, having previously passed from the expression for the tangent β in (21) to the sine β:

$$s = L\mathrm{ctg}\beta_R\sqrt{\sin^2\varphi + \mathrm{tg}^2\beta_R}. \tag{22}$$

When constructing the knife surface, the parameter s changes from zero to the value (22). Let the helical knife be given by the following design parameters: $L = 0.72$ m, $R = 0.25$ m, $\tau = 20°$, $\varphi = 65°$, $u_o = 0.1$ m. The necessary parameters for constructing the knife surface can be found by equations (15). According to (18) $r = 0.2266$ m. By formula (19), the limits of the variable parameter u are determined: $u = 0.006 \ldots 0.106$ m. The angle of elevation β of the guide helix for the radius r is determined by formula (21), where $\beta_R = 90° - \tau = 70°$: $\beta = 71.75°$. The limits of the change in the length of the helix are determined by formula (22): $s = 0 \ldots 0.758$ m. These data are sufficient to construct the surface of the knife according to equations (15), taking into account (14) at $p = 1$ and its bending at other values of p. In this case, the radius r acts as a constant a. However, the surface of the one-sheeted hyperboloid of revolution, to which the surface of the knife is bent at $p = 0$, is interesting. The hyperboloid of revolution is constructed in Figure 5, from which it can be seen that it is very close to a truncated cone, which can be considered an approximate sweep of the knife, that is, a flat blank for its manufacture. The cone, in turn, is very close to a cylinder with a height h. From this, we can conclude that the sweep of the knife will be close to a rectilinear strip.

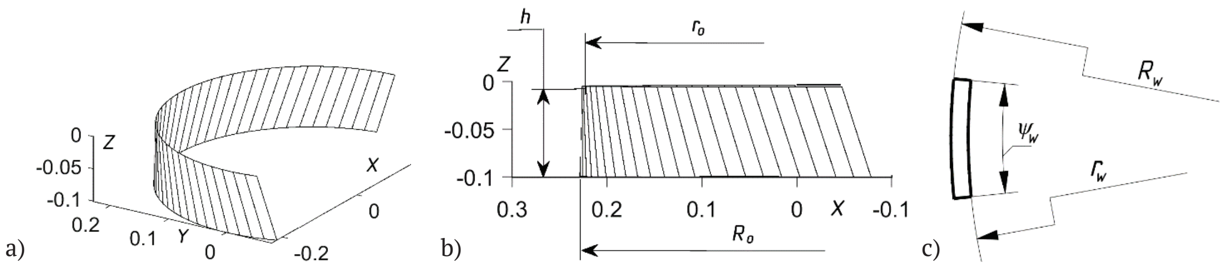

Figure 5. Section of a one-sheeted hyperboloid of revolution on which a knife has bent

Note: a) axonometric image; b) frontal projection with dimensions; c) approximate sweep of the knife: X, Y, Z – coordinate axes, units of measurement – m; R_o – radius of the lower parallel of the one-sheeted hyperboloid of revolution; r_o – radius of the upper parallel of the single-cavity hyperboloid of revolution; h – height of the compartment of the one-sheeted hyperboloid of revolution; R_w – radius of the blade arc on a flat knife blank; r_w – radius of the inner edge arc on a flat knife blank; ψ_w – central angle that limits the flat blank along the length

Source: developed by the authors based on research conducted

It is necessary to find the dimensions of the truncated cone (Fig. 5b). The variable radius ρ, which characterises the helical lines on the surface of the knife and depends on the variable u, must be found at $p=0$. In this case, according to (14) $a=r$, $b=0$. For these data from the first two equations (15):

$$\rho = \sqrt{X^2+Y^2} = \sqrt{r^2+u^2\cos^2\beta}. \tag{23}$$

At $u=0.006$ and $\beta=71.75°$, according to (22) the radius of the upper base of the truncated cone can be found $r_o=0.2266\ m$ (Fig. 5b). Practically $r_o=r$, since $u=0.006\ m$ is a small value. At $u=0.106$ and the same value of $\beta=71.75°$, according to (22), the radius of the lower base of the truncated cone can be found: $R_o=0.229\ m$. The height h is determined from the last equation (15) at $p=0$, (at which $b=0$), as the difference of heights at $u=0.006$ and $u=0.106$. From here it can be found: $h=0.095\ m$. With this data known, as well as the known length s of the upper base of radius r_o ($s=0.758\ m$), it is possible to construct a scan of a truncated cone, which is an approximate flat blank of a helical knife. The described sequence of finding the dimensions of a truncated cone, which approximates the surface of a helical knife, can be generalised. The formulas, which include only the design parameters of the knife, have the form:

$$R_0 = \frac{R\sin\varphi}{\sin\tau\sqrt{\sin^2\varphi+\mathrm{ctg}^2\tau}}; \tag{24}$$

$$r_0 = \sin\varphi\sqrt{R^2+\frac{(u_0-R\cos\varphi)^2}{\sin^2\varphi+\mathrm{ctg}^2\tau}}; \tag{25}$$

$$h = \frac{u_0\,\mathrm{ctg}\tau}{\sqrt{\sin^2\varphi+\mathrm{ctg}^2\tau}}. \tag{26}$$

Given the design parameters of the knife $L=0.72\ m$, $R=0.25\ m$, $\tau=20°$, $\varphi=65°$, $u_o=0.1\ m$, according to formulas (23), (24), (25), one can obtain: $R_o=0.229\ m$, $r=0.2266\ m$, $h=0.095\ m$. The next stage is finding the sweep of the truncated cone, which will be a flat blank for the helical knife. The dimensions of the sweep are found by the well-known formulas:

$$R_w = \frac{R_0}{R_0-r_0}\sqrt{(R_0-r_0)^2+h^2};$$
$$r_w = \frac{r_0}{R_0-r_0}\sqrt{(R_0-r_0)^2+h^2}. \tag{27}$$

where R_w is the radius of the knife blade on a flat workpiece, r_w is the radius of the inner edge (Fig. 5c). The length of the blade on the workpiece is equal to the length of the larger base of the truncated cone, which is not closed (Fig. 5a). It can be determined from a right triangle (Fig. 4b):

$$s_w = \frac{L}{\sin\beta_R} = \frac{L}{\cos\tau}. \tag{28}$$

From formulas (27), (28), one can obtain: $R_w=9.07\ m$, $r_w=8.97\ m$, $s_w=0.77\ m$. The knife blade on the workpiece rests on the central angle ψ_w (Fig. 5c), which is determined from the expression (for the considered case $\psi_w=0.08$ rad or 4.8°):

$$\psi_w = \frac{L}{R_0\cos\tau}. \tag{29}$$

Given that helical surfaces are widespread in technology, great attention is paid to their manufacture. From an engineering point of view, they all fall under the general definition associated with a helical conoid – the common name in technology of "screw". However, from a geometric point of view, there is a difference between the methods of forming helical surfaces. This difference is taken into account in the study. And it is as follows: in a helical conoid, which is also called a direct closed helicoid, the rectilinear generators intersect the axis of the surface, and in a direct open helicoid, they are parallel to the axis.

It is noteworthy that in the article, the finding of the approximate sweep of the knife surface is closely related to the theoretical description of the process of its bending. According to the theory of differential geometry of surfaces, any helical surface can be bent into a surface of revolution and vice versa. This implies the invariance of the lengths of lines on the surface and its area during the bending process. The surface thickness is assumed to be zero. This is a disadvantage of the method. However, with a relatively small surface thickness, this method gives acceptable results for practice.

In the theoretical description of the bending of helical surfaces in the surface of revolution, it is important to obtain reliable results. In the conducted study, this is confirmed by the coefficients of the first quadratic forms of the surface of the open helical conoid and the one-sheeted hyperboloid of revolution. The correspondence of these forms is accompanied by the found coefficients (10) for the helical surface and the corresponding coefficients (16) for its bending.

The construction of the sweep of a helical knife has its specifics. The fact is that the angle of elevation of the helix (knife blade) is quite large: $\beta_R=70°$. With a drum radius of $R=0.25\ m$, this corresponds to a surface pitch of $H=4.3\ m$. If there were only one knife on the drum, then for its continuous operation, it would have to have a length of $L=4.3\ m$. $L=0.72\ m$ was taken, which requires mounting 6 knives on the drum for continuous operation. The approximate sweep of the sixth part of the full turn of the helical knife is close to a straight strip. The small curvature of the knife blade is also indicated by the radius found on a flat workpiece – $R_w=9.07\ m$. With a blade length of $s_w=0.77\ m$ and such a radius, the workpiece can be replaced with a straight strip. However, the importance of the result is that it is directly related to the process of bending the workpiece into the surface of the knife. As its length increases, the effect of taking into account the curved shape of the flat workpiece will increase.

Numerous studies have been devoted to the construction of developable surfaces. F. Taş & R. Ziatdinov (2023) investigated developable ruled surfaces, which are formed using the curvature axis of a spatial curve. The authors analysed the geometric properties of such surfaces and their construction. The work of A.S.M. Kamarudzaman & M.Y. Misro (2024) is devoted to the comparison of enveloping developable surfaces constructed based on quintic trigonometric Bezier surfaces. The study was conducted in the context of evaluating their geometric properties for use in computer modeling and surface design. T.G. Nelson *et al.* (2019) analysed how developable mechanisms can be integrated into curvilinear structures while maintaining the ability to fold and developable. This opens up new possibilities for creating flexible engineering solutions, particularly in robotics, aerospace, and biomedical devices. The design of a helical blade of an agricultural tool from a planar surface is proposed in the article by S. Pylypaka *et al.* (2024). In this case, the planar surface can be precise, which minimises deformation during bending, but in return, there is a significant limitation of the study. The main difference in the design of surfaces in this work is that the surface is non-planar.

The issue of constructing non-developable surfaces is more complex from a mathematical point of view and is of interest to many researchers. Scientists A. Bankova *et al.* (2024) outlined a method for constructing intersection lines at the transition of sheet material between different surfaces, as well as designing the sweep of such a surface. The research is aimed at improving the processes of designing and manufacturing parts from sheet materials in mechanical engineering and construction. Research of L. Zawallich & R. Pajarola (2024) is devoted to the method of developable 3D models by approximating the mesh using surface flows. The authors propose an algorithm that optimises the developable process of complex geometric shapes, while preserving their structure and minimising deformations.

E. Güler & Y. Yayli (2023) considered the local isometry of generalised helicoidal surfaces in four-dimensional space. The authors investigated the conditions under which such surfaces are locally isometric to each other, which is important for the geometry of multidimensional objects and the theory of surfaces. The article of E. Güler & N.C. Turgay (2024) is devoted to the study of geometric isometries of helical surfaces in five-dimensional Euclidean space. The authors analyse the properties of such surfaces and their behaviour under various transformations, which is important for multidimensional differential geometry and mathematical modelling.

A. Kumar *et al.* (2024) investigated multi-scale surface folding during metalworking. The authors analysed the mechanisms of fold formation and their impact on the surface quality and characteristics of the machined parts, which is important for optimising cutting processes in modern manufacturing. W. Zhang *et al*. (2024) proposed an approach to selecting machining parameters when milling helical surfaces, taking into account spindle vibrations, to increase the efficiency and quality of machining in high-precision machining processes. Research of I. Hevko *et al*. (2018) is devoted to the synthesis of methods for winding screw spirals, which is an important part of the development and improvement of screw mechanism manufacturing technology. The authors analysed various winding methods that allow achieving optimal parameters to ensure the effective operation of screw systems in various industries, such as material processing or agriculture. M. Pylypets *et al*. (2021) analysed the prerequisites for the development of combined operations for the manufacture of screw and auger blanks by the method of metal processing by pressure. The authors considered the latest technologies that combine various processing methods to improve the efficiency of manufacturing such blanks, in particular to reduce material consumption and increase manufacturing accuracy in modern mechanical engineering.

Research of O. Liashuk *et al*. (2019) is devoted to the feasibility study of the manufacturing process of screw working bodies to improve their manufacturing process. S. Pylypaka *et al*. (2017) considered the bounding surfaces of a one-parameter set of planes, as well as methods for their construction and the construction of sweeps. The authors focused their attention on the mathematical and geometric aspects of creating such surfaces, which can be useful for the development of new technologies in mechanical engineering and architectural design. Zh. Li & J. Liqiang (2013) proposed an innovative approach to the design and manufacture of combined propeller blades for use in various industrial applications, in particular in turbine and pump systems. This allowed for to improvement of the technology of manufacturing propeller blades, increasing the accuracy and efficiency of their operation. Ch.-M. Tan & G.-Y. Lin (2016) proposed an innovative mould design for the production of propeller blades for lawn mowers. The authors developed effective methods for optimising the casting process of such blades, which include improving the quality of their manufacture and increasing the productivity of the process.

V. Tarelnyk *et al.* (2019a) investigated the influence of the main technological parameters on the microgeometry, structure, and properties of electroerosion coatings created using combined coatings and surface plastic deformation. The main attention is paid to improving the quality of surface layers by optimising processing modes. Research by V. Tarelnyk *et al.* (2019b) is devoted to the analysis of the stress-strain state of the surface layer after surface plastic deformation of electroerosion coatings. However, the influence of surface geometry on these characteristics was not taken into account at the design stage, which creates prospects for further scientific research in this direction.

Similar to this work V. Khropost & T.A. Kresan (2023) considered finding the sweep of a section of a straight open helicoid due to its bending onto a surface of revolution. However, the description of the bending process was carried out in a Cartesian coordinate system without involving the vector equation of the surface and Frenet formulas. Ultimately, a result similar to that obtained in this study was obtained, i.e., the surface of revolution is a single-cavity hyperboloid. In addition, the construction of an approximate sweep was carried out for an entire turn without giving generalised formulas.

Thus, many scientific works are devoted to the study of the properties, features of geometry, and methods of constructing helical non-developable and expandable surfaces. At the same time, a significant part of these studies is mainly theoretical and is aimed at solving purely mathematical problems, without detailed consideration of the practical aspects of their use in real structures and technological processes. In contrast, within the framework of this study, attention is focused not only on theoretical principles but also on applied aspects, which makes it more oriented towards solving engineering problems.

CONCLUSIONS

A mathematical model of the process of gradual bending of the surface of a helical knife into a surface of revolution has been developed. For this purpose, the theory of differential geometry regarding the bending of helical surfaces is used. It is based on the well-known position that any helical surface can be bent into a surface of revolution by reducing its pitch to zero. In this case, the helical lines are transformed into parallels of the surface of revolution. Based on this position, parametric equations of gradual bending of a straight open helicoid into a surface of revolution have been derived. These include the bending parameter p, which can be given constant values in the range from unity to zero. At $p = 1$, the equations describe the initial helical surface, and at $p = 0$, the surface of revolution. At intermediate values of the parameter p from unity to zero, the helical surface gradually bends into a surface of revolution. In the obtained equations of gradual bending of the surface corresponding to a helical knife, a transition was made from constant values to the design parameters of the knife. This allowed us to describe the surface of revolution at $p = 0$, which is a one-sheeted hyperboloid of revolution, through the parameters of the knife. For example, with a drum radius $R = 0.25$ m, an angular elevation of the helix (knife blade) $\beta_R = 70°$ and a knife length $L = 0.72$ m, a section of a one-sheeted hyperboloid of revolution was obtained with a larger parallel of radius $R_0 = 0.229$ m and a smaller parallel $r_0 = 0.2266$ m and a distance between them $h = 0.095$ m. These dimensions were taken as the dimensions of a truncated cone, which closely approximates the surface of a single-cavity hyperboloid. After that, an exact sweep of the truncated cone was obtained, which is an approximate sweep of a helical knife. It is a flat ring with an outer radius $R_w = 9.07$ m and an inner radius $r_w = 8.97$ m.

The obtained result of constructing an approximate sweep of a helical knife is directly related to the mathematical model of the surface bending process, therefore, it is logical. The prospects for further research are to study the surface of helical blades for their improvement from a geometric point of view and simplification of the manufacturing technology.

ACKNOWLEDGEMENTS

The authors of the article express their gratitude to the soldiers of the Armed Forces of Ukraine, thanks to whose courage, Ukrainian scientists have the opportunity to engage in science.

FUNDING

None.

CONFLICT OF INTEREST

None.

REFERENCES

[1] Bankova, A., Tenev, S., Atanasov, A., Nikolov, P., Mehmedov, I., & Neveda, N. (2024). Construction of the intersection lines of a sheet material transition and design of the unfolding of its surface. *5th International conference on communications, information, electronic and energy systems (CIEES)* (pp. 1-5). Veliko Tarnovo: IEEE. doi: 10.1109/CIEES62939.2024.10811193.

[2] Bulgakov, V., Rucins, A., Holovach, I., Trokhaniak, O., Klendii, M., Popa, L., & Kutsenko, A. (2024). Theoretical study of traction resistance of harrows with helical working bodies. *INMATEH – Agricultural Engineering*, 74(3), 380-387. doi: 10.35633/inmateh-74-33.

[3] Chen, J., Zhu, R., Chen, W., Li, M., & Yin, X. (2024). General meshing modeling and dynamic characteristics analysis of helical gear pair with tooth surface deviation. *Iranian Journal of Science and Technology Transactions of Mechanical Engineering*, 48(1), 1623-1641. doi: 10.1007/s40997-024-00751-4.

[4] Filimonov, S., & Bacherikov, D. (2022). Model of screw linear piezoelectric motor. *Bulletin of Cherkasy State Technological University*, 27(4), 13-22. doi: 10.24025/2306-4412.4.2022.268445.

[5] Güler, E., & Turgay, N.C. (2024). Analyzing geometric isometries of helical surfaces in five-dimensional Euclidean space. *Filomat*, 38(23), 8121-8129.

[6] Güler, E., & Yayli, Y. (2023). Local isometry of the generalised helicoidal surfaces family in 4-space. *Malaya Journal of Matematik*, 11(2), 210-218. doi: 10.26637/mjm1102/009.

[7] Hevko, I.B., Hud, V.Z., & Kruhlik, O.A. (2018). Synthesis of methods for helical winding of screw conveyors. *Prospective Technologies and Devices*, 12, 39-47.

[8] Kamarudzaman, A.S.M., & Misro, M.Y. (2024). Developability comparison of enveloping developable quintic trigonometric Bézier surface. *5th International Conference on Mathematical Sciences (ICMS5)*, 3150, article number 030005. doi: 10.1063/5.0228304.

[9] Khropost, V.I., & Kresan, T.A. (2023). Design of an open helicoid turn from a flat blank. *Applied Geometry and Engineering Graphics*, 105, 213-221. doi: 10.32347/0131-579X.2023.105.213-221.

[10] Kumar, A., Chandan, A., & Mahato, A. (2024). Multi-scale surface folding in metal cutting. *Journal of Manufacturing Processes*, 120, 628-640. doi: 10.1016/j.jmapro.2024.04.070.

[11] Li, Zh., & Liqiang, J. (2013). Design of combined helical blade manufacturing device. *Advanced Materials Research*, 753-755, 1386-1390. doi: 10.4028/www.scientific.net/AMR.753-755.1386.

[12] Liashuk, O.L., Diachun, A.Ye., Tretiakov, O.L., Navrotska, T.D., & Kruhlik, O.A. (2019). Technical and economic justification of the manufacturing process for helical working bodies. *Bulletin of the Kharkiv Petro Vasylenko National Technical University of Agriculture. Mechanization of Agricultural Production*, 198, 244-251.

[13] Liu, H. (2024). The forming theory and computer simulation of the rotary cutting tools with helical teeth and complex surfaces. *Computer and Information Science*, 20241(4), 158-162. doi: 10.5539/cis.v1n4p158.

[14] Liu, S., Li, B., Gan, R., & Xu, Y. (2023). Surrogate-based optimization design for surface texture of helical pair in helical hydraulic rotary actuator. *Scientific Reports*, 13(1), article number 20259. doi: 10.1038/s41598-023-47509-7.

[15] Mushtruk, M., Gudzenko, M., Palamarchuk, I., Vasyliv, V., Slobodyanyuk, N., Kuts, A., Nychyk, O., Salavor, O., & Bober, A. (2020). Mathematical modeling of the oil extrusion process with pre-grinding of raw materials in a twin-screw extruder. *Potravinarstvo Slovak Journal of Food Sciences*, 14, 937-944. doi: 10.5219/1436.

[16] Nelson, T.G., Zimmerman, T.K., Magleby, S.P., Lang, R.J., & Howell, L.L. (2019). Developable mechanisms on developable surfaces. *Science Robotics*, 4(27), article number eaau5171. doi: 10.1126/scirobotics.aau5171.

[17] Ortiz, J.C.P., Rubio-Clemente, A., & Chica, E. (2024). Optimization of a Gorlov helical turbine for hydrokinetic application using the response surface methodology and experimental tests. *Energies*, 17(22), article number 5747. doi: 10.3390/en17225747.

[18] Pull-type forage harvesters and flail harvester. (n.d.). Retrieved from https://assets.cnhindustrial.com/nhag/apac/en/assets/pdf/forage-harvesters/pull-type-brochure-apac-en.pdf.

[19] Pylypaka, S., Hropost, V., Nesvidomin, V., Volina, T., Kalenyk, M., Volokha, M., Zalevska, O., Shuliak, I., Dieniezhnikov, S., & Motsak, S. (2024). Designing a helical knife for a shredding drum using a sweep surface. *Eastern-European Journal of Enterprise Technologies*, 4(1(130)), 37-44. doi: 10.15587/1729-4061.2024.308195.

[20] Pylypaka, S.F., Kresan, T.A., & Hryshchenko, I.Yu. (2017). *Enveloping surfaces of a single-parameter set of planes: Design, section cutting, and development construction*. Kyiv: CP “KOMPRINT”.

[21] Pylypets, M.I., Vasylykiv, V.V., Radyk, D.L., & Pylypets, O.M. (2021). Prerequisites for the development of combined operations for manufacturing helical and screw blanks by metal forming methods. *Prospective Technologies and Devices*, 18, 112-123. doi: 10.36910/6775-2313-5352-2021-18-17.

[22] Rucins, A., Bulgakov, V., Holovach, I., Trokhaniak, O., Klendii, M., Popa, L., & Yaremenko, V. (2024). Research on power parameters of a screw conveyor with bladed operating body for transporting agricultural materials. *INMATEH - Agricultural Engineering*, 74(3), 428-435. doi: 10.35633/inmateh-74-38.

[23] Tan, Ch.-M., & Lin, G.-Y. (2016). An innovative compression mold design for manufacture of reel mower helical blades. *Applied Mechanics and Materials*, 851, 255-258. doi: 10.4028/www.scientific.net/AMM.851.255.

[24] Tarelnyk, V.B., Gaponova, O.P., Konoplianchenko, Ye.V., Martsynkovskyy, V.S., Tarelnyk, N.V., & Vasylenko, O.O. (2019a). Improvement of quality of the surface electroerosive alloyed layers by the combined coatings and the surface plastic deformation. III. The influence of the main technological parameters on microgeometry, structure and properties of electrolytic erosion coatings. *Metallofizika i Noveishie Tekhnologii*, 41(3), 313-335. doi: 10.15407/mfint.41.03.0313.

[25] Tarelnyk, V.B., Gaponova, O.P., Konoplianchenko, Ye.V., Martsynkovskyy, V.S., Tarelnyk, N.V., & Vasylenko, O.O. (2019b). Improvement of quality of the surface electroerosive alloyed layers by the combined coatings and the surface plastic deformation. II. The analysis of a stressedly-deformed state of surface layer after a surface plastic deformation of electroerosive coatings. *Metallofizika i Noveishie Tekhnologii*, 41(2), 173-192. doi: 10.15407/mfint.41.02.0173.

[26] Taş, F., & Ziatdinov, R. (2023). Developable ruled surfaces generated by the curvature axis of a curve. *Axioms*, 12(12), article number 1090. doi: 10.3390/axioms12121090.

[27] Zawallich, L., & Pajarola, R. (2024). Unfolding via mesh approximation using surface flows. *Computer Graphics Forum*, 43(2), article number e15031. doi: 10.1111/cgf.15031.

[28] Zhang, W., Sun, X., Yang, H., Liu, Y., & Dong, Zh. (2024). A process parameters decision approach considering spindle vibration in helical surface milling for minimizing energy consumption and surface roughness value. *Journal of the Brazilian Society of Mechanical Sciences and Engineering*, 46, article number 675. doi: 10.21203/rs.3.rs-4166187/v1.

[29] Zhao, J., Ma, Ch., Li, Zh., Yu, X., & Sheng, W. (2024). Evolution of tooth surface morphology and tribological properties of helical gears during mixed lubrication sliding wear. *Surface Topography: Metrology and Properties*, 12(3), article number 035037. doi: 10.1088/2051-672X/ad76c3.

Андрій Несвідомін
Кандидат технічних наук, доцент
Національний університет біоресурсів і природокористування України
03041, вул. Героїв Оборони, 15, м. Київ, Україна
https://orcid.org/0000-0002-9227-4652

Сергій Пилипака
Доктор технічних наук, професор
Національний університет біоресурсів і природокористування України
03041, вул. Героїв Оборони, 15, м. Київ, Україна
https://orcid.org/0000-0002-1496-4615

Тетяна Воліна
Доктор технічних наук, доцент
Національний університет біоресурсів і природокористування України
03041, вул. Героїв Оборони, 15, м. Київ, Україна
https://orcid.org/0000-0001-8610-2208

Микола Лохоня
Доктор філософії
Сумський державний педагогічний університет імені А.С. Макаренка
40002, вул. Роменська, 87, м. Суми, Україна
https://orcid.org/0000-0003-0778-252X

Яна Бородай
Старший викладач
Сумський національний аграрний університет
40021, вул. Герасима Кондратьєва, 160, м. Суми, Україна
https://orcid.org/0000-0003-0048-815X

Формування гвинтоподібних ножів із плоских заготовок за умови мінімальних деформацій

Анотація. У конструкціях кормозбиральної техніки все ширше використовуються гвинтоподібні ножі, які демонструють кращі характеристики різання порівняно з традиційними плоскими, проте їх виготовлення ускладнюється нерозгортною формою поверхні. Проблема створення точної плоскої заготовки для таких ножів зумовлює потребу в математичному описі їх геометрії. Метою дослідження було визначення аналітичного способу побудови плоскої заготовки для гвинтоподібного ножа з урахуванням мінімального опору при пластичній деформації заготовки. Для досягнення поставленої мети застосовано методи диференціальної геометрії, зокрема векторний аналіз гвинтових поверхонь, побудова тригранника Френе та аналіз першої квадратичної форми поверхні. Встановлено, що робоча поверхня ножа є прямим відкритим гелікоїдом, який може бути зігнутий у поверхню обертання без зміни першої квадратичної форми. Побудовано параметричні рівняння згинання поверхні ножа з використанням змінного параметра, що описує процес перетворення гелікоїда в однопорожнинний гіперболоїд обертання. Доведено, що останній із високою точністю апроксимується зрізаним конусом, розгортка якого визначається через конструктивні параметри ножа. Отримано формули для обчислення геометричних розмірів розгортки за відомими параметрами ножа, зокрема радіусами основ і висотою зрізаного конуса. Показано, що довжина дуги леза та центральний кут, який окреслює заготовку, дозволяють точно описати її форму. Практична цінність дослідження полягає у створенні ефективної методики побудови найбільш точної плоскої заготовки для виготовлення гвинтоподібного ножа, що дозволяє мінімізувати опір при формуванні, знизити трудомісткість і підвищити точність виготовлення деталей подрібнювальних барабанів

Ключові слова: формули Френе; кривина; скрут; векторне рівняння поверхні; перша квадратична форма

Machinery & Energetics
Vol. 16, No. 3. 2025

Journal homepage:
https://technicalscience.com.ua/en

UDC 621.01:631.31
DOI: 10.31548/machinery/3.2025.20

Stanislav Nikolayenko
Doctor of Pedagogical Sciences, Professor,
Academician of the National Academy of Agrarian Sciences of Ukraine
National University of Life and Environmental Sciences of Ukraine
03041, 15 Heroiv Oborony Str., Kyiv, Ukraine
https://orcid.org/0000-0001-5271-1777

Gennadii Virchenko
Doctor of Technical Sciences, Professor
National Technical University of Ukraine "Igor Sikorsky Kyiv Polytechnic Institute"
03056, 37 Beresteisky Ave., Kyiv, Ukraine
https://orcid.org/0000-0001-9586-4538

Mykola Volokha*
Doctor of Technical Sciences, Senior Researcher
National Technical University of Ukraine "Igor Sikorsky Kyiv Polytechnic Institute"
03056, 37 Beresteisky Ave., Kyiv, Ukraine
https://orcid.org/0000-0002-0112-7324

Oleksii Vorobiov
Postgraduate Student
National Technical University of Ukraine "Igor Sikorsky Kyiv Polytechnic Institute"
03056, 37 Beresteisky Ave., Kyiv, Ukraine
https://orcid.org/0000-0001-5314-1075

Yuliia Lazarchuk-Vorobiova
Postgraduate Student
National Technical University of Ukraine "Igor Sikorsky Kyiv Polytechnic Institute"
03056, 37 Beresteisky Ave., Kyiv, Ukraine
https://orcid.org/0000-0002-7866-3299

Improving energy efficiency of double-disc coulters using boundary estimation method of seed furrow profile influence

Abstract. The relevance of this study lies in the global demand to increase the energy efficiency of agricultural implements while maintaining high agronomic performance. The purpose of the article was to analytically assess the effect of furrow profile parameters on the operational energy performance of tillage tools, using double-disc openers as an example. The methodology was based on geometric modelling of the working components of the coulter in a Cartesian coordinate system, derivation of parametric equations for furrow contours, and analytical calculation of the furrow cross-sectional area depending on tillage depth, disc diameter, and disc alignment angles. The study demonstrated that the furrow area for discs with a 350 mm diameter increased from 415 mm^2 to 4106 mm^2 as the tillage depth rose from 20 mm to 80 mm. With a fixed depth of 50 mm and angles $\alpha = 50°$, $\beta = 20°$, the furrow area varied from 1762 mm^2 to 1935 mm^2 as the disc diameter changed from 300 mm to 400 mm. A quadratic approximation formula was proposed to express this dependence.

Article's History: Received: 15.05.2025; Revised: 19.08.2025; Accepted: 23.09.2025.

Suggested Citation:
Nikolayenko, S., Virchenko, G., Volokha, M., Vorobiov, O., & Lazarchuk-Vorobiova, Yu. (2025). Improving energy efficiency of double-disc coulters using boundary estimation method of seed furrow profile influence. *Machinery & Energetics,* 16(3), 20-32. doi: 10.31548/machinery/3.2025.20.

*Corresponding author

The results showed that reducing the tillage depth from 50 mm to 45 mm led to a decrease in furrow area from 1851 mm^2 to 1277 mm^2, while increasing the depth to 55 mm resulted in an increase to 2516 mm^2. The influence of disc inclination angles on the cross-sectional area was also demonstrated: decreasing the angles to $\alpha = 40°$ and $\beta = 15°$ reduced the area to 1522 mm^2. The proposed approach enabled further configuration optimisation of coulters under real conditions. The methodology presented in this publication makes it possible to determine the most rational configuration of tillage tools for the existing circumstances through appropriate analysis

Keywords: energy efficiency of agricultural machinery; disc tillage tools; mathematical modelling; computer-aided design; computer information technology

INTRODUCTION

In the context of increasing demands for sustainable agriculture and resource-efficient food production, improving the energy performance of tillage implements remains a pressing technical challenge. With the rising cost of fuel, depletion of non-renewable resources, and the need to reduce environmental impacts, modern agricultural machinery must be designed to ensure high productivity with minimal energy input. This necessitates the optimisation of structural and operational parameters of tillage tools, particularly those adapted for conservation agriculture, such as disc-type openers.

V. Damanauskas & A. Janulevičius (2022) noted that due to the existing high environmental requirements and the need to ensure proper energy efficiency, the intensity of tillage is now significantly decreasing. Using the example of a cultivator with elastic tines and a disc harrow, they show that the required soil structure and the desired application of plant residues are realised by fuel consumption, which is determined by the type of tractor, its speed, tillage depth, and soil condition. It is recommended to save energy resources by reducing the depth of cultivation rather than reducing the speed of agricultural units. M. Malasli & A. Çelik (2023) studied the effect of ploughing depth, angles of discs in the horizontal plane and relative to the vertical, emphasising the importance of these parameters for furrow formation, traction forces, and energy consumption. This information shows the relevance of determining the optimal position of tillage tools during their operation. The geometric modelling of furrow profiles of disc tillage tools is the subject of a study by P. Yablonskyi *et al.* (2023; 2025). O. Vorobiov (2024) outlined the principles of analytical and computer reproduction of the structural and operational parameters and characteristics of these tillage tools.

The authors A. Hamid & A. Alsabbagh (2023) studied the effect of shelf types, depths, and cultivation speeds on the obtained agrotechnical characteristics. The prospects of disc tools are associated with the current progressive trends in minimum tillage. Discs, unlike shelf ploughs, significantly reduce energy costs, ensure soil moisture retention, and contribute to its erosion resistance. G. Xu *et al.* (2023) and Z. Zeng *et al.* (2021) performed an experimental study of several disc tillage tools to compare their effectiveness at different furrow profiles, measuring the acting forces and crushing of plant residues. K. Aikins *et al.* (2020) investigated the basic characteristics of coulters, including soil destruction, low traction resistance, and accurate seed and fertiliser placement. D. Parihar *et al*. (2023) compared openers in terms of furrow formation, energy consumption and sowing performance. The publication of F. Chandio *et al.* (2020) is devoted to the mathematical prediction of the forces acting on the discs and the resulting soil deformations depending on the speed and depth of cultivation. O. Ranta *et al.* (2021) note that there is a growing interest in farming, which involves sowing into untreated soil by forming the necessary furrows. This preserves moisture in the soil and prevents soil erosion. Several types of discs and sowing speeds have been studied to define rational agronomic regimes. It is emphasised that more attention should be paid to the design of soil-adapted coulters, as well as the possibility of their real-time adjustment to improve the quality of work performed. In the work of S. Nikolaenko *et al.* (2021) indicated that the training of mechanical engineers, technologists and designers in agricultural higher education institutions requires innovative integrated approaches that provide relevant in-depth theoretical knowledge, sufficient practical skills, and an appropriate level of proficiency in modern computer information technologies. In this regard, the information presented in this publication will also be quite useful. Thus, the analysis of existing approaches shows that further improvement of disc tillage tools is quite relevant. This is due to the need to solve urgent problems of food security with minimal energy costs.

This article is aimed at solving some of the problems of this topic. In particular, this concerns optimisation of the operation of double-disc openers by selecting rational disc diameters, their installation angles, tillage depths, travel speeds, etc. The scientific novelty of the study lies in the proposed method of boundary estimates of the influence of the furrow profile on the operational energy characteristics of tillage tools, presented on the example of double-disc coulters.

MATERIALS AND METHODS

For soil cultivation, their main components (Fig. 1) were the riser 1, axle 2 and flat discs 3. Such components as seed pipes, wrappers, etc. that were not essential for determining the required furrow were not considered in the cited articles. This also applied to additional structural elements that can remove the ridge formed between the discs and the soil from the furrow walls. These tasks should be the subject of further scientific research.

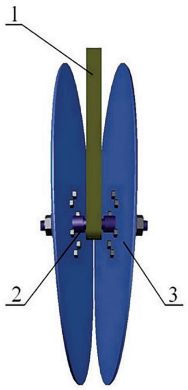

Figure 1. Main tillage components of the double disc coulter

Note: 1 – riser, 2 – axle, 3 – disc with hub and rolling element

Source: developed by the authors

The image in Figure 1 corresponds to the view in the direction of travel of the opener. The round flat discs are placed symmetrically with respect to the longitudinal vertical plane of symmetry of the implement. They are positioned in the Cartesian coordinate system *Oxyz* with the origin *O* at the point of intersection of the disc axes, the *x*-axis opposite to the direction of the coulter movement, the horizontal plane *Oxy* and the vertical axis *z*. The discs are rotated by an angle of α relative to the *x*-axis in the horizontal plane and deviated by an angle β from the vertical. During operation, they rotate around their axes, cut, spread and compact the soil to form a furrow. Its profile, i.e. cross section, depends on the diameter *D* of the discs, the required processing depth *a*, and the angles α and β. The latter also determine the location of the convergence point *S*, which corresponds to the minimum distance between the discs (Fig. 2). To simplify the analytical calculations, the original *Oxyz* coordinate system was moved to the centre of the left disc by parallel transfer.

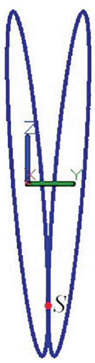

Figure 2. Point S of disc convergence

Source: developed by the authors

According to O. Vorobiov (2024), the parametric equations of the contours are as follows:

- for the left (first) disc:

$$x(u)=\frac{D}{2}(cos\alpha\ cos(u)+sin\alpha\ sin\beta\ sin(u)),$$
$$y(u)=\frac{D}{2}(cos\alpha\ sin\beta\ sin(u)-sin\alpha\ cos(u)),\ z(u)=-\frac{D}{2}cos\beta\ sin(u);\quad(1)$$

- for the right (second) disc:

$$x(u)=\frac{D}{2}(cos\alpha\ cos(u)+sin\alpha\ sin\beta\ sin(u)),$$
$$y(u)=2_{yS}+\frac{D}{2}(sin\alpha\ cos(u)-cos\alpha\ sin\beta\ sin(u)),$$
$$z(u)=-\frac{D}{2}\ cos\beta\ sin(u),\quad(2)$$

where *D* is the diameter of the discs; α ∈ (0°, 90°), β ∈ (0°, 90°) are the intervals of change in the angles α and β; y_s is the ordinate of the point *S* of the discs' convergence; *u* ∈ [0°, 360°] is a parameter corresponding to the angle in the plane of the disc with the vertex in its centre, the base side directed to the rear point of the horizontal diameter (Fig. 2), and is counted counterclockwise, looking against the direction of the *y*-axis. Conforming to O. Vorobiov (2024) shows that the vanishing point *S* corresponds to the parameter:

$$u_s=\text{arctg}(-\text{ctg}\cdot sin\beta)+180°.\quad(3)$$

By substituting the value from expression (3) into expression (1), the required value of y_s for the ordinate *y* in ratio (2) is obtained. The furrow pattern of a double disc coulter is illustrated in Figure 3, where *h* is the distance from the centre of the discs to the ground.

The applications of formulas (1) and (2) show that for the lowest positions of the first and second discs the parameter *u* = 90°. Then the distance between these points (Fig. 3):

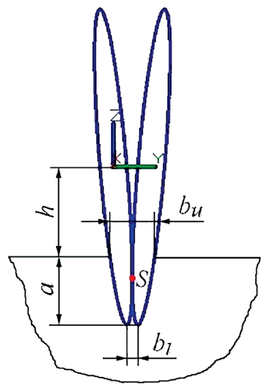

Figure 3. Furrow profile depending on the tillage depth *a*

Note: *h* – distance from the centre of the discs to the ground; *a* – tillage depth; *S* – point of minimum distance between discs; b_l – distance between the lowest points of the discs; b_u – width of the top of the furrow profile

Source: developed by the authors

$$b_l=2y_S+\frac{D}{2}(sin\alpha\ cos(90°)-cos\alpha\ sin\beta\ \sin(90°))-$$
$$-\frac{D}{2}(cos\alpha\ sin\beta\ sin(90°)-sin\alpha\ cos(90°))=2y_S-D\ cos\alpha\ sin\beta.\quad(4)$$

In practice, considering the gap d_S between the discs at the point of their convergence, the following expression is obtained:

$$b_l = 2y_S - D\cos\alpha \sin\beta + d_S. \quad (5)$$

The study by O. Vorobiov (2024) shows that the initial upper position of the furrow profile is determined by the parameter:

$$u_u = arcsin\left(1 - \frac{2a}{D\cos\beta}\right). \quad (6)$$

The maximum processing depth $a_{\max}$ of the disc at twothirds of its radius corresponds to the gap:

$$u \in [u_{\min}, u_{\max}] = [19.5°, 160.5°], \quad (7)$$

For a specific furrow:

$$u \in [u_u, 180° - u_u], \quad (8)$$

where:

$$u_u \in [u_{\min}, 90°). \quad (9)$$

As can be seen from Figure 3 and expressions (1) and (2), the width b_u of the top of the furrow profile is equal to:

$$b_u = 2y_S + \frac{D}{2}(\sin\alpha \cos(u_u) - \cos\alpha \sin\beta \sin(u_u)) - \\ - \frac{D}{2}(\cos\alpha \sin\beta \sin(u_u) - \sin\alpha \cos(u_u)) = \\ = 2y_S + D(\sin\alpha \cos(u_u) - \cos\alpha \sin\beta \sin(u_u)). \quad (10)$$

Considering the minimum distance d_S between the discs at the point of their convergence, the following expression is obtained:

$$b_u = 2y_S + D(\sin\alpha \cos(u_u) - \cos\alpha \sin\beta \sin(u_u)) + d_S. \quad (11)$$

Thus, relations (1)-(11) for the double disc coulters under consideration make it possible to analytically determine the theoretical profile of the furrow they form. These data are necessary, but not sufficient for rational management of the energy efficiency of the studied agricultural implements. The useful work performed by a tillage implement W_{ti} under stable operating conditions (or proper average values over a certain period of time) is determined by the formula:

$$W_{ti} = F_{ti} \cdot L_{ti}, \quad (12)$$

where F_{ti} is the force of resistance of the soil and the implement; L_{ti} is the distance travelled.

In dependence (12), it is assumed that the tillage tools are moving in a straight line with a constant speed. Therefore, the total traction force applied to them acts along the specified trajectory, is equal to the resistance force of the soil and the implement, and has the opposite direction to it. The term "total traction force" refers to the total effect of traction. For example, driving downhill reduces the actual traction force of the tractor, while driving uphill increases it, and so on. Also, the "soil and implement resistance force" includes both the direct resistance of the deformed soil and additional components related, in particular, to the features of the structure used, its operational condition, etc. It is once again emphasised that the method of boundary estimation of the influence of the furrow profile on the operational energy characteristics of tillage tools, as proposed in this study, is based on parameters and properties averaged over a specified time interval T_{ti}.

By dividing both left and right sides of expression (12) by the interval T_{ti} under study, the following result is obtained:

$$P_{ti} = \frac{W_{ti}}{T_{ti}} = F_{ti} \cdot \frac{L_{ti}}{T_{ti}} = F_{ti} \cdot V_{ti}, \quad (13)$$

where P_{ti} is the required power; V_{ti} is the operating speed of the implement. The components F_{ti} and V_{ti} of formula (13) are functions of many different factors. For example:

$$F_{ti} = f_{ti}(SP, TI, PP, \ldots), \quad (14)$$

where soil properties:

$$SP = (MC, SST, SM, PC, HM, SA, \ldots); \quad (15)$$

its mechanical composition:

$$MC = (SS, CS, LM, BS, \ldots), \quad (16)$$

where *SS* – sandy soils, *CS* – clay soils, *LM* – loams, *BS* – black soil; soil structure:

$$SST = (SLST, LMST, LSST, \ldots), \quad (17)$$

where *SLST* – solid, *LMST* – lumpy, *LSST* – loose; *SM* – soil moisture, *PC* – previous crops, *HM* – humus, *SA* – soil aeration; tillage implements:

$$TI = (MLB, DSC, CHL, \ldots), \quad (18)$$

where *MLB* – moldboard, *DSC* – disc, *CHL* – chisel; processing parameters:

$$PP = (a, V_{ti}, A, \ldots), \quad (19)$$

where a is tillage depth, V_{ti} is the speed of the tillage tool, and A is the area of the furrow profile. The functional dependence for the speed of the implement as a component of the tractor unit can be represented as:

$$V_{ti} = \frac{P_{tr} \cdot k_{ptr}}{n_{ti} \cdot F_{ti}}, \quad (20)$$

where P_{tr} is the nominal power of the tractor; power transmission ratio of the tractor to agricultural implements:

$$0 < k_{pt_{tr}} < 1, \quad (21)$$

n_{ti} is Thus, operational energy performance, see expressions (12)-(21), depends on many parameters and characteristics (see for example Ya. Pavlova & D. Litvinov (2024)). Therefore, it is quite problematic to accurately reflect them with one universal analytical mathematical apparatus. It is proposed to solve this complex problem by dividing the latter into several simpler ones.

An increase in the operational speed (20) of agricultural implements increases the productivity of agricultural processes. The analysis of this formula shows that this is facilitated by an increase in tractor power and the coefficient of its transmission to tillage tools. However, the former requires adequate energy, financial and other costs. The second approach is more economical but has certain limitations (21). An increase in the number of aggregated implements n_{ti} slows down their speed but increases the area worked. Therefore, this value requires the definition of an optimal value. The most appropriate is to reduce the force F_{ti} of soil and tool resistance. This article is devoted to these issues.

The main idea is to use the experience gained in cultivating certain agricultural lands. This applies to both small and large farms. Each of them cultivates fields with certain soil properties (15), their mechanical composition (16), and structure (17). There is also statistical information available, at the required time periods, on soil moisture, humus, aeration, previous crops, etc. There is data on the tillage tools used, the appropriate tillage parameters (19), the tractor fleet used, and its technical characteristics. There are also corresponding farming results. The question is whether the latter can be improved, for example, in terms of increased yields, labour productivity, reduced energy and financial costs, etc.

The above studies, approaches, mathematical apparatus and considerations served as the basis for determining the methodology for conducting scientific research aimed at improving the energy efficiency of tillage tools on the example of double-disc coulters. The proposed methods consist in establishing analytical dependencies between certain parameters of the design of agricultural implements (for the studied openers, these are the diameter of the discs D, the minimum distance d_s between them, the installation angles α, β) and the resulting operational characteristics associated with energy consumption (in this case, these are the depth of cultivation a, the furrow profile and its area A).

Their increase or decrease enables the estimation of the relative increase or decrease in fuel consumption for the implementation of the technological process. The following general approach of marginal estimates, illustrated on the example of double disc coulters, can be extended to other tillage tools and other, not only agricultural, equipment. However, this is the subject of further research. The proposed methodology for some aspects of improving the energy efficiency of agricultural tillage tools, presented on the example of double-disc openers, is as follows. The accumulated cultivation experience is selected as the starting point for the optimisation. The direction of the desired improvements is determined based on analytically determined limit estimates of the influence of the furrow profile on the operational energy characteristics of tillage tools.

RESULTS AND DISCUSSION

As can be seen from formulas (13)-(21), for certain existing soil properties (mechanical composition, structure, moisture, previous crops, etc.), the tools used (in this case, double-disc coulters), cultivation parameters (in the form of the required depth, operating speed, furrow profile, furrow area) and the available technical park, certain agricultural results are achieved due to specific energy inputs (tractor power).

Increasing productivity, i.e. V_{ti} and n_{ti}, by increasing the power P_{tr} of tractors, see dependence (20), is obvious, but it does not improve energy efficiency. Increasing the coefficient k_{pttr} is important, but does not correspond to the chosen topic of this research. An effective way is to reduce the resistance force F_{ti} of the soil and the implement. Then, with other operating parameters remaining constant, labour productivity increases due to an increase in V_{ti} or energy costs are reduced by reducing the required power P_{tr}.

Based on expressions (1)-(11) and Figure 3, an analytical determination of the area A of the furrow profile formed by a double disc coulter is carried out, as this parameter is particularly significant for the resistance force F < sub > ti</sub> acting between the soil and the tool. To do this, move the *Oxyz* coordinate system vertically downwards so that the *Oxy* plane coincides with the level of the furrow bottom. Then the applications in relations (1) and (2) will be equal to:

$$z(u) = -\frac{D}{2}cos\beta\ sin(u) + \frac{D}{2}cos\beta = \frac{D}{2}cos\beta(1 - sin(u)). \qquad (22)$$

Further, based on the integral for calculating the area of the curved trapezoid bounded by the parametric curve and the symmetry of the furrow profile relative to the vertical axis passing through the point S of the discs' convergence, the following is obtained:

$$A = 2 \cdot \left(\left(y_S - y_u + \frac{d_S}{2}\right) \cdot a - \int_{u_u}^{u_s} z(u) y'(u)\, du\right), \qquad (23)$$

where $y(u)$ is the ordinate of the first disc, $z(u)$ is determined according to formula (22). The components of dependence (23) are as follows:

$$y_S = y(u_S) = \frac{D}{2}(cos\alpha\ sin\beta\ sin(u_S) - sin\alpha\ cos(u_S)),$$
$$y_u = y(u_u) = \frac{D}{2}(cos\alpha\ sin\beta\ sin(u_u) - sin\alpha\ cos(u_u)), \qquad (24)$$

where $u_s = arctg(-ctg\alpha \cdot sin\beta) + 180°$, $u_u = arcsin(1 - 2a/(D \cdot cos\beta))$;

$$y'(u) = \frac{D}{2}(cos\,\alpha\ sin\beta\ cos(u) + sin\,\alpha\ sin(u)),$$
$$\int_{u_u}^{u_s} z(u)y'(u)du = \int_{u_u}^{u_s} \frac{D}{2} cos\,\beta\,(1 - sin(u)) \cdot \frac{D}{2}(cos\,\alpha\ sin\beta\ cos(u) + sin\,\alpha\ sin(u))du =$$
$$= \frac{D^2}{4} cos\,\beta\,(cos\,\alpha\ sin\beta \int_{u_u}^{u_s} cos(u)du + sin\,\alpha \int_{u_u}^{u_s} sin(u)du -$$
$$- cos\,\alpha\, sin\,\beta \int_{u_u}^{u_s} sin(u)\, cos(u)du - sin\,\alpha \int_{u_u}^{u_s} sin^2(u)du =$$
$$= \frac{D^2}{4} cos\,\beta\,(cos\,\alpha\ sin\beta\ sin(u)\left.\right|_{u_S}^{u_u} - sin\,\alpha\, cos(u)\left.\right|_{u_S}^{u_u} -$$
$$\frac{- cos\,\alpha\, sin\,\beta\, sin^2(u)\left.\right|_{u_S}^{u_u}}{2} - sin\,\alpha\left(\frac{u}{2} - \frac{sin(2u)}{4}\left.\right|_{u_S}^{u_u}\right), \qquad (25)$$

where angles α, β , parameters u_s, u_u are measured in radians. Expressions (23) and (25) make possible to determine the area A of the furrow profile of a two-disc coulter with diameters D of the discs and the minimum distance d_s between them, their installation angles α and β. To illustrate the proposed approach, the furrow profile defined by the design parameters of the opener in O. Vorobiov (2024) is used as the initial condition:

$$D = 350 \text{ mm}, \alpha = 5°, \beta = 20°. \tag{26}$$

In addition to the values specified in expression (26), it is necessary to consider a zero minimum distance between the discs and working range of tillage depths.

$$a \in [20 \text{ mm}, 80 \text{ mm}]. \tag{27}$$

The proper furrow profile is illustrated in Figure 4. The second image shows the ridge that forms at the bottom of the furrow. Its width at heights greater than one millimetre is mostly less than a millimetre. In other words, in practice, the shape of this ridge would be described by an approximately equilateral trapezoid with a height of 1 to 1.5 mm and a lower and upper base of 3 mm and 1 mm, respectively. These geometric parameters are acceptable. These aspects will not be considered in further detail.

Table 1 contains the results of calculations based on expressions (23)-(27) of the area A of the furrow profile for $D = 350$ mm, $\alpha = 5°$, $\beta = 20°$ depending on the depth a of tillage.

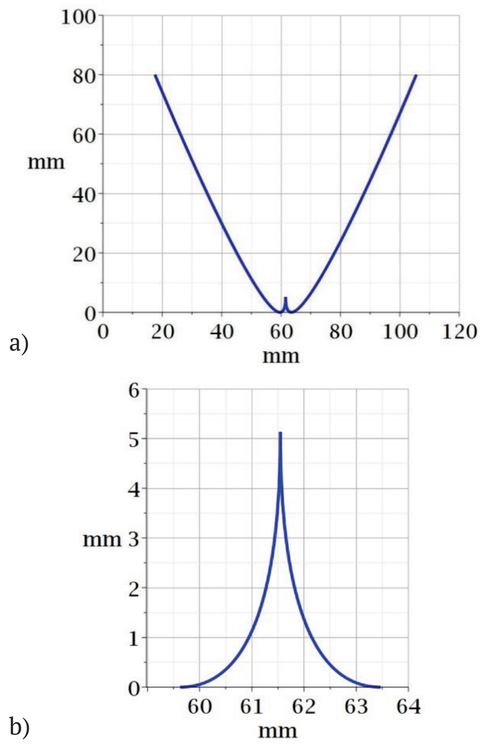

Figure 4. Furrow profile for $D = 350$ mm, $\alpha = 5°$, $\beta = 20°$
Note: a) general view; b) crest
Source: developed by the authors

Table 1. Variation of furrow profile area A for $D = 350$ mm, $\alpha = 5°$, $\beta = 20°$

Tillage depth a, mm	20	30	40	50	60	70	80
Furrow profile area A, mm²	415	796	1,277	1,851	2,516	3,268	4,106

Source: compiled by the authors

The corresponding quadratic approximation formula is:

$$A(a) = k_2\, a^2 + k_1\, a + k_0, \tag{28}$$

where $k_2 = 91/200$, $k_1 = 1{,}129/70$, $k_0 = -1{,}305/14$. The corresponding graph is shown in Figure 5.

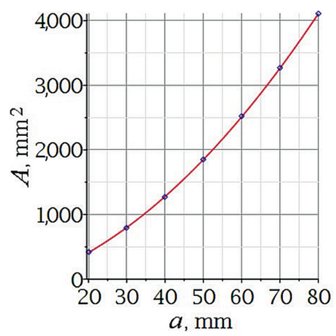

Figure 5. Visualisation of expression (28)
Source: developed by the authors

It is obvious that the first depth saves energy and financial costs, but can lead to a deterioration in agronomic performance. In the second case, the opposite is true. The assessment of agrotechnical factors, unlike energy factors, is not the subject of this publication. Consideration is given to a case where the current tillage depth is $a_0 = 50$ mm, and the suitability of two alternative depths, $a_1 = 45$ mm and $a_2 = 55$ mm, is evaluated. To determine the most appropriate option, the following procedure is applied. It is obvious that the first depth saves energy and financial costs, but can lead to a deterioration in agronomic performance. In the second case, the opposite is true. The assessment of agrotechnical factors, unlike energy factors, is not the subject of this publication. In accordance with the proposed approach, expression (28) provides a means to determine the limits of variation in energy costs, whether increasing or decreasing.

$$A(a_0) = 1{,}851 \text{ mm}^2, A(a_1) = 1{,}554 \text{ mm}^2, A(a_2) = 2{,}170 \text{ mm}^2. \tag{29}$$

Using the data provided in expression (29), the following boundary estimates of R (rating) are obtained, reflecting the impact of changes in the furrow profile on the operational energy characteristics of the double disc coulter under consideration.

$$R_1 = \frac{A(a_0)}{A(a_1)} = \frac{1{,}851 \text{ mm}^2}{1{,}554 \text{ mm}^2} \approx 1.19,$$
$$R_2 = \frac{A(a_0)}{A(a_2)} = \frac{1{,}851 \text{ mm}^2}{2{,}170 \text{ mm}^2} \approx 0.85. \tag{30}$$

The values of (30) show that the savings *Sav* (saving) of energy resources and their overspending *Ovs* (overspending) are approximately:

$$Sav = (1 - 1/R_1) \cdot 100\% \approx 16\%,$$
$$Ovs = (1/R_2 - 1) \cdot 100\% \approx 17\%. \qquad (31)$$

Thus, if the savings (31) of energy resources in financial terms cover the possible losses from the deterioration of agronomic performance, then the analysed tillage depth $a_1 = 45$ mm is appropriate, otherwise – not. By analogy, if the additional costs (31) are less than the gains from improved agronomic performance, then the new tillage depth $a_2 = 55$ mm is appropriate, otherwise it is not. In the following, the financial efficiency of the proposed changes in the furrow profile is assessed in a similar way and is therefore no longer emphasised. The mathematical apparatus presented above makes it possible to assess the influence of disc diameters *D* on the energy efficiency of the coulter. It is assumed that the values presented in Table 2 need to be calculated.

Table 2. Variation of furrow profile area *A* for $a = 50$ mm, $\alpha = 5°$, $\beta = 20°$

Diameter *D* of discs, mm	300	320	350	380	400
Furrow profile area *A*, mm²	1762	1,798	1,851	1,902	1,935

Source: compiled by the authors

The proper expression of the quadratic approximation is:

$$A(D) = k_2 D^2 + k_1 D + k_0, \qquad (32)$$

where $k_2 = 0.000981$, $k_1 = 2.41766$, $k_0 = 1{,}124.9387$. The corresponding graph is shown in Figure 6.

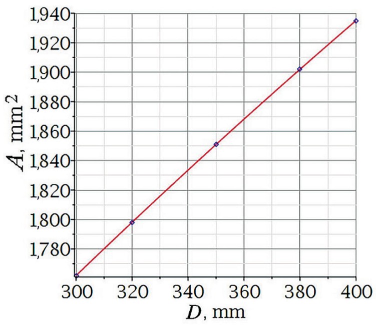

Figure 6. Visualisation of dependency (32)
Source: developed by the authors

Figure 7 shows the variation of the furrow ridge for two disc diameters *D*.

Suppose that from the point of view of agrotechnical requirements, the ridge of Figure 7b is too large, and the furrow variant of Figure 7a is acceptable. In the latter case, the energy savings will be:

$$Sav = \left(1 - \frac{A(D=320\text{ mm})}{A(D=350\text{ mm})}\right) \cdot 100\% =$$
$$= \left(1 - \frac{1{,}798\text{ mm}^2}{1{,}851\text{ mm}^2}\right) \cdot 100\% \approx 2.9\%. \qquad (33)$$

The formula (32) allows processing arbitrary disc diameters from the range:

$$D \in [300\text{ mm}, 400\text{ mm}]. \qquad (34)$$

By comparing the respective values of expressions (31) and (33), it is concluded that the depth *a* of tillage has a significantly greater impact on energy saving than the diameters *D* of the discs used. The integrated effect of the considered operational and design parameters is possible. For instance, given $a = 45$ mm, $\alpha = 50$, $\beta = 200$, and $D = 320$ mm, the following result is obtained:

$$Sav = \left(1 - \frac{A(a=45\text{ mm}, \alpha=5^0, \beta=20^0, D=320\text{ mm})}{A(a=50\text{ mm}, \alpha=5^0, \beta=20^0, D=350\text{ mm})}\right) \cdot$$
$$\cdot\, 100\% = \left(1 - \frac{1{,}507\text{ mm}^2}{1{,}851\text{ mm}^2}\right) \cdot 100\% \approx 18.6\%. \qquad (35)$$

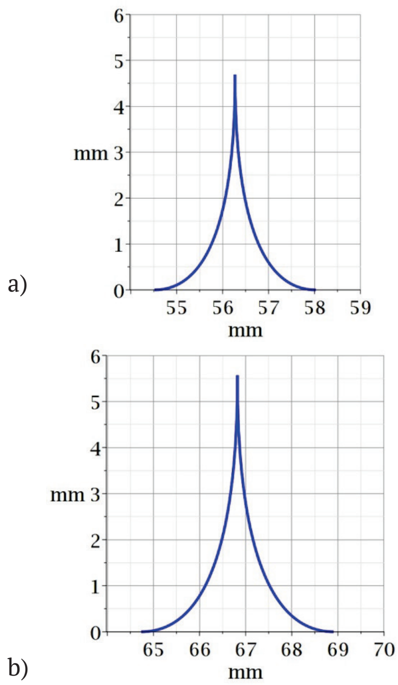

Figure 7. Furrow ridges for $a = 50$ mm, $\alpha = 5°$, $\beta = 20°$
Note: a) $D = 320$ mm; b) $D = 380$ mm
Source: developed by the authors

The value (35) describes the relative estimate of the energy reduction. A proper furrow profile is shown in Figure 8.

The dependencies (23) and (25), for example, for $\alpha = 5°$, $\beta = 20°$ and the intervals (27) and (34), can be visualised using Table 3. The previously calculated values by expressions (28) and (32) are highlighted in blue.

Figure 9 illustrates the calculated results.

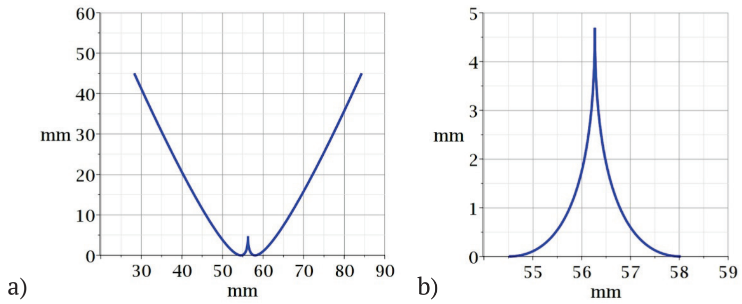

Figure 8. Furrow profile for $D = 320$ mm, $\alpha = 5°$, $\beta = 20°$, $a = 45$ mm
Note: a) general view; b) crest
Source: developed by the authors

Table 3. Furrow profile area A, mm²

Tillage depth a, mm	Diameters of discs				
	$D = 300$ mm	$D = 320$ mm	$D = 350$ mm	$D = 380$ mm	$D = 400$ mm
20	390	400	415	430	440
30	753	771	796	822	838
40	1,212	1,238	1,277	1,314	1,338
50	1,762	1,798	1,851	1,902	1,935
60	2,401	2,448	2,516	2,591	2,624
70	3,126	3,184	3,268	3,350	3,402
80	3,933	4,004	4,106	4,205	4,269

Source: compiled by the authors

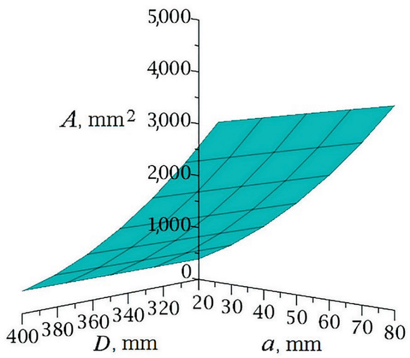

Figure 9. Dependence of the area A of the furrow profile for $\alpha = 5°$, $\beta = 20°$
Source: developed by the authors

The proper formulas are as follows:

$$A(D, a) = k_2(D) \cdot a^2 + k_1(D) \cdot a + k_0(D), \tag{36}$$

where $k_2(D) = -13/2046240000 \cdot D^2 + 16361/70992000 \cdot D + 7254577/19325600$, $k_1(D) = -6803/204624000 \cdot D^2 + 9618$ $1/1987776 \cdot D + 6261669/1932560$, $k_0(D) = 281/426300 \cdot D^2 - 231883/414120 \cdot D + 2184507/96628$. Figure 10 shows, for example, the effect of changing the angles α and β of the discs on the resulting furrow profile.

In the first and second cases, the furrow profile area is respectively:

$$A_1 = 1{,}330 \text{ mm}^2, A_2 = 1{,}160 \text{ mm}^2. \tag{37}$$

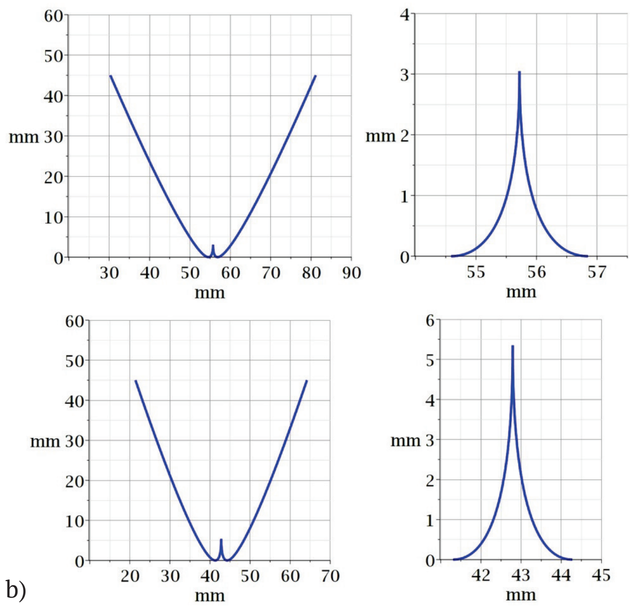

Figure 10. Furrow profiles and ridges for $D = 320$ mm, $a = 45$ mm
Note: a) $\alpha = 4°$, $\beta = 20°$; b) $\alpha = 4°$, $\beta = 15°$
Source: developed by the authors

As evidenced by the values of (37), reducing the angles α and β significantly affects the decrease in the furrow profile area. However, it is necessary to take into account, in addition to agrotechnical indicators, the possibility of constructive implementation of the analysed geometric parameters. Thus, compared to the initial state, the reduction in energy resources can be as follows:

$$Sav_1 = \left(1 - \frac{A(a{=}45\,\text{mm},\, \alpha{=}4^0,\, \beta{=}20^0,\, D{=}320\text{ mm})}{A(a{=}50\,\text{mm},\, \alpha{=}5^0,\, \beta{=}20^0,\, D{=}350\text{ mm})}\right)\cdot 100\% = \left(1 - \frac{1{,}330\text{ mm}^2}{1{,}851\text{ mm}^2}\right)\cdot 100\% \approx 28\%,$$
$$Sav_2 = \left(1 - \frac{A(a{=}45\text{ mm},\, \alpha{=}4^0,\, \beta{=}15^0,\, D{=}320\text{ mm})}{A(a{=}50\text{ mm},\, \alpha{=}5^0,\, \beta{=}20^0,\, D{=}350\text{ mm})}\right)\cdot 100\% = \left(1 - \frac{1{,}160\text{ mm}^2}{1{,}851\text{ mm}^2}\right)\cdot 100\% \approx 37\%. \quad (38)$$

The values of (38) show that energy consumption varies widely for different crops grown. However, the issue of ensuring flexible adaptation of coulters to specific operating conditions is not clear. It is understood that these actions should have positive generalised effects, and not lead to an increase in the cost of adjusting the openers It should also be noted that the methods described above allow for the calculation, for the angles α and β, of the dependencies of the form (36) reflecting their influence on the size of the area A of the furrow profile and, accordingly, on energy efficiency.

To compare the results obtained with similar studies by other authors, additional study of the available literature on the selected topic was conducted, see Figure 11. Common and distinctive features of the approaches and methods employed, the nature of the aspects investigated, as well as the theoretical and practical significance of the results, have been identified. Thus, the publication of M. Sadek *et al.* (2021) is devoted to the prediction of traction force during high-speed (12 km/h and more) tillage with disc tools. These parameters are important dynamic components of these energy processes. As mathematical and computer tools, the discrete element method was used, which is designed to analyse the movement of a large number of specific particles that interact with each other as a result of external influences on them. It is shown that, compared to real values, the model error ranges from 8% to 14%. To eliminate this defect, the model was adapted and an accuracy of 1% was achieved. After that, the influence of the angles of deviation of the disc from the vertical and horizontal planes, its diameter, depth, and tillage speed on the traction force was evaluated. The advantage of the considered methodology is the sufficient accuracy of the description of these parameters in limited intervals of their change for a certain state of the analysed soil. It should be noted that the results obtained will be satisfactory in practice only if the existing conditions coincide with the studied ones, which is generally unlikely. The approach proposed by the authors of this article, in order to optimise the operational energy characteristics of agricultural implements, is based on the existing circumstances of the latter's functioning. This ensures the necessary adequacy of the applied theoretical model to the specific conditions of practice (Pavlova & Litvinov, 2024).

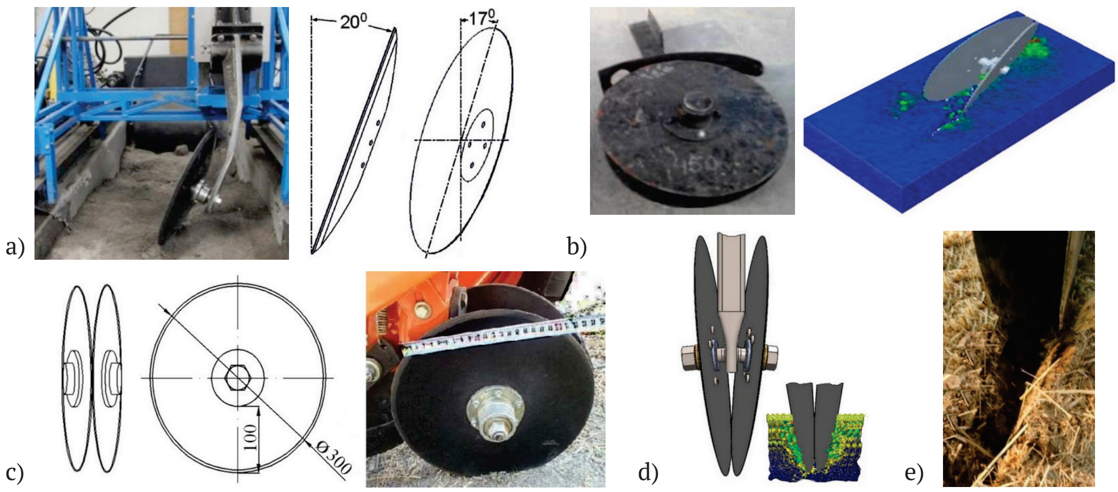

Figure 11. Graphic illustrations of the results of works on the selected topic by other authors
Note: a) M. Sadek *et al.* (2021); b) F. Ahmad *et al.* (2020); c) D. Karayel *et al.* (2024); d) A. Sugirbay *et al.* (2023); e) B. Rosu *et al.* (2024)
Source: developed by the authors

F. Ahmad *et al.* (2020) used the discrete element method to study several different designs of disc coulters. The emphasis is placed on various mechanical properties of the soil, such as its density, shear modulus, Poisson's ratio, friction coefficients, etc. The error between the calculated and actual values of the required traction force, depending on the speed of the double-disc coulter, ranges from 1% to 21%. This information to some extent complements the information presented in the previous paragraph. But, unfortunately, in reality, there are a huge number of such possible combinations of parameters and characteristics. Therefore, the probability of the existence of the options considered in advance in specific business circumstances is quite small. The described methodology is of practical value for direct application in the relevant agricultural fields, as indicated in the title of this publication. D. Karayel *et al.* (2024) studied the issue of ensuring the required productivity of a seeder without plowing by finding the right balance between the design of the coulter and the available soil coverage with plant residues. Corn sowing after wheat harvest was analysed. Plain and ripple coulters were tested as variant components of the seeder. Recommendations for their practical use were formulated. This work demonstrates the relevance of analysing, in addition to conventional discs, also their design modifications.

A double-disc coulter for a no-till seeder with simultaneous fertiliser and seed application is presented by A. Sugirbay *et al.* (2023). The proposed design is based on an improvement of the conventional coulter shown in Figure 11d. In the furrow, granular fertilisers are placed 2 cm deeper than the level of wheat seeds. Comparative experiments of the basic and developed double-disc coulters were conducted in a soil bunker. Horizontal and vertical forces were determined, and the accuracy of fertiliser and seed placement was analysed. The behaviour of soil particles interacting with the coulter was simulated using the discrete element method. The agreement between the modelling results and physical experiments is satisfactory. Based on the information presented in this publication, it can be concluded that the design of multifunctional implements based on double-disc openers and the proper use of computer software implementations of the discrete element method are promising.

B. Rosu *et al.* (2024) believed that agricultural specialists should pay more attention to the capabilities of disc tools, their adaptation to specific operating conditions by adjusting the angles of the discs, speed, etc. in order to increase the accuracy of sowing, especially for no-till cultivation, see Figure 11e. This emphasises the aspect of changes in parameters such as the size and weight of the coulter discs due to soil contact. For the studied range of openers, it was found that, on average, the discs thinned by about 0.25 mm per 100 hectares sown, and their diameter decreased by 0.17-0.35% for the sown area from 80 to 380 hectares. It is noted that new research is needed to generalise the results obtained for other types of seeders, as well as to determine the dependence of the above values on various soil properties. Thus, the analysed publication from the standpoint of a systematic approach properly complements the above methodology for the creation and use of double-disc coulters. N. Kumar *et al.* (2021 examined the shredding of plant residues using various disc coulters by different disc coulters (plain, notch, curved teeth, cutter bar and star wheel).

Thus, the considered literary sources were analysed similar design and operational parameters of openers (disc diameters, their installation angles, depth of cultivation), but for certain working speeds and tractors, used soils, their condition, etc. As can be seen from formulas (12)-(21), the number of possible combinatorial variants of the above factors is almost infinite. In other words, the research carried out makes practical sense only if the existing specific conditions of agricultural production coincide with the analysed ones quite accurately. In cases where these conditions differ, there is a need for a more flexible methodological approach. To some extent, the approach proposed in this article is aimed at resolving this complex issue. Its basic idea is, so to speak, to start from the existing economic circumstances and identify promising areas for their improvement. In particular, this applies to the increase in energy efficiency of tillage tools considered on the example of double-disc coulters without deterioration of the agrotechnical indicators obtained.

The conducted study confirmed the feasibility and practical value of a methodological approach based on marginal estimates of the impact of the furrow profile on the energy characteristics of tillage tools. Using the example of double-disc openers, the analytical relationships between design parameters and energy performance indicators were derived and validated, allowing for justified optimisation decisions. The obtained results demonstrate that even minor adjustments in disc diameter, installation angles, or tillage depth may lead to significant variations in energy consumption, offering a potential reserve for resource savings.

CONCLUSIONS

Improving the energy efficiency of tillage implements, in particular seed sowing machines, while ensuring a high level of agrotechnical and environmental requirements is an urgent scientific and applied problem. In this direction, the double-disc coulters of modern seeders are quite promising, and at the same time, the most used in production. The article analytically evaluates the influence of the parameters of the seeding furrow profile on the energy performance of double-disc openers. By geometric modelling of the working surfaces of the coulter, the parametric equations of the contours of the seed furrow in the Cartesian coordinate system were derived and the analytical calculation of its cross-sectional area was performed depending on the depth of cultivation, disc diameter, and disc alignment angles. Using a quadratic approximation formula, it was found that the furrow area for a disc with a diameter of, for example, 350 mm increased from 415 to 4106 mm^2 when the processing depth increased from 20 to 80 mm. With a fixed depth of 50 mm and alignment angles of $\alpha = 50°$, $\beta = 20°$, varying the disc diameter from 300 to 400 mm changes the furrow area from 1762 to 1935 mm^2. Reducing the working depth by 5 mm leads to a decrease in the furrow area from 1851 to 1277 mm^2, while increasing the working depth by the same amount, the furrow area increases to 2516 mm^2. At the same time, when the angles α and β are reduced to 40° and 15°, respectively, the cross-sectional area of the seed furrow decreases to 1522 mm^2.

Thus, the method of boundary estimates of the influence of the seed furrow profile on the energy characteristics of the seeder proposed in this publication is the main scientific and applied achievement of this work, and the methodological approach on the example of disc coulters with the help of appropriate analysis allows optimising the configuration of the working surfaces of disc tillage tools in real-world conditions. The main difficulty in this case is the need to properly take into account the rather different conditions associated with the geometry of specific working surfaces of the disc type, soil condition, size and weight of the sown seeds, the energy used, the peculiarities of agricultural technology, etc. The presented information needs to be generalised and extended to other agricultural tillage tools, which determines the directions of further research on this topic.

ACKNOWLEDGEMENTS

The study was carried out in accordance with the research topic "Automated variant geometric modelling of technical objects", state registration number 0114U002701, which is being carried out at the Department of Descriptive Geometry, Engineering and Computer Graphics of the National Technical University of Ukraine "Igor Sikorsky Kyiv Polytechnic Institute".

FUNDING

None.

CONFLICT OF INTEREST

None.

REFERENCES

[1] Ahmad, F., Qiu, B., Ding, O., Ding, W., Khan, Z., Shoaib, M., Chandio, F., Rehim, A., & Khaliq, A. (2020). Discrete element method simulation of disc type furrow openers in paddy soil. *International Journal of Agricultural and Biological Engineering*, 13(4), 103-110. doi: 10.25165/j.ijabe.20201304.4800.

[2] Aikins, K., Barr, J., Ucgul, M., Jensen, T., Antille, D., & Desbiolles, J. (2020). No tillage furrow opener performance: A review of tool geometry, settings and interactions with soil and crop residue. *Soil Research*, 58(7), 603-621. doi: 10.1071/SR19153.

[3] Chandio, F., Li, Y., Xu, L., Ma, Z., Ahmad, F., Cuong, D., & Lakhiar, I. (2020). Predicting 3D forces of disc tool and soil disturbance area using fuzzy logic model under sensor-based soil-bin. *International Journal of Agricultural and Biological Engineering*, 13(4), 77-84. doi: 10.25165/j.ijabe.20201304.5115.

[4] Damanauskas, V., & Janulevičius, A. (2022). Effect of tillage implement (spring tine cultivator, disc harrow), soil texture, forward speed, and tillage depth on fuel consumption and tillage quality. *Journal of Agricultural Engineering*, 53(3), article number 1371. doi: 10.4081/jae.2022.

[5] Hamid, A., & Alsabbagh, A. (2023). Effect of Moldboard types, Two depths of tillage and two speeds of tractor in some physical properties and pulverisation of soil. *Kufa Journal for Agricultural Sciences*, 15(1), 105-116. doi: 10.36077/kjas/2023/v15i1.10334.

[6] Karayel, D., Jotautiene, E., & Šarauskis, E. (2024). the effect of furrow opener and disc coulter configurations on seeding performance under different residue cover densities. *AgriEngineering*, 6(2), 1277-1288. doi: 10.3390/agriengineering6020073.

[7] Kumar, N., Sawant, C., Sharma, R., Chhokar, R., Tiwari, P., Singh, D., Roul, A., Tripathi, S., Gill, S., & Singh, G. (2021). Combined effect of disc coulters and operational speeds on soil disturbance and crop residue cutting under no-tillage system in soil bin. *Journal of Scientific & Industrial Research*, 80(9), 739-749. doi: 10.56042/jsir.v80i09.40333.

[8] Malasli, M., & Çelik, A. (2023). Effects of the disc and tilt angle of a single disc-type furrow opener of a no-till seeder on residue distribution and the furrow profile. *Turkish Journal of Agriculture and Forestry*, 47(6), article number 19. doi: 10.55730/1300-011X.3146.

[9] Nikolaenko, S., Bondar, M., Bulgakova, O., Vasileva, V., & Vartukapteinis, K. (2021). Studying requirements for substantial list of professional knowledge for students of agricultural engineering specialities. In *20th international scientific conference: Engineering for rural development* (pp. 1519-1525). Jelgava: Latvia University of Life Sciences and Technologies. doi: 10.22616/ERDev.2021.20.

[10] Parihar, D., Dogra, B., & Narang, M. (2023). Performance evaluation of different furrow openers for sustainable tillage: A review. *Indian Journal of Ecology*, 50(4), 1133-1142. doi: 10.55362/IJE/2023/4025.

[11] Pavlova, Ya., & Litvinov, D. (2024). The influence of previous crops and tillage on available moisture reserves of chernozem typical for growing spring barley. *Plant and Soil Science*, 15(2), 32-41. doi: 10.31548/plant2.2024.32.

[12] Ranta, O., Gheţe, A., Stănilă, S., Muntean, M., Marian, O., & Molnar-Irimie, A. (2021). Influence of design of the disc furrow opener of no-till sowing machines on the seedbed quality. *Romanian Agricultural Research*, 38, 239-249. doi: 10.59665/rar3826.

[13] Rosu, B., Voicu, G., Constantin, G., Tudor, P., & Stefan, E. (2024). Aspects regarding the physical parameters and wear in the work process of the disc openers for seeding machines. *Agriculture*, 14(7), article number 1066. doi: 10.3390/agriculture14071066.

[14] Sadek, M., Chen, Y., & Zeng, Z. (2021). Draft force prediction for a high-speed disc implement using discrete element modelling. *Biosystems Engineering*, 202, 133-141. doi: 10.1016/j.biosystemseng.2020.12.009.

[15] Sugirbay, A., *et al.* (2023). Double disc colter for a no-till seeder simultaneously applying granular fertilisers and wheat seeds. *Agriculture*, 13(5), article number 1102. doi: 10.3390/agriculture13051102.

[16] Vorobiov, O. (2024). Computer modelling of basic design and operational geometrical parameters of double disc coulters. *Bulletin of Sumy National Agrarian University. The Series: Mechanisation and Automation of Production Processes,* 4(58), 12-20. doi: 10.32782/msnau.2024.4.

[17] Xu, G., Xie, Y., Peng, S., Liang, L., & Ding, Q. (2023). Performance evaluation of vertical discs and disc coulters for conservation tillage in an intensive rice-wheat rotation system. *Agronomy*, 13(5), article number 1336. doi: 10.3390/agronomy13051336.

[18] Yablonskyi, P., Rogovskii, I., Sobczuk, H., Virchenko, G., Volokha, M., & Vorobiov, O. (2024). Computational approach to geometric modelling of plough bodies. *Journal of Engineering Sciences*, 11(1), E9-E18. doi: 10.21272/jes.2024.11(1).e2.

[19] Yablonskyi, P., Rogovskii, I., Virchenko, G., Borek, K., Volokha, M., & Golova, O. (2025). Geometric modelling of disc furrow profile. *Journal of Engineering Sciences*, 12(1), E1-E8. doi: 10.21272/jes.2025.12(1).e1.

[20] Zeng, Z., Thoms, D., Chen, Y., & Ma, X. (2021). Comparison of soil and corn residue cutting performance of different discs used for vertical tillage. *Scientific Reports*, 11, article number 2537. doi: 10.1038/s41598-021-82270-9.

Станіслав Ніколаєнко
Доктор педагогічних наук, професор, академік Національної академії аграрних наук
Національний університет біоресурсів і природокористування України
03041, вул. Героїв Оборони, 15, м. Київ, Україна
https://orcid.org/0000-0001-5271-1777

Геннадій Вірченко
Доктор технічних наук, професор
Національний технічний університет України
«Київський політехнічний інститут імені Ігоря Сікорського»
03056, просп. Берестейський, 37, м. Київ, Україна
https://orcid.org/0000-0001-9586-4538

Микола Волоха
Доктор технічних наук, старший науковий співробітник
Національний технічний університет України
«Київський політехнічний інститут імені Ігоря Сікорського»
03056, просп. Берестейський, 37, м. Київ, Україна
https://orcid.org/0000-0002-0112-7324

Олексій Воробйов
Аспірант
Національний технічний університет України
«Київський політехнічний інститут імені Ігоря Сікорського»
03056, просп. Берестейський, 37, м. Київ, Україна
https://orcid.org/0000-0001-5314-1075

Юлія Лазарчук-Воробйова
Аспірант
Національний технічний університет України
«Київський політехнічний інститут імені Ігоря Сікорського»
03056, просп. Берестейський, 37, м. Київ, Україна
https://orcid.org/0000-0002-7866-3299

Підвищення енергоефективності дводискових сошників на основі методу граничних оцінок впливу профілю посівної борозни

Анотація. Актуальність дослідження полягає у світовій необхідності підвищення енергоефективності сільськогосподарських знарядь при збереженні високих агротехнічних показників. Метою статті було аналітично оцінити вплив параметрів профілю борозни на експлуатаційні енергетичні характеристики ґрунтообробних знарядь на прикладі дводискових сошників. Методологія ґрунтувалася на геометричному моделюванні робочих компонентів сошника в декартовій системі координат, виведенні параметричних рівнянь контурів борозни та аналітичному обчисленні площі її поперечного перерізу залежно від глибини обробітку, діаметра дисків і кутів їх встановлення. У ході дослідження було встановлено, що площа борозни для дисків діаметром 350 мм зростала від 415 мм^2 до 4106 мм^2 зі збільшенням глибини обробітку від 20 мм до 80 мм. За фіксованої глибини 50 мм і кутів $\alpha = 50°$, $\beta = 20°$, площа борозни змінювалася від 1762 мм^2 до 1935 мм^2 залежно від зміни діаметра дисків від 300 мм до 400 мм. Було запропоновано квадратичну апроксимацію для опису цієї залежності. Результати показали, що зменшення глибини обробітку з 50 мм до 45 мм зменшувало площу борозни з 1851 мм^2 до 1277 мм^2, а її збільшення до 55 мм призводило до зростання площі до 2516 мм^2. Також було продемонстровано вплив кутів встановлення дисків: при зменшенні до $\alpha = 40°$ і $\beta = 15°$ площа борозни зменшувалася до 1522 мм^2. Запропонований підхід дозволив здійснити подальшу оптимізацію конфігурації сошників у реальних умовах. Методика, представлена в даній публікації, дозволяє визначити найбільш раціональну конфігурацію ґрунтообробних знарядь для існуючих обставин шляхом проведення відповідного аналізу

Ключові слова: енергоефективність сільськогосподарської техніки; дискові ґрунтообробні знаряддя; математичне моделювання; автоматизоване проєктування; комп'ютерні інформаційні технології

Machinery & Energetics
Vol. 16, No. 3. 2025

Journal homepage:
https://technicalscience.com.ua/en

UDC 631.365
Doi: 10.31548/machinery/3.2025.33

Borys Kotov

Doctor of Technical Sciences, Professor
Higher Educational Institution "Podillia State University"
32316, 12 Shevchenko Str., Kamianets-Podilskyi, Ukraine
https://orcid.org/0000-0001-6369-3025

Valerii Voitiuk

Doctor of Technical Sciences, Professor
National University of Life and Environmental Sciences of Ukraine
03041, 15 Heroiv Oborony Str., Kyiv, Ukraine
https://orcid.org/0000-0001-6344-0706

Roman Kalinichenko

PhD in Technical Sciences
National University of Life and Environmental Sciences of Ukraine
03041, 15 Heroiv Oborony Str., Kyiv, Ukraine
https://orcid.org/0000-0001-9325-1551

Serhii Stepanenko*

Doctor of Technical Sciences
Institute of Mechanics and Automation of Agro-Industrial Production
of the National Academy of Agrarian Sciences of Ukraine
08631, 11/1 Vokzalna Str., Hlevakha village, Kyiv region, Ukraine
https://orcid.org/0000-0002-8331-4632

Alvian Kuzmych

PhD in Technical Sciences, Senior Researcher
Institute of Mechanics and Automation of Agro-Industrial Production
of the National Academy of Agrarian Sciences of Ukraine
08631, 11/1 Vokzalna Str., Hlevakha village, Kyiv region, Ukraine
https://orcid.org/0000-0003-3102-0840

Mathematical modelling and investigation of the grain drying process in bunker units with radial supply of drying agent

Abstract. One of the key tasks of modern grain processing equipment is to increase the efficiency of drying in bunker installations with a ring-cylindrical grain bed. The aim of this study was to investigate the unsteady processes of heat and mass transfer in the annular layer of grain in a bin-type dryer with a radial supply of drying agent to assess the uniformity of temperature and moisture distribution and determine the effect of drying parameters on dehydration efficiency. To improve the energy efficiency and quality of drying, a two-level mathematical model was proposed to study the processes of internal heat and mass transfer and external heat and mass transfer. At the first level, the drying kinetics of a single grain in the form of a sphere in contact with a drying agent of constant temperature and humidity was modelled. The second level described the process of filtration drying of a dense ring-cylindrical layer of grain with a radial supply of the

Article's History: Received: 28.04.2025; Revised: 30.07.2025; Accepted: 23.09.2025.

Suggested Citation:
Kotov, B., Voitiuk, V., Kalinichenko, R., Stepanenko, S., & Kuzmych, A. (2025). Mathematical modelling and investigation of the grain drying process in bunker units with radial supply of drying agent. *Machinery & Energetics,* 16(3), 33-47. doi: 10.31548/machinery/3.2025.33.

*Corresponding author

drying agent. The thermophysical coefficients of the models were identified based on the results of field experiments. The obtained analytical and numerical solutions of the presented mathematical models made it possible to determine the rational design parameters and calculate energy-efficient operating modes of bunker-type grain dryers depending on the initial grain parameters. It was substantiated that the highest efficiency is achieved when using a periodic circulation mode, which ensures uniform heating and dehydration of the grain mass along the radial coordinate of the bed. The dependences of the influence of temperature, moisture content and air filtration rate on the exposure of grain drying in the bed were determined, which allows for flexible control of the drying process depending on the operating conditions. The study results confirmed that the use of a batch-circulating drying mode allows achieving high uniformity of the final grain moisture content, increasing the energy efficiency of the process and significantly reducing the unevenness of grain heating compared to traditional continuous modes of drying grain in a thick radial layer. The results can be used both for the modernisation of existing drying plants and for the design of new energy-saving grain dryers

Keywords: mathematical modelling; heat and mass transfer; bunker dryer; cyclic-periodic mode; ring-cylindrical layer

INTRODUCTION

Grain drying is a mandatory post-harvest process that serves as a crucial step in preparing crops for long-term storage and subsequent processing. Freshly harvested grain continues to undergo post-harvest ripening processes; therefore, drying not only reduces moisture content but also accelerates maturation, inhibits the development of pathogenic microflora, and homogenises the grain mass in terms of ripeness. Drying also significantly enhances the technological efficiency of subsequent grain processing in mills and groat factories.

The primary method for grain drying in agricultural enterprises is thermal drying with convective heat supply. Despite its numerous advantages, this method has significant drawbacks, including the high energy consumption of the process and the low efficiency of dryers due to substantial heat losses with the exhaust drying agent. Consequently, optimising the parameters of the convective drying process is critically important by H.S. El-Mesery *et al.* (2024). Most grain drying installations utilise straight-through shaft designs with gas distribution boxes, commonly known as shaft dryers, with capacities ranging from 24 to 50 tons per hour. These dryers are characterised by their high metal consumption and uneven grain heating as shown in the study by P. Demissie *et al.* (2019). This unevenness arises from the large contact area between the distribution boxes and the grain, leading to localised overheating. Such localised overheating significantly contributes to drying non-uniformity. Non-uniform drying poses significant microbiological risks and ultimately results in a reduction in the quality of the final dried product.

In high-temperature convective drying, the distribution of the air flow and the heat carrier supply modes significantly impact drying efficiency. According to research by W. Wang *et al.* (2020), implementing an effective heat carrier distribution within the grain layer can reduce localised overheating and increase drying efficiency. The high throughput of shaft dryers complicates the processing of small grain batches, as highlighted in a review by K.A. Jimoh *et al.* (2023), which emphasised the low flexibility of such installations for decentralised processing. For micro, small, and medium-sized enterprises involved in grain production, the application of column and batch dryers presents an effective solution. Studies by A. Sokolenko *et al.* (2020) demonstrated that these dryers offer lower metal consumption and cost while providing sufficient capacity. Similar conclusions were drawn by A.I. Onderová *et al.* (2019), who investigated the drying processes of biomaterials in vacuum dryers and noted their adaptability to various grain types and batch volumes. The use of column dryers in conjunction with heat generators powered by solid alternative fuels significantly reduces drying costs. However, this approach necessitates a separate bunker for grain cooling. This requirement was analysed by Z.Y. Xu *et al.* (2019), who explored the prospects of low-temperature heat recovery and its potential application in grain drying infrastructure.

Improving the technological and energy efficiency of grain dryers is intrinsically linked to the intensification of heat and mass transfer processes and the utilisation of new heat supply schemes for grain material. The fundamentals, methods, and means of drying intensification were identified by I. Palamarchuk *et al.* (2023). Among the effective methods are: vibro-loosening of the grain layer, non-contact infrared (IR) and microwave energy supply, and ozonation of the drying agent. These methods substantially accelerate the dehydration process, thereby increasing dryer productivity. While microwave drying offers some advantages, it also presents limitations, including uneven heating, limited penetration into thick materials, and the risk of surface damage due to excessively rapid moisture evaporation. Therefore, researchers N. Ahmad *et al.* (2021) were studying the combined application of microwave drying with other technologies to integrate the benefits of each method, enhance drying efficiency, and improve grain quality. Combining microwave and infrared drying enhances process efficiency and optimises energy utilisation. Microwave heating penetrates deep into the material, heating it through the oscillation of water molecules, while infrared radiation primarily heats the surface, rapidly increasing its temperature. This combined approach was investigated by P. Mukwevho & M.N. Emmambux (2022). Infrared (IR) drying technology is a promising method for moisture removal due to its high energy conversion efficiency and direct transfer of thermal energy to the material's surface. V.R.G. Nascimento *et al.* (2019) noted that unlike traditional hot-air drying, IR drying minimises heat losses to the environment, ensures a rapid increase in product temperature, and allows operation at lower temperatures. This contributes to a reduced process duration and decreased energy consumption.

However, the limited penetration depth of IR radiation reduces its effectiveness when processing thick-layer or low-moisture materials. Therefore, N.D.S. Timm *et al.* (2020) combined this technology with other drying methods to enhance the overall process efficiency. P. Yu *et al*. (2025) determined that one common challenge with the aforementioned methods for increasing dryer productivity is that they often lead to higher capital or operational costs due to increased power requirements, equipment complexity, and energy consumption. An alternative approach is to optimise dryer operating modes and technological schemes to ensure stable productivity with minimal energy consumption.

This optimisation necessitates accurate mathematical models that describe heat and mass transfer in specific drying configurations. Research by O. Tsurkan *et al.* (2022) confirmed the feasibility of using combined analytical and numerical modelling methods for convective drying to predict temperature and moisture fields. However, aspects such as the distribution of temperature and moisture along the radius of thick-layer annular dryers with radial air flow remain insufficiently studied.

The aim of this study was to investigate unsteady heat and mass transfer processes in the annular grain layer of a bunker-type dryer with radial supply of the drying agent to assess temperature and moisture distribution uniformity and evaluate the impact of drying parameters on dehydration efficiency.

Research objectives:

- to develop a mathematical model of unsteady heat and mass transfer in a ring-cylindrical layer of grain mass, taking into account changes in the radial coordinate of temperature, moisture content, and filtration rate of the drying agent;
- to identify thermo physical coefficients (effective thermal conductivity, effective diffusion), similarity criteria (heat and mass transfer Bio) from classical analytical solutions of heat and mass transfer equations for a spherical body to calculate the heating and drying coefficients of the external heat and mass transfer model.

The scientific novelty of the study was that a mathematical model of unsteady heat and mass transfer in the grain layer of a bunker dryer was developed, taking into account changes in the radial flow rate of the drying agent and the empirical dependence of grain equilibrium moisture content on drying parameters. The model allowed identifying the distribution patterns of temperature and humidity along the bed height and radius, as well as the risk zones of overdrying or underdrying. A new approach to reducing uneven drying by means of cyclic grain mixing was substantiated, suitable for implementation in single or serially connected bunker-type dryers.

MATERIALS AND METHODS

To determine the rational modes of drying grain (seed) material and optimise the technological and structural parameters of grain dryers, it was necessary to study the kinetics of dehydration and heating of both single grains and the entire dense layer of grain in its interaction with the drying agent. The drying kinetics of individual grains was determined by interrelated processes of internal heat and mass transfer, and the drying of the grain layer was determined by the hydrodynamic regime of drying agent filtration in the intergrain space of the moving material. At the same time, the parameters of the drying agent changed both in time and in the coordinates of the drying volume of the grain dryer. Therefore, the research was based on an analytical and experimental method based on a two-level mathematical model of internal heat and mass transfer and external heat and moisture exchange of grain with the drying agent.

At the first level (micro level), a mathematical description of the drying kinetics (changes in moisture content and temperature) of a single spherical grain in the form of a ball when it interacts with a drying agent with time-variable parameters was formulated. The thermophysical coefficients of the mathematical model were identified from the experimental data. At the second level (macro kinetics), a two-stream mathematical model of heat and mass transfer of the drying agent, variable parameters, and a gravitationally moving ring-cylindrical grain layer during radial filtration of the drying agent was formulated.

The interconnected transfer of heat and mass (in the form of liquid and vapor) inside a wet material is described, as is well known, by the system of differential equations by I. Palamarchuk *et al.* (2023), which were written in the form:

$$\begin{cases} \frac{\partial \theta}{\partial \tau} = a_T \nabla^2 \theta + \frac{\varepsilon r_v}{c} \frac{\partial U}{\partial \tau} \\ \frac{\partial U}{\partial \tau} = a_m \nabla^2 U + a_m \delta_T \nabla^2 \theta + \varepsilon \frac{\partial U}{\partial \tau}, \end{cases} \tag{1}$$

where θ, U – temperature and moisture content of the material; a_T, a_m, δ_T – coefficients of thermal conductivity, moisture conductivity, and thermo gradient coefficient; ε – the phase transformation coefficient; c – specific heat capacity of the material; r_v – specific heat of vaporisation; $\nabla\theta$, ∇U – gradients of the temperature and moisture content field in the body.

The system of equations (1) can be solved numerically with the defined coefficients a_m, a_T, ε, δ_T. However, existing methods for determining the transfer coefficients involve separate experiments for each coefficient, which leads to rather complicated empirical dependencies that complicate calculations and reduce their reliability. The problem arose of determining the coefficients of the equations from experimental information using known analytical solutions of the equations of thermal conductivity and mass transfer separately. To do this, the equations of system (1) were simplified.

The second term on the right-hand side of the first equation determines the amount of heat for moisture evaporation. Using the Rebinder criterion $Rb = \frac{c}{r}\cdot\frac{\partial\theta}{\partial U}$, was replaced $r\cdot\left(-\frac{\partial U}{\partial\tau}\right) = \frac{c}{Rb}\cdot\frac{\partial\theta}{\partial\tau}$. The coefficient of thermal and moisture conductivity is set to zero, given the practical absence of thermogradient moisture transfer in the grain under the adopted drying regimes.

It was supposed that the grain shape is a sphere with an equivalent radius:

$$R = \frac{1}{2}\sqrt{\frac{6V_g}{\pi}}, \tag{2}$$

where V_g – volume of the grain.

Taking into account the adopted simplifications, the equations of heat and mass transfer in a single grain can be written in the form:

$$\frac{\partial\theta(r,\tau)}{\partial\tau} = a_{ef}\cdot\left(\frac{\partial^2\theta(r,\tau)}{\partial^2 r} + \frac{2}{r}\frac{\partial\theta(r,\tau)}{\partial r}\right); \tag{3}$$

$$\frac{\partial U(r,\tau)}{\partial\tau} = a_{mef}\cdot\left(\frac{\partial^2 U(r,\tau)}{\partial^2 r} + \frac{2}{r}\frac{\partial U(r,\tau)}{\partial r}\right), \tag{4}$$

where $a_{ef} = \frac{a_T}{1-\frac{\varepsilon}{Rb}}$ – coefficient of effective thermal conductivity; $a_{mef} = \frac{a_m}{1-\varepsilon}$ – coefficient of effective moisture conductivity; $\varepsilon = \frac{dU_{ev}}{dU}$; r – coordinate of the measurement point.

Interphase heat and moisture exchange (grain – drying agent) occurs by convective-diffusion, therefore, boundary conditions of the third kind were used to solve equations (3) and (4):

$$-\frac{\partial\theta(R,\tau)}{\partial r} + \frac{\alpha}{\lambda}\cdot(t_c - \theta(R,\tau)) = 0;\ \frac{\partial\theta(R,\tau)}{\partial r} = 0, \tag{5}$$

$$\frac{\partial U(R,\tau)}{\partial R} - \frac{\beta}{a_m}\cdot\left(U(R,\tau) - U_{riv}(t,\varphi)\right) = 0;\ \frac{\partial U(R,\tau)}{\partial R} = 0. \tag{6}$$

Initial conditions:

$$\theta(\bar{R},\bar{\tau}) = \bar{\theta}_0;\ U(\bar{R},\bar{\tau}) = \bar{U}_0. \tag{7}$$

The solutions of equations (3), (4) under boundary conditions (5-7) are known (Kaletnik *et al.*, 2024) and for changes in time of the average (over the radius) values of the sought parameters $\theta(\tau)$ and $U(\tau)$ take the form:

$$\bar{\theta}(\tau) = t_c - (t_c - \theta_0)\cdot\sum_{n=1}^{\infty}\frac{6\cdot Bi^2}{\mu_n^2\cdot[\mu_n^2 + Bi^2 - Bi]}\cdot e^{-\frac{a_{ef}}{R^2}\cdot\tau\cdot\mu_n^2}, \tag{8}$$

$$\bar{U}(\tau) = U_{riv} + (U_0 - U_{riv})\cdot\sum_{n=1}^{\infty}\frac{6\cdot Bi_m^2}{\mu_n^2\cdot[\mu_n^2 + Bi_m^2 - Bi_m]}\cdot e^{-\frac{a_{mef}}{R^2}\cdot\tau\cdot\mu_n^2}, \tag{9}$$

$$tg\mu = -\frac{\mu}{Bi-1}, \tag{10}$$

where μ_n – roots of characteristic equation (10); $Bi = \frac{\alpha\cdot R}{\lambda}$; $Bi_m = \frac{\beta\cdot R}{a_{mef}}$ – heat and mass transfer criterion "Bio"; α – heat transfer coefficients (W/(m^2·K)); β – moisture transfer coefficient (m/s); λ – thermal conductivity coefficient, W/(m·K); a_{mef} – coefficient of effective moisture conductivity (m^2/s); a_{ef} – coefficient of effective thermal conductivity (m^2/s); t_c – temperature of drying agent (°C); U_{riv} (t, φ) – equilibrium moisture content (kg/kg); φ – relative humidity of drying agent (%).

To reduce the influence of random experimental errors on the result of calculating the coefficients of equations (8), (9), the obtained experimental kinetics data were approximated by dependencies in the form of equations:

$$\theta(\tau) = t_2 - (t_2 - \theta_1)\ e^{-k_1\tau}; \tag{11}$$

$$U(\tau) = U_2 + (U_1 - U_2)\ e^{-k_2\tau}, \tag{12}$$

where θ_1, U_1, t_2, U_2 – initial and final values of the parameters; k_1, k_2 – heating and dehumidification coefficients, respectively. For calculations and numerical modelling, the mathematical software Mathcad was used, enabling the solution of transcendental equations and implementation of the Levenberg-Marquardt algorithm via the genfit function. The Statistica 10 package was employed for approximation and construction of empirical dependencies, allowing for highly accurate polynomial models with strong correlation coefficients.

RESULTS AND DISCUSSION

To search for unknown coefficients in equations (8), (9) using the inverse problem method, numerous solutions of the transcendental equation (10), obtained in the mathematical environment Mathcad, are approximated by empirical dependencies. Figure 1 shows a screen fragment of the numerical solution of equation (10).

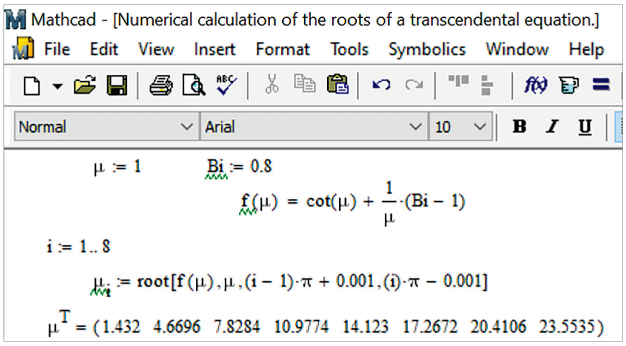

Figure 1. Numerical determination of the roots of the transcendental equation (10) in the mathematical package Mathcad

Source: compiled by the authors

For μ_1, after numerical experiments with various approximating mathematical structures in the Statistica 10 package, an empirical dependence with the highest level of multiple correlation (R = 0.99981) of the form:

$$\mu_1 = b_0 + b_1\ Bi + b_2\ Bi^{b_3}, \tag{13}$$

where the coefficients: b_0 = -0.090821; b_1 = -0.27041; b_2 = 1.924477; b_3 = 0.461608; Bi = 0.02 ÷ 10.5. For μ_2 - μ_6 the approximating dependences on the Bio criterion are defined as a polynomial of the second degree:

$$\mu = b_0 + b_1\ Bi + b_2\ Bi^2. \tag{14}$$

The values of the dependence coefficients (14) were determined in the Statistica 10 package and are given in Table 1.

Table 1. Values of dependence coefficients (13)

μ	b_0	b_1	b_2	R (multiple correlation coefficient)
$\mu2$	4.49427	0.228132	-0.0108	0.9998
$\mu3$	7.72303	0.136715	-0.00428	0.9999
$\mu4$	10.90255	0.09611	-0.00206	0.9999
$\mu5$	14.06520	0.07373	-0.00112	0.9999
$\mu6$	17.22012	0.05973	-0.00067	0.9999

Source: compiled by the authors

Substitute the determined dependencies μ_1 - μ_6 into dependency (8) and (9) and, using the built-in genfit function in the Mathcad mathematical package implementing the Levenberg-Marquardt algorithm. Determine the values of Bi, Bi_m and a_{ef}, a_{mef} at which dependencies (8) and (9) will most accurately describe the sets of given points determined from (11) and (12). Take the initial a priori approximate values of Bi, Bi_m and a_{ef}, a_{mef} for the given parameters of the heating and drying process in the elementary layer of wheat grain from reference books and preliminary studies (Kaletnik *et al.*, 2024). A screen fragment of calculations of *a* and *Bi* by formulas (8), (13)-(14) in the Mathcad package is illustrated in Figure 2.

Figure 3 shows graphs of changes in moisture content and grain temperature in a layer 0.02 m thick during air filtration with a temperature of t_c = 60°C and a velocity at the entrance to the layer of 0.22 m/s. The graphs show points obtained from empirical dependencies (11) and (12) and a curve determined by the genfit function in MathCad according to equations (8) and (9).

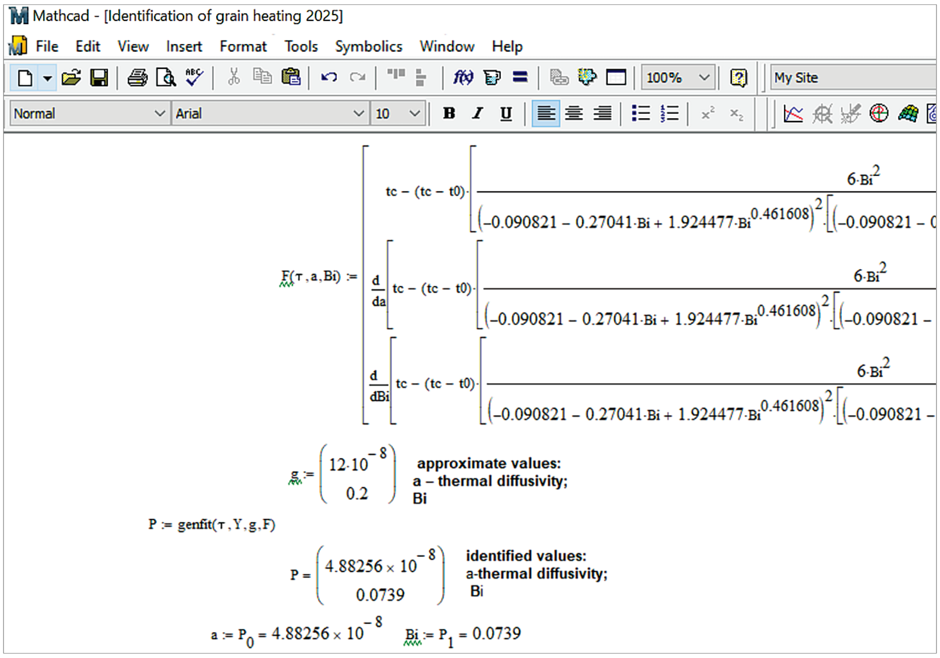

Figure 2. Screen fragment of the implementation of the genfit function in the Mathcad mathematical package for determining the thermal diffusivity coefficient a and the criterion *Bi*

Source: compiled by the authors

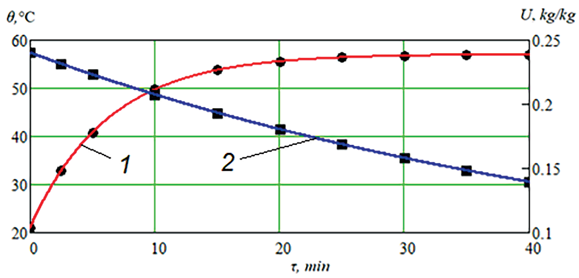

Figure 3. Kinetics of grain temperature 1 and grain moisture content 2

Note: temperature of drying agent t_c = 60°C; velocity at the entrance to the layer υ_{r_0} = 0.22 m/s

Source: compiled by the authors

For further analytical studies, simplify equations (8) and (9). As is known, in the stage of regular mode, the functions that describe the drying and heating processes can be described by one (first) term of the series and the dependence (8) and (9) can be presented in a simplified form:

$$\bar{\theta}(\tau) - \bar{\theta}_0 = B_1 \cdot (t_c - t_0) \cdot e^{-\frac{a_{ef}}{R^2}\tau\mu_1^2}; \tag{15}$$

$$\bar{U}(\tau) - \bar{U}_p = B_2 \cdot (U_0 - U_p) \cdot e^{-\frac{a_{mef}}{R^2}\tau\mu_1^2}, \tag{16}$$

where $B_1 = \frac{6\cdot Bi^2}{\mu_1^2\cdot[\mu_1^2+Bi^2-Bi]}$; $B_2 = \frac{6\cdot Bi_m^2}{\mu_1^2\cdot[\mu_1^2+Bi_m^2-Bi_m]}$; $\mu_1^2 = \left(\frac{1}{\pi}+\frac{1}{3\cdot Bi_m}\right)^{-1} \approx \left(\frac{1}{3}+\frac{1}{Bi}\right)^{-1}$.

The rate of change of temperature and moisture content of grain in time was determined by differentiating equations (15) and (16) with respect to time. After differentiating equations (15) and (16) and comparing the obtained derivatives with (15) and (16), B_1 and B_2 were eliminated, and the following was obtained:

$$\frac{d\bar{\theta}(\tau)}{d\tau} = k_t \cdot (t_c - \theta(\tau)); \tag{17}$$

$$\frac{d\bar{U}(\tau)}{d\tau} = -k_c \cdot \left(\bar{U}(\tau) - U_{riv}(t,\varphi)\right), \tag{18}$$

where $k_t = \frac{a_{ef}}{R^2}\left(\frac{1}{\pi}+\frac{1}{3\cdot Bi_m}\right)^{-1}$; $k_c = \frac{a_{mef}}{R^2}\left(\frac{1}{\pi}+\frac{1}{3\cdot Bi_m}\right)^{-1}$.

The equilibrium moisture content of grain is usually determined as a function of temperature t and relative humidity φ of the drying agent and can be calculated using the empirical formula obtained from research:

$$U_{riv}(t,\varphi) = b_0 + b_1 \cdot t + b_2 \cdot \varphi, \tag{19}$$

where $b_0 = 0.02343$; $b_1 = 0.114 \cdot 10^{-3}$; $b_2 = 0.002067$; t – temperature of the drying agent (°C); φ – relative humidity of the drying agent (%). But a more informative parameter of air is the moisture content d, therefore formula (18) is approximated as dependence:

$$U_{riv}(t,d) = b_0 \cdot t^{b_1} \cdot d^{b_2}, \tag{20}$$

where $b_0 = 0.725$; $b_1 = -1.2133$; $b_2 = 0.8826$; d – absolute humidity of the drying agent (g/m³). Equations (15) and (16) are obtained under the condition that the temperature of the drying agent is constant over time. However, when air is filtered through a dense layer of grain material, its temperature changes both in time and along the coordinate r.

The calculation diagram of the grain material drying process in a bunker dryer with radial supply of the drying agent is shown in Figure 4.

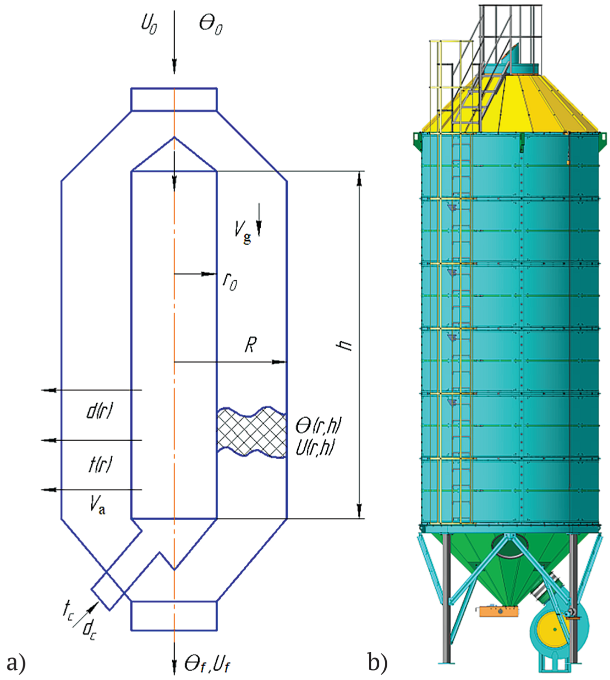

Figure 4. Calculation diagram of the grain material drying process in a bunker dryer with radial supply of drying agent (a) and general view of the bunker type dryer (b)

Note: U_0, is the initial moisture content of grain, kg/kg; U_f is the final average moisture content of grain, kg/kg; θ_0 is the initial temperature of grain, °C; θ_f is the final average temperature of grain, °C; r_0 is the radius of the inner cylinder of the bunker, m; R is the radius of the outer cylinder of the bunker, m; r is a variable radial coordinate, m; h is a variable vertical coordinate, m; t_c is the temperature of the drying agent at the inlet to the grain layer, °C; d_c is the moisture content of the drying agent at the inlet to the grain layer, g/m³; $t(r)$ is the variable temperature of the drying agent at the radial coefficient, °C; $d(r)$ is the variable moisture content of the drying agent at the radial coefficient, g/m³; $V_a(r)$ is the filtration rate of the drying agent in the grain layer, at the radial coordinate, m/s; $V_g(h)$ is the speed of grain movement, by vertical coordinate, m/min; $\theta(r, h)$ is the temperature of grain by radial and vertical coordinates, °C; $U(r, h)$ is the moisture content of grain by radial and vertical coordinates, kg/kg

Source: compiled by the authors

To formulate a mathematical model of unsteady heat and mass transfer in the process of grain drying in a moving annular-cylindrical layer (macro level model), will expand the full differentials in equations (17) and (18) were expanded: $d\theta=\frac{\partial\theta}{\partial\tau}d\tau+\frac{\partial U}{\partial h}dh$; $dU=\frac{\partial U}{\partial\tau}d\tau+\frac{\partial U}{\partial h}dh$. Considering that $\frac{dh}{d\tau}=\upsilon_{gr}$ – velocity of grain material and using (19) the following was obtained:

$$\frac{\partial\theta}{\partial\tau}+\upsilon_{gr}\frac{\partial\theta}{\partial h}=k_t\cdot(t_c-\theta); \tag{21}$$

$$\frac{\partial U}{\partial\tau}+\upsilon_{gr}\frac{\partial U}{\partial h}=-k_c\cdot(U-b_0\cdot t^{b_1}\cdot d^{b_2}). \tag{22}$$

The heat balance equation for the drying agent can be written as:

$$-m_p\cdot c_p\cdot d\bar{d}=m_{gr}\cdot c_{gr}\cdot d\bar{\theta}-m_0\cdot r\cdot d\bar{U}. \tag{23}$$

Considering the complete differentials $d\bar{d}, d\bar{\theta}, d\bar{U}$ and taking into account the obvious signs: $m_{gr}=V_{sp}\cdot\rho_{gr}$; $m_0=V_{sp}\cdot\rho_0$; $m_p=V_p\cdot\rho_p$; $\varepsilon=V_p/V_{sp}$, equation (23) was rewritten as:

$$\varepsilon\cdot\rho_p\cdot c_p\cdot\left(\frac{\partial t}{\partial\tau}+\upsilon_r\frac{\partial t}{\partial r}\right)=\rho_{gr}\cdot c_{gr}\cdot$$
$$\cdot\left(\frac{\partial\theta}{\partial\tau}+\upsilon_{gr}\frac{\partial\theta}{\partial h}\right)-\rho_0\cdot r_0\cdot\left(\frac{\partial U}{\partial\tau}+\upsilon_{gr}\frac{\partial U}{\partial h}\right). \tag{24}$$

The equation for the material balance sheet was similar:

$$\varepsilon\cdot\rho_p\cdot\left(\frac{\partial d}{\partial\tau}+\upsilon_r\frac{\partial d}{\partial r}\right)=\rho_0\cdot\left(\frac{\partial U}{\partial\tau}+\upsilon_{gr}\frac{\partial U}{\partial h}\right). \tag{25}$$

Thus, the dynamic drying regime of grain material was determined by solving the system of equations (21, 22, 24, 25) under the following boundary and initial conditions:

$$U(0,h)=U_0;\ \theta(0,h)=\theta_0;\ t(\tau,0)=t_1;\ d(\tau,0)=d_1. \tag{26}$$

In equations (24)-(25), the value $V_r=V(r)$ is the actual filtration speed of the drying object through the layer. The overall, calculated for the entire cross-section of the unfilled volume υ_r is related to the actual speed of the drying agent by the ratio $\upsilon_{c,a}=\frac{\upsilon_r(r)}{\varepsilon}$, and the overall speed varies along the coordinate in the direction of movement:

$$\upsilon_r=\frac{L_{c.a}}{2\cdot\pi\cdot H\cdot r}, \tag{27}$$

where $L_{c.a}$ – volumetric flow rate of drying agent; H – height of the working zone of the grain dryer. In the stationary mode of operation of the drying unit, the process parameters at each point of the drying volume will have values that do not vary in time; therefore, time derivatives can be excluded from the differential equations.

The stationary operating mode of the grain drying process in a gravitationally moving annular-cylindrical layer describes the following level system:

$$\begin{cases}\upsilon(r)\frac{\partial t}{\partial r}=\frac{\rho_{gr}\cdot c_{gr}}{\varepsilon\cdot\rho_p\cdot c_p}\upsilon_{gr}\frac{\partial\theta}{\partial h}-\frac{\rho_0\cdot r_0}{\varepsilon\cdot\rho_p\cdot c_p}\upsilon_{gr}\frac{\partial U}{\partial h}\\ \upsilon(r)\frac{\partial d}{\partial r}=-\frac{\rho_{gr}}{\rho_p\cdot\varepsilon}\upsilon_{gr}\frac{\partial U}{\partial h}\\ \upsilon_{gr}\frac{\partial\theta}{\partial h}=k_t\cdot(t_c-\theta)\\ \upsilon_{gr}\frac{\partial U}{\partial h}=-k_c(U-b_0\cdot t^{b_1}\cdot d^{b_2})\end{cases}. \tag{28}$$

Since the relative speed of the drying agent in the grain layer (filtration rate) varies along the coordinate, it is necessary to take into account the change in the intensity of heat supply to the material and the intensity of moisture removal, which leads to a change in the parameters of the drying agent $t(r)$, $d(r)$. For this, it is necessary to have a dependence of the heat exchange criterion Bi and the mass exchange Bi_m on the filtration speed of the drying agent υ_r, its temperature t for the mass exchange criterion: $Bi(\upsilon_r)$, $Bi_m(\upsilon_r, t)$.

The dependence of the Bio heat transfer criterion on the speed of the drying agent (due to the fact that the value of Bi is practically independent of t, d) can be used with the known criterion dependencies Bi(Nu), namely:

$$Bi(Nu)=Nu\cdot\frac{R}{l}\cdot\frac{\lambda_c}{\lambda_g}, \tag{29}$$

where $Nu=0.0745\cdot Re^{0.625}$; $Re=\frac{\upsilon_r}{\nu}\frac{2}{3}\frac{\varepsilon\cdot d_{e.g}}{1-\varepsilon}$; ε – porosity of the grain layer; $d_{e.g}$ – equivalent diameter of grains; $l=\pi R$; λ_c, λ_g – coefficients of thermal conductivity of the drying agent and grains; ν – coefficient of kinematic viscosity of the drying agent.

From the expanded mathematical expression (29) it follows:

$$Bi(\upsilon_r)=0.0745\frac{\lambda_c}{\pi\cdot\lambda_g}\left(\frac{2\varepsilon\cdot d_{e.g}}{3\nu(1-\varepsilon)}\right)^{0.625}\upsilon_r^{0.625}. \tag{30}$$

The dependence $Bi_m(\upsilon_r, t, d)$ can be determined from the relation for k_c:

$$k_c=\frac{a_m}{(1+Rb^{-1})\cdot R^2}\cdot\left(0.2+\frac{1}{Bi_m}\right)^{-1}. \tag{31}$$

Then:

$$Bi_m(\upsilon_r)=\left(\frac{a_m}{(1+Rb^{-1})\cdot k_c\cdot R^2}-0.2\right)^{-1}. \tag{32}$$

The drying coefficient k_c is also determined directly from the data of the experimental determination of drying kinetics according to the well-known formula (Kaletnik *et al.*, 2024):

$$k_c=\frac{1}{\tau_c}\cdot ln\frac{u_1-u_p}{u_2-u_p}, \tag{33}$$

where τ_c – drying time from grain moisture content u_1 to u_2.

Based on the generalisation of tabular data from the work of P.C. Coradi & Â.F. Lemes (2019), the experimental studies of H. Kaletnik *et al.* (2024), and the approximation of dependence (31), empirical relationships of the drying coefficient with the drying agent parameters were obtained, which, for wheat grain, take the form:

$$k_c(\upsilon_r, t)=0.025t\upsilon_r^{0.625}, \tag{34}$$

where k_c – drying coefficient (1/h); t – temperature of the drying agent (°C); υ_r – filtration speed of the drying agent, (m/s).

The dependence of the mass transfer criterion Bi_m on the parameters of the drying agent, respectively:

$$Bi_m(v_r, t) = \left(\frac{a_m}{(1+Rb^{-1})\cdot k_c(v_r,t)\cdot R^2} - 0.2\right)^{-1}. \quad (35)$$

The results of solving the system of equations (28) under boundary conditions:

$$r = r_0;\ t(h, r_0) = t_1;\ d(h, R_0) = d_1;\ h = 0;\ \theta(0, r) = \theta_1;\ U(0, r) = U_1.$$

Taking into account (31-32, 34-35), numerical solutions were obtained in the Mathematica computer environment in the form of changes in grain parameters $\theta(r, h)$, $U(r, h)$and drying agent according to the coordinates of the drying space of the bunker dryer. Calculations were carried out with the following ranges of initial data: height of the drying space 6.8 m², thickness of the grain layer $r_0 = 0.4 - 0.6$ m, $R = 1.54$ m specific consumption of the drying agent L = 3,000-4,000 m³/(hour·ton) of dried grain; W_0 – initial moisture 20%. The final grain moisture, which is allowed by the standards for grain dryers 14.0-15.5%, is determined as the grain humidity in the outer grain layer. The temperature of the drying agent at the entrance to the grain material layer was 80-100°C.

A graphical interpretation of the numerical calculation of the wheat grain drying process parameters according to model (28) in the Mathematica mathematical environment is shown in Figure 5. The calculated data correlate well with the experimental data of grain wheat drying in the SBS-5 bunker dryer. The uneven distribution of grain moisture at the dryer outlet is up to 20% ($\Delta\omega = 16.1 - 12.8\%$). The uniformity of drying, i.e. the difference in grain moisture in the zones of the inner and outer cylinder of the dryer, can be increased by increasing the consumption of the drying agent Figure 6, but at the same time the energy losses with the spent drying agent increase several times.

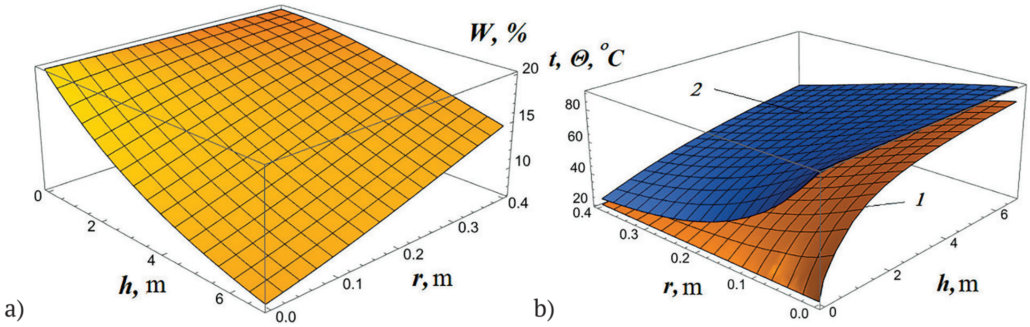

Figure 5. Simulation results with parameters $L = 3{,}000$ m³/(hour·ton); $R - r_0 = 0.4$ m; $W_0 = 20\%$; $t = 90$°C
Note: a) – field of moisture content of the grain layer; b) – temperature fields: 1 – grain layer; 2 – drying agent in the grain layer
Source: compiled by the authors

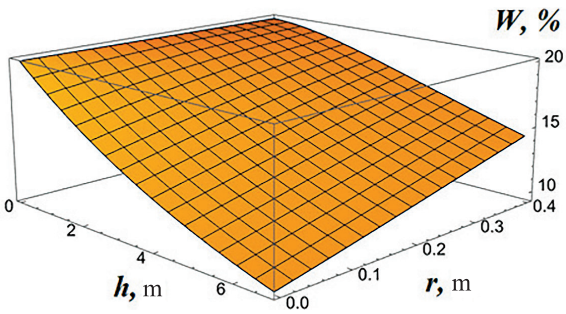

Figure 6. Grain layer moisture content field
Note: $L = 4{,}000$ m³/(hour·ton); $R - r_0 = 0.4$ m $W_0 = 20\%$; $t = 90$°C
Source: compiled by the authors

To simplify numerical calculations of the periodic circulation mode, it was assumed that after each cycle of grain passing through the drying zone, the grain material was completely mixed, and its parameters were averaged along the radial coordinate:

$$U_{out}(r) = \bar{U}_{out.a};\ \theta_{out}(r) = \bar{U}_{out.a}, \quad (36)$$

where $U_{out}(r)$, $\theta_{out}(r)$ – distribution of moisture content and temperature along the radius at the exit from the drying zone when $h = H$. The magnitude of the average values of temperature and moisture content is determined by the obtained formulas:

$$\bar{\theta}_{out.gr} = \frac{2}{R^2}\int_{r_0}^{R} r \cdot \theta(r)dr; \quad (37)$$

$$\bar{U}_{out.gr} = \frac{2}{R^2}\int_{r_0}^{R} r \cdot U(r)dr. \quad (38)$$

The scheme of implementation of the process of periodic-circulating grain drying is shown in Figure 7.

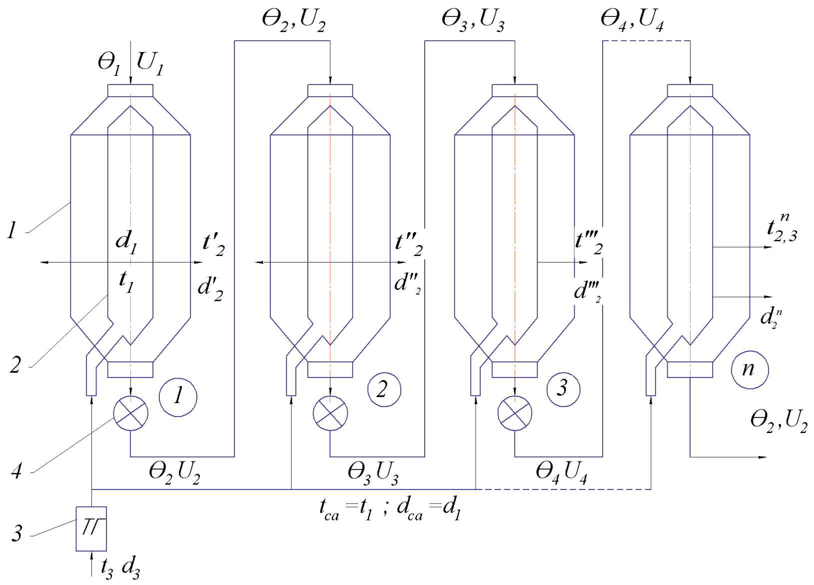

Figure 7. Technological scheme for implementing the process of cyclic drying of grain in a bunker unit
Note: 1 – outer cylinder of the bunker; 2 – inner distribution cylinder; 3 – heat generator; 4 – grain material mixer
Source: compiled by the authors

The schematic diagram of the calculation of the process of periodic-cyclic drying of grain in a moving annular-cylindrical layer is shown in Figure 8, which is based on the mathematical description (model) of the equations of the system (28) taking into account (33), (37), (38).

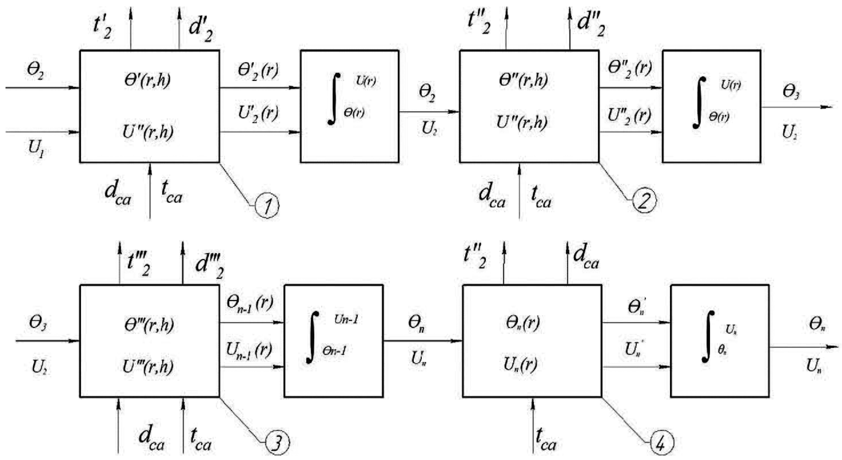

Figure 8. Schematic diagram of the calculation of periodic-cyclic drying of grain in a moving annular layer
Note: 1, 2, 3…n – cycle; θ_k, U_k – final values
Source: compiled by the authors

Calculation algorithm for periodic circulation drying (based on model (28) and illustrated in Figure 9) consists of the following steps:

1. Selection of the number of cycles $n = 1\text{-}5…n(\tau_c)$.
2. Calculation of the speed of movement of a gravitationally directed grain:

$$V_g = \frac{H \cdot n(\tau_c)}{\tau_c}, \qquad (39)$$

where τ_c – drying time; H – height of the drying agent distributor.

3. Calculation in the first cycle of grain drying under the following boundary conditions: $h = 0$; $\theta(r, 0) = \theta_1$; $U(r, 0) = U_1$; $t_{c.a} = t_1$; $d_{c.a} = d_1$; $h = H$; $\theta(r, H) = \theta_2(r)$; $U(r, H) = U_2(r)$.
4. Determination of the average values of θ_2 (r) and $U_2(r)$ of the grain parameters at the exit from the drying zone $h = H$ using equations (37) and (38) $\theta_2(r) = \bar{\theta}_2$ and $U_2(r) = \bar{U}_2$.
5. The obtained average values of $\bar{\theta}_2$ and $2\bar{U}_2$ are required as boundary (initial conditions) parameters of the grain at the entrance to the drying zone during the second drying cycle.

6. Next, the modelling scheme of the process of changing the temperature and moisture content of grain is repeated for the following cycles. The parameters of the drying agent at the entrance to the grain layer remain unchanged throughout the grain drying process.

7. Drying time (residence time) of grain in the dryer after reaching the conditional value of average moisture content – $\bar{U}_k = 17\%$ ($W = 14\%$):

$$\tau = \frac{\sum h \cdot n}{V_g}. \tag{40}$$

Figure 9 shows a test graph of changes in grain parameters along the length of the "drying path" $L = H_c \cdot n$.

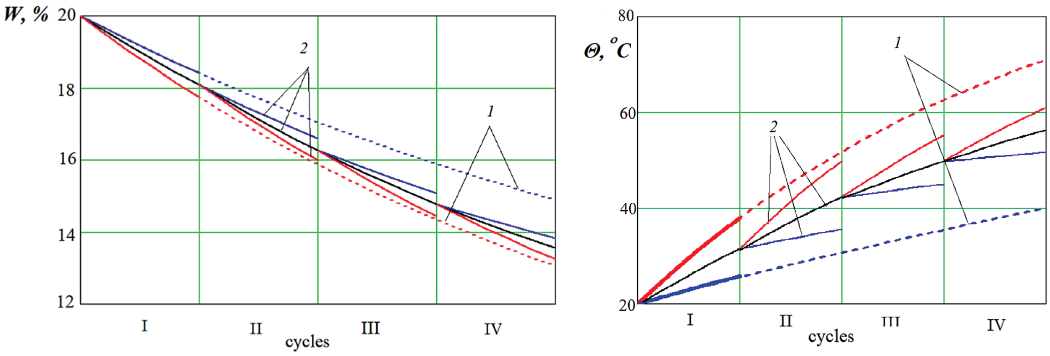

Figure 9. Kinetics of drying (a) and heating (b) of grain

Note: 1 – on the inner and outer wall of the layer in a continuous process, 2 – on the inner, outer and average value in a cyclic-periodic process

Source: compiled by the authors

Convective drying of grain in a dense, thick ring-cylindrical moving layer is a complex physical and technical process accompanied by simultaneous heat and mass transfer and complex dynamic interaction between the solid and gas phases. As substantiated in the study by V. Messerle & A. Ustimenko (2024), an adequate description of this process requires solving a system of nonlinear partial differential equations that take into account external and internal heat and mass transfer, changes in parameters, and hydrodynamic conditions of the medium. Such equations, even in a simplified form, can be effectively solved only by numerical methods. The results of the numerical modelling conducted in this study allowed for a detailed analysis of the patterns of temperature and humidity distribution in a thick grain layer of a bunker dryer with a cross-feed drying agent, and enabled the establishment of optimal drying modes. The proposed model takes into account unsteady processes and features of drying agent filtration in the ring-cylindrical layer, which is an adequate simulation of the geometry of the grain dryer. Preliminary analytical solutions of mathematical models for bodies of classical shape, particularly the work by Y. Sniezhkin & Z. Petrova (2023) provided a theoretical description only for constant thermophysical coefficients. The present work demonstrates the effectiveness of the inverse problem method for identifying thermophysical coefficients based on the experimental kinetics of grain drying and heating. This approach allowed modelling the development of temperature and humidity fields in a single grain modelled as a sphere. However, analytical mathematical solutions are cumbersome and unsuitable for practical engineering use, so it is advisable to use simplified balance models to describe processes in a thick grain layer.

This observation aligns with the findings by Sh.A. Sultanova *et al.* (2024), who demonstrated that energy-based mathematical modelling enables the precise control of temperature fields within a rotary thermosyphon dryer. Their model accounted for the dynamics of heat and mass transfer during the drying of pumpkin seeds, confirming that simulation tools can accurately reflect the kinetics of moisture removal and inform the selection of optimal drying trajectories. Importantly, they highlighted the critical role of boundary conditions – such as internal airflow velocity and rotating drum speed – in determining drying efficiency, suggesting that unified models must be sensitive to geometric and operational variability. A similar perspective is found in the work by H. Kaletnik *et al.* (2024), where a vibratory mill with spatial circulation was applied as the basis for constructing a drying rig. Their research underscored the benefit of incorporating elements of forced particle movement to overcome stagnation zones and non-uniform heat distribution. The proposed technical configuration improved the intensity of convective flows and reduced local temperature differentials, pointing to the advantages of mechanical agitation for energy-efficient moisture extraction. Notably, their design was adapted for granular agricultural products with high bulk density – highlighting the relevance of process-specific parameterisation.

The approach developed in the current study, which recommends precise regulation of bed thickness and filtration velocity, is particularly relevant when integrated with findings from by I. Kuznietsova *et al.* (2020), who applied differential scanning calorimetry (DSC) to evaluate the thermal behaviour of tomato tissue during drying. The DSC analysis enabled the identification of critical temperature thresholds associated with structural collapse or case hardening, indicating that empirical calibration of mathematical models with thermal analysis data can significantly improve predictive capacity. Their results confirmed that even slight deviations in thermal input could result in non-linear responses in moisture migration, which reinforces the need for adaptive control strategies in drying systems. The obtained results confirm the effectiveness of using mathematical modelling to optimise key technological parameters such as temperature, moisture content and duration of drying. A similar modelling approach was applied by R. Chuiuk (2025), who developed a kinetic model of the transesterification process of waste oils into biodiesel. In his work, the dynamic changes in the concentrations of reactants and products were taken into account, along with temperature-dependent reaction rates. This modelling enabled the identification of optimal process conditions to ensure high yield and energy efficiency. These findings further demonstrate the versatility of mathematical models as tools for improving technological processes in different fields.

Taken together, the reviewed studies validate the integration of physical modelling and experimental diagnostics as a robust framework for the development of energy-optimised drying processes. They also emphasise the necessity of tailoring model parameters to reflect material-specific properties and equipment geometry, thereby supporting the direction adopted in this work. Numerical modelling of the effect of drying agent temperature confirmed that increasing the temperature from 80°C to 100°C reduces the drying time by 25-30%, which is consistent with the results of A. Kraiem *et al.* (2023). However, further analysis showed that an excessive increase in the temperature of the drying agent leads to overheating of the grain, especially in areas near the inner cylinder of the dryer (up to 72°C), which can negatively affect the sowing quality of the grain. It is recommended to use a drying agent temperature in the range of 85-90°C, which ensures sufficient process intensity and reduces the risk of thermal damage to the grain. The analysis of the effect of air flow rate confirmed the conclusions of I. Shevchenko & E. Aliiev (2020) that it is inexpedient to increase it above 0.5 m/s, as this leads to an unreasonable increase in energy costs (up to 6 MJ/kg of evaporated moisture) without a significant improvement in dryer performance. The optimum air flow rate was determined to be 0.3 m/s at the entrance to the grain layer up to 0.4 m thick, which ensures an acceptable moisture gradient and minimal energy losses.

Modelling of the drying process for different radial layer thicknesses (0.3, 0.4, 0.5 m) at a drying agent temperature of 90°C and an air flow rate of 0.3 m/s showed that the optimal vertical movement rate of the layer was 0.17, 0.13, and 0.10 m/min, respectively. At the same time, the dryer's productivity was 19.9, 20.2, and 19.5 t/h, the average grain outlet temperature was about 50°C, and the temperature difference between the inner and outer walls increased from 13 to 18°C with increasing layer thickness. The humidity unevenness according to the layer thickness ranged from 6% to 9%, and the energy consumption for moisture evaporation decreased from 5.2 to 4.2 MJ/kg. The results clearly demonstrate the existence of a discrepancy between energy efficiency and drying quality: increasing the layer thickness reduces energy consumption but increases drying unevenness and the risk of overheating of the inner layers, while reducing the thickness leads to lower performance and increased energy losses with the spent drying agent.

The organisation of a cyclic-periodic drying regime with grain stirring is proposed in this paper as a rational solution to eliminate these contradictions. This ensures uniformity of drying with a moisture deviation of 1-1.5% and avoids overheating of the grain material. In addition, stirring promotes the activation of further moisture transfer due to the diffusion of moisture from the inner layers of the grain to its surface during the stirring period, which is confirmed by an increase in the moisture transfer coefficient β by 8-14% after stirring, according to the identified mass transfer criteria Bio for different process regulations.

Comparison of the results with the modes implemented in serial grain dryers by Fratelli Pedrotti, Agrimec, Mecmar, Agrex and others (Fig. 10) showed that although these installations provide high uniformity of drying, the intensity of mixing in them is much higher, which leads to increased grain injury in the augers and increased energy costs for mixing.

a)

b)

Figure 10. Appearance of grain dryers
Note: a) Fratelli Pedrotti XL-420; b) Agrimec AS 1150
Source: Fratelli Pedrotti mobile grain dryers (n.d.), Agrimec grain dryer (mobile) (n.d.)

The results of the study confirm that the specific energy consumption for the evaporation of 1 kg of moisture in the proposed periodic-circulation drying mode ranges from 4.2 to 5.2 MJ/kg, which is fully consistent with the values characteristic of modern energy-efficient grain dryers. This range correlates with the findings of I. Bezbah *et al.* (2022), who developed new dryer constructions aimed at reducing energy costs without compromising drying quality, and with the results of P.C. Coradi & Â.F. Lemes (2019), who applied CFD-based optimisation to improve energy utilisation in silo-dryer systems. The obtained results highlight the high energy-saving potential of bunker-type dryers operating under periodic regimes, especially when combined with adaptive control of the drying agent flow and the vertical movement rate of the grain layer.

An important direction in increasing energy efficiency is the integration of waste heat recovery technologies. The study confirmed the relevance and applicability of such approaches in bunker systems, which resonates with the work by F. Huang *et al.* (2017), who investigated industrial-scale heat recovery schemes, and by Z.Y. Xu *et al.* (2019), who emphasised the feasibility of low-temperature waste heat recovery in agricultural drying systems. According to these studies, up to 20-30% of thermal losses in conventional dryers can be recuperated using plate or rotary-type heat exchangers. In the present research, the modelling results suggest that up to 27% of the exhaust heat energy can be effectively returned to the drying process without compromising the thermal stability of the system. This effect is especially evident when using a two-stage heating zone with variable drying agent temperatures and flow control, which stabilises the internal gradients of temperature and humidity within the grain mass. This effect is especially evident when using a two-stage heating zone with variable drying agent temperatures and flow control, which stabilises the internal gradients of temperature and humidity within the grain mass.

Moreover, the numerical experiments conducted in the Mathematica environment confirm that energy savings are not only a result of improved insulation or material properties, but also strongly depend on the rational configuration of drying cycles and the reduction of peak thermal loads. The integration of heat recovery modules becomes particularly effective when combined with periodic grain mixing, which equalises thermal fields and enhances the efficiency of heat transfer in the layer. These findings support the thesis that future dryer designs should be guided by the principle of thermal self-sufficiency, where the waste heat of the system is partially or fully reintegrated into the process, reducing the reliance on external thermal energy sources. Such an approach is not only economically viable, but also aligns with the broader goals of sustainable agriculture and carbon footprint reduction.

Thus, the numerical modelling confirmed the high sensitivity of the process to the technological and design parameters of the plants and allowed for the formulation of new approaches to the design of efficient grain dryers with radial drying agent feeding. The proposed mathematical models can be used to create automated control systems for the drying process with feedback based on the temperature and humidity of the drying agent and grain, which will help reduce energy costs and ensure consistently high quality of finished products.

CONCLUSIONS

The developed two-level mathematical model of the process of drying seed material in bunker dryers with radial supply of the drying agent allows to adequately describe the kinetics of dehydration and heating of both a single grain and a dense ring-cylindrical layer of grain. This provides a reliable theoretical basis for further optimisation of drying regimes. The thermo physical coefficients of the models are identified based on the results of experimental studies, which allows for quick engineering calculations and prediction of results when changing the input parameters of drying, such as temperature, speed, and moisture content of the agent.

A significant effect of the distribution of temperature and humidity of the drying agent along the radius of the bed was found, which increases the unevenness of drying. The largest energy losses and a decrease in drying quality are observed in a single direct-flow mode due to uneven heating of the grain mass. The use of a periodic-circulating drying mode based on the repeated passage of grain through the drying zone with subsequent mixing is proposed. This allows to significantly reduce the moisture difference between the inner and outer layers of the grain mass and increase the overall energy efficiency of the process. Based on modelling and calculations, the rational design parameters of bin dryers (layer thickness, filtration rate, height of the working area) were determined, which ensure the lowest energy losses while maintaining high grain quality.

Further research should focus on determining the optimal number of grain mixing cycles depending on initial moisture content, considering energy consumption and drying quality. Promising directions include studying heat and mass transfer under variable drying agent feed and grain movement rates, which may enable uniform drying without mixing. This will require refining mathematical models by incorporating dynamic moisture changes into the drying coefficient. Particular attention should be given to the impact of high-temperature regimes on the biological characteristics of grain, including seed viability and nutritional quality. In addition, the synthesis and implementation of automated control systems based on modern microprocessor feedback devices-especially computer vision sensors, real-time grain moisture sensors, and artificial intelligence elements – remain highly relevant for adaptive regulation of drying parameters.

ACKNOWLEDGEMENTS

None.

FUNDING

None.

CONFLICT OF INTEREST

None.

REFERENCES

[1] Agrimec grain dryer (mobile). (n.d.). Retrieved from https://www.eridon-tech.com.ua/agrimec-mobile-dryers/.
[2] Ahmad, N., *et al.* (2021). Impact of thermal extrusion and microwave vacuum drying on fatty acids profile during fish powder preparation. *Food Science and Nutrition*, 9, 2743-2753. doi: 10.1002/fsn3.2236.
[3] Bezbah, I., Zykov, A., Mordynskyi, V., Osadchuk, P., Phylipova, L., Bandura, V., Yarovyi, I., & Marenchenko, E. (2022). Designing the structure and determining the mode characteristics of the grain dryer based on thermosiphons. *Eastern-European Journal of Enterprise Technologies*, 2(8-116), 54-61. doi: 10.15587/1729-4061.2022.253977.
[4] Chuiuk, R. (2025). Mathematical model of the process of converting waste oils into diesel biofuel. *Scientific Reports of the National University of Life and Environmental Sciences of Ukraine*, 21(1),28-43. doi: 10.31548/dopovidi/1.2025.28.
[5] Coradi, P.C., & Lemes, Â.F. (2019). Experimental prototype of silo-dryer-aerator of grains using computational fluid dynamics (CFD) system. *Acta Scientiarum. Technology*, 41, article number e36949. doi: 10.4025/actascitechnol.v41i1.36949.
[6] Demissie, P., Hayelom, M., Kassaye, A., Hailesilassie, A., Gebrehiwot, M.G., & Vanierschot, M. (2019). Design, development and CFD modeling of indirect solar food dryer. *Energy Procedia*, 158, 3721-3726. doi: 10.1016/j.egypro.2019.01.278.
[7] El-Mesery, H.S., Qenawy, M., Ali, M., Hu, Z., Adelusi, O.A., & Njobeh, P.B. (2024). Artificial intelligence as a tool for predicting the quality attributes of garlic (*Allium sativum* L.) slices during continuous infrared-assisted hot air drying. *Journal of Food Science*, 89(11), 7693-7712. doi: 10.1111/1750-3841.17373.
[8] Fratelli Pedrotti mobile grain dryers. (n.d.). Retrieved from https://zernosusharka.com/.
[9] Huang, F., Zheng, J., Baleynaud, J.M., & Lu, J. (2017). Heat recovery potentials and technologies in industrial zones. *Journal of the Energy Institute*, 90(6), 951-961. doi: 10.1016/j.joei.2016.07.012.
[10] Jimoh, K.A., Hashim, N., Shamsudin, R., Che Man, H., Jahari, M., & Onwude, D.I. (2023). Recent advances in the drying process of grains. *Food Engineering Reviews*, 15, 548-576. doi: 10.1007/s12393-023-09333-7.
[11] Kaletnik, H., Solona, O., Kotov, B., Stepanenko, S., Shvydia, V., Kalinichenko, R., Tverdokhlib, I., & Polievoda, Y. (2024a). The usage of the elemental base of the vibratory mill with the spatial circulation movement of material to create drying rig. *Przegląd Elektrotechniczny*, 1, 234-239. doi: 10.15199/48.2024.03.41.
[12] Kraiem, A., Madiouli, J., Shigidi, I., & Sghaier, J. (2023). Experimental analysis of drying conditions' effect on the drying kinetics and moisture desorption isotherms at several temperatures on food materials: Corn case study. *Processes*, 11(1), article number 184. doi: 10.3390/pr11010184.
[13] Kuznietsova, I., Bandura, V., Paziuk, V., Tokarchuk, O., & Kupchuk, I. (2020). Application of the differential scanning calorimetry method in the study of the tomato fruits drying process. *Agraarteadus*, 31(2), 173-180. doi: 10.15159/jas.20.14.
[14] Messerle, V., & Ustimenko, A. (2024). Plasma processing of rubber powder from end-of-life tires: Numerical analysis and experiment. *Processes*, 12, article number 994. doi: 10.3390/pr12050994.
[15] Mukwevho, P., & Emmambux, M.N. (2022). Effect of infrared and microwave treatments alone and in combination on the functional properties of resulting flours from Bambara groundnut seeds. *LWT – Food Science and Technology*, 153, article number 112448. doi: 10.1016/j.lwt.2021.112448.
[16] Nascimento, V.R.G., Biagi, J.D., Oliveira, R.A.D., Arantes, C.C., & Rossi, L.A. (2019). Infrared radiation drying of Moringa oleifera grains for use in water treatment. *Revista Brasileira de Engenharia Agrícola e Ambiental*, 23, 768-775. doi: 10.1590/1807-1929/agriambi.v23n10p768-775.
[17] Onderová, A.I., Cacko, B.V., Šooš, C.L., & Ondruška, D.J. (2019). Drying of biological materials in the dryer with controlled vacuum chambers. In *2019 international council of environmental engineering education – technologies of environmental protection* (pp. 201-205). Starý Smokovec: IEEE. doi: 10.1109/ICTEP48662.2019.8968950.
[18] Palamarchuk, I., Palamarchuk, V., Paziuk, V., Hulevych, R., Kalizhanova, A., & Sarsembayev, M. (2023). Analysis of power and energy parameters of the conveyor infrared dryer of oil-containing raw materials. *Informatyka, Automatyka, Pomiary w Gospodarce i Ochronie Środowiska*, 13(2), 10-14. doi: 10.35784/iapgos.3487.
[19] Shevchenko, I., & Aliiev, E. (2020). Improving the efficiency of the process of continuous flow mixing of bulk components. *Eastern-European Journal of Enterprise Technologies*, 6/1(108), 6-13. doi: 10.15587/1729-4061.2020.216409.
[20] Sniezhkin, Y., & Petrova, Z. (2023). Energy consumption and environmental aspects of drying processes. *Science and Innovation*, 19(2), 44-55. doi: 10.15407/scine19.02.044.
[21] Sokolenko, A., Shevchenko, O., Koval, O., Maksymenko, I., & Shevchenko, A. (2020). Phase transitions in food production technologies. *Ukrainian Food Journal*, 9(4), 889-900. doi: 10.24263/2304-974X-2020-9-4-13.
[22] Sultanova, Sh.A., Imanova, G.T., Safarov, J.E., Usenov, A.B., Ait-Kaddour, A., & Azimov, A.T. (2024). Mathematical modelling of pumpkin seed drying in a rotary thermosyphon dryer. *Materials Research Innovations*, 28(7), 503-508. doi: 10.1080/14328917.2024.2366581.

[23] Timm, N.D.S., Lang, G.H., Ferreira, C.D., Pohndorf, R.S., & De Oliveira, M. (2020). Infrared radiation drying of parboiled rice: Influence of temperature and grain bed depth in quality aspects. *Journal of Food Process Engineering*, 43, article number e13375. doi: 10.1111/JFPE.13375.

[24] Tsurkan, O., Prysiazhniuk, Y., Spirin, A., Borysiuk, D., Tverdokhlib, I., & Polievoda, Y. (2022). Research of the process of vibroozone drying of grain. *Przegląd Elektrotechniczny*, 98(12), 329-333. doi: 10.15199/48.2022.12.76.

[25] Wang, W., Wang, W., Wang, Y., Yang, R., Tang, J., & Zhao, Y. (2020). Hot-air assisted continuous radio frequency heating for improving drying efficiency and retaining quality of inshell hazelnuts (*Corylus avellana* L. Cv. Barcelona). *Journal of Food Engineering*, 279, article number 109956. doi: 10.1016/j.jfoodeng.2020.109956.

[26] Xu, Z.Y., Wang, R.Z., & Chun, Y. (2019). Perspectives for low-temperature waste heat recovery. *Energy*, 176, 1037-1043. doi: 10.1016/j.energy.2019.04.001.

[27] Yu, P., Zhu, W., Shen, C., Qiao, Y., Zhang, W., Zhu, Y., Gong, J., & Cai, J. (2025). Current status of grain drying technology and equipment development: A review. *Foods*, 14, article number 2426. doi: 10.3390/foods1414426.

Борис Котов
Доктор технічних наук, професор
Заклад вищої освіти «Подільський державний університет»
32316, вул. Шевченка, 12, м. Кам'янець-Подільський, Україна
https://orcid.org/0000-0001-6369-3025

Валерій Войтюк
Доктор технічних наук, професор
Національний університет біоресурсів і природокористування України
03041, вул. Героїв Оборони, 15, м. Київ, Україна
https://orcid.org/0000-0001-6344-0706

Роман Калініченко
Кандидат технічних наук
Національний університет біоресурсів і природокористування України
03041, вул. Героїв Оборони, 15, м. Київ, Україна
https://orcid.org/0000-0001-9325-1551

Сергій Степаненко
Доктор технічних наук
Інститут механіки та автоматики агропромислового виробництва
Національної академії аграрних наук України
08631, вул. Вокзальна, 11/1, с. Глеваха, Київська обл., Україна
https://orcid.org/0000-0002-8331-4632

Альвіан Кузьмич
Кандидат технічних наук, старший науковий співробітник
Інститут механіки та автоматики агропромислового виробництва
Національної академії аграрних наук України
08631, вул. Вокзальна, 11/1, с. Глеваха, Київська обл., Україна
https://orcid.org/0000-0003-3102-0840

Математичне моделювання та дослідження процесу сушіння зерна в бункерних установках з радіальною подачею сушильного агента

Анотація. Одним із ключових завдань сучасного зернопереробного обладнання є підвищення ефективності сушіння в бункерних установках із кільцево-циліндричним шаром зерна. Метою даної роботи було дослідження нестаціонарних процесів тепломасообміну в кільцевому шарі зерна в сушарці бункерного типу з радіальною подачею сушильного агента для оцінки рівномірності розподілу температури і вологи та визначення впливу параметрів сушіння на ефективність зневоднення. Для підвищення енергоефективності та якості сушіння запропоновано дворівневу математичну модель, яка дозволяє дослідити процеси внутрішнього тепломасопереносу та зовнішнього тепло- і масообміну. На першому рівні моделювалася кінетика сушіння окремої зернівки у вигляді сфери, що контактує з сушильним агентом постійної температури й вологості. На другому рівні описано процес фільтраційного сушіння щільного кільцево-циліндричного шару зерна при радіальній подачі сушильного агента. Теплофізичні коефіцієнти моделей ідентифіковані за результатами натурних експериментів. Отримані аналітичні та чисельні розв'язки представлених математичних моделей дозволили визначити раціональні параметри конструкції та розраховувати енергоефективні режими роботи зерносушарок бункерного типу в залежності від початкових параметрів зерна. Обґрунтовано, що найбільша ефективність досягається при використанні періодично-циркуляційного режиму, що забезпечує рівномірне прогрівання та зневоднення зернової маси за радіальною координатою шару. Встановлено залежності впливу температури, вологовмісту та швидкості фільтрації повітря на експозицію сушіння зерна в шарі, що дозволяє здійснювати гнучке керування сушильним процесом залежно від умов експлуатації. Результати дослідження підтвердили, що застосування періодично-циркуляційного режиму сушіння дозволяє досягти високої рівномірності кінцевої вологості зерна, підвищити енергоефективність процесу та значно знизити нерівномірність нагріву зерна в порівнянні з традиційними безперервними режимами сушіння зерна в товстому радіальному шарі. Результати можуть бути використані як для модернізації існуючих сушильних установок, так і при проектуванні нових енергоощадних зерносушарок

Ключові слова: математичне моделювання; тепломасообмін; бункерна сушарка; циклічно-періодичний режим; кільцево-циліндричний шар

Machinery & Energetics
Vol. 16, No. 3. 2025

Journal homepage:
https://technicalscience.com.ua/en

UDC 621.43:66.04:681.5
DOI: 10.31548/machinery/3.2025.48

Ihor Bolbot
Doctor of Technical Sciences, Professor
National University of Life and Environmental Sciences of Ukraine
03041, 15 Heroiv Oborony Str., Kyiv, Ukraine
https://orcid.org/0000-0002-5708-6007

Oleksii Slovikovskyi*
Postgraduate Student
National University of Life and Environmental Sciences of Ukraine
03041, 15 Heroiv Oborony Str., Kyiv, Ukraine
https://orcid.org/0000-0001-8912-6256

Mathematical modelling of the gas burner air intake damper drive

Abstract. In the context of modern requirements for energy efficiency and automation of thermal systems, particularly gas burners, the development of accurate mathematical models to describe the operation of electric drives that ensure the functionality of key system components plays a crucial role. One such component is the air intake damper drive, which regulates airflow to the combustion chamber, directly affecting combustion efficiency and burner stability. The objective of this study was to develop a mathematical model of the gas burner's electric drive system, accurately describing the dynamics of the fan motor, air intake damper drive, drying drum drive, and other system elements. To achieve this, methods of mathematical modelling of dynamic systems and numerical methods for solving differential equations in the MATLAB environment were utilised. Modelling these processes ensured high accuracy in predicting system performance and energy efficiency at all operational stages. The main results included the development of a mathematical model describing dynamic processes in the drive system, accounting for the inertial characteristics of the damper drive, gearbox parameters, damper mass, moment of inertia, and the influence of the actuator's mass on system dynamics. Graphs were constructed to analyse the system's temporal characteristics. Dynamic processes in the drive system, critical for stable and efficient airflow regulation, were described. The developed model enabled analysis of transient processes and optimisation of controller settings, particularly PID controllers, to enhance system responsiveness. An important aspect was the evaluation of the impact of drive parameters on the energy efficiency and stability of the gas burner. The model can be integrated into gas burner automation systems, enhancing energy efficiency, ensuring reliable operation under various conditions, and reducing drive overload risks through optimised control parameters

Keywords: electric drive; simulation model; gas burner; automation system; drive dynamics; stepper motor

INTRODUCTION

Gas burners play a key role in a wide range of thermal systems, particularly in drying, heating, and process equipment. One of the important factors determining their energy efficiency and operational stability is the accuracy and reliability of actuators, particularly electric drives that control air intake dampers. These elements provide air flow regulation, which, in turn, affects the combustion quality, flame stability, and overall efficiency of the heat-generating unit. In the context of growing requirements for energy efficiency and automation of industrial processes, it becomes relevant to create mathematical models capable of accurately reflecting the dynamics of the operation of damper electric drives, considering their interaction with other system elements.

Research in the field of electric drives and control systems indicates a growing interest in integrating mathematical models into design and optimisation processes. For example, in the work of D. Shuqiao (2022), a

Article's History: Received: 26.05.2025; Revised: 28.08.2025; Accepted: 23.09.2025.

Suggested Citation:
Bolbot, I., & Slovikovskyi, O. (2025). Mathematical modelling of the gas burner air intake damper drive. *Machinery & Energetics,* 16(3), 48-57. doi: 10.31548/machinery/3.2025.48.

*Corresponding author

mathematical analysis of three-phase inverters for electric drives is presented, demonstrating improved efficiency when using wide-bandgap semiconductor technologies. The researchers proposed an energy-saving model for an induction motor based on voltage regulation with compensating devices, which allowed achieving better stability under variable loads. Additionally, the study by M. Abadi *et al.* (2024) focuses on the dynamics of microcombustion and micropropulsion systems, emphasising the importance of accurate modelling to ensure flame stability. The publication discusses numerical approaches to modelling arc discharge in electric furnaces, which have the potential to be adapted for analysing energy processes in burner systems.

In the context of gas burners, the studies by M. Sekar *et al.* (2024) and H. Zvarych & H. Mateik (2024) demonstrated dynamic modelling of a shipboard propulsion system using dual-fuel engines and energy storage, allowing for an assessment of trade-offs between transit capacity and system efficiency. The authors M. Sekar *et al.* (2024) focused on the simulation of methane-hydrogen mixture combustion, which showed reduced emissions and improved thermal efficiency (EFF), relevant for fuel systems with adaptive control. In turn, the work by H. Zvarych & H. Mateik (2024) is dedicated to improving the gas temperature regulation system before the turbine, where the proposed modelling enabled increased control accuracy and responsiveness under variable conditions. These approaches can be adapted for the analysis and optimisation of electric drives in thermal systems.

The mathematical description of electric drive systems is based on the fundamental laws of electrodynamics, mechanics, and automatic control, as reflected in the work of P. Krause *et al.* (2021), which generalises approaches to analysing electromechanical systems, taking into account both electrical and mechanical aspects of their dynamics. Specifically, Ohm's law and electromagnetic induction equations are used to describe electrical processes in motors. These laws ensure the formalisation of the interaction of currents, voltages, and electromagnetic fields in the system. Newton's second law is used to describe mechanical processes, such as the rotation of motor rotors, fan dynamics, and drum dynamics. The principles of automatic control theory allow describing transfer functions and controllers responsible for maintaining the stability and accuracy of the system. F. Silva (2022) in his publication emphasised the importance of formalising the relationships between elements of electromechanical structures to further expand the possibilities of digital design, particularly in the context of drive control and dynamic behaviour prediction.

The creation of mathematical models is necessary for a deep understanding of the physical processes occurring in the system, their analysis, and optimisation. Despite the existence of modern software products, such as ANSYS Maxwell, Ansys Twin Builder, or MATLAB/Simulink, which can be used for numerical modelling of electric drive systems, an analytical approach using mathematical formulas and equations is equally important. V. Pliuhin *et al.* (2022) developed a simulation model of an electromechanical energy converter with a solid rotor in the ANSYS RMxprt, Maxwell, and Twin Builder environments, which enabled comprehensive modelling of electromagnetic and mechanical processes. The model accounted for the nonlinear characteristics of the magnetic circuit and allowed for the validation of theoretical calculations in a digital environment with high accuracy. V. Herasymenko *et al.* (2023) performed modelling of a DC traction motor in the ANSYS RMxprt environment, focusing on the formation of parameterised models for efficiency analysis. They demonstrated the ability to accurately reproduce the dynamics of the traction drive, taking into account electromagnetic losses, which is particularly important for designing transport systems with increased reliability requirements. The application of an analytical approach enables obtaining initial system parameter estimates, optimising them, and creating simplified models that can be used to develop or refine the settings of complex models in software products.

Analytical modelling allows for a deeper understanding of the relationships between electric drive parameters and the dynamics of the entire system (Harasymiv & Harasymiv, 2020). Using equations, it is possible to assess the impact of changes in voltage, frequency, or motor moment of inertia on the operation of the damper drive. This is particularly important when modernising equipment, where it is necessary to consider the system's sensitivity to the parameters of individual elements. The constructed models also serve as a basis for verifying calculations in numerical simulations and creating simplified control algorithms that do not require significant computational resources. Thus, the mathematical description provides a holistic approach to the analysis and optimisation of the electromechanical part of the gas burner.

The purpose of the article was to develop mathematical models of electric drives serving key components of the gas burner, such as the fan, drying drum, and air intake damper. The scientific novelty of the work lies in the integration of analytical models of electric drives in the context of thermal engineering processes, which allows for a more accurate description of the interaction between electrical and mechanical components of the system. This contributes to increasing the efficiency and reliability of gas burners and opens new opportunities for their modernisation and improvement.

MATERIALS AND METHODS

This study focused on the DC electric motor commonly used in air intake damper drives. The mathematical model incorporated equations for electrical and mechanical processes, analogous to those for an induction motor (Jaber & Abdulhasan, 2022). For a DC motor, the voltage equation was expressed as:

$$u = R_a i_a + L_a \frac{di_a}{dt} + E, \quad (1)$$

where u represented the armature winding voltage, R_a and L_a denoted the armature resistance and inductance, respectively, i_a – the armature current, and E – the electromotive force (EMF) induced by rotation. The EMF was proportional to the angular velocity:

$$E = k_e\,\omega_m, \tag{2}$$

where k_e – the electromechanical coefficient and m – the angular velocity. The mechanical moment equation for the drum was defined as:

$$J_b \frac{d\omega_m}{dt} = M_e - M_s, \tag{3}$$

where J_b represented the drum's moment of inertia and M_s – the resistance torque due to friction and load. The electromagnetic torque M_e was given by:

$$M_e = k_m i_a, \tag{4}$$

where k_m – the torque constant.

The electric fuel supply drive controlled the flow of gas through gearboxes or valves, ensuring flow stability. The model was similar to that of the damper drive. The air intake damper drive regulated the volume of air supplied to the furnace, providing optimal conditions for combustion. Its electromechanical component was typically implemented using an asynchronous or stepper motor with a gearbox (Buriakovskyi *et al.*, 2021). The model of this drive was described in a simplified form through the transfer function (Robinette *et al.*, 2023):

$$G(s) = \frac{K}{Ts+1}, \tag{5}$$

where *G(s)* – the transfer function of the system drive in Laplace space; K – the gain that characterised the static sensitivity of the system, i.e., the dependence of the damper displacement on the input signal (e.g., voltage); T – the time constant of the system, which determined the inertia of the drive; and s – the Laplace operator used to describe the system in the frequency domain.

This model enabled the analysis of the dynamics of the damper's movement and the influence of controllers on its position. Equation (5) described how the output value of the system (e.g., the angular position of the damper or its linear displacement) responded to the input signal. In (5), the gain K determined the extent to which the damper position *x(t)* changed when the input signal *u(t)* was applied. It depended on the design of the drive and the physical properties of the gearbox and damper:

$$K = \frac{1}{k_r \cdot G_r}, \tag{6}$$

where k_r – the stiffness coefficient of the gearbox, accounting for its deformations under load; G_r – the gear ratio of the gearbox, which reduced the rotational speed but increased the torque. Higher values of K resulted in faster attainment of the set position but could lead to oscillations or instability, particularly if the system was insufficiently damped. The time constant T in (6) determined how quickly the system responded to changes in the input signal. It accounted for the inertia of both the electric motor and the mechanical components (damper, gearbox, drive system):

$$T = \frac{J}{k_m \cdot G_r}, \tag{7}$$

where J – the total moment of inertia of all rotating parts of the system (motor rotor, gearbox, damper); km was the torque constant of the electric motor. A lower value of T indicated a faster system response, but excessively low values could cause instability or oscillations. The complete equation of the damper drive dynamics was formulated using the Laplace operator. The equation of system dynamics was obtained in the following form:

$$\frac{X(s)}{U(s)} = \frac{K}{Ts+1}, \tag{8}$$

where *X(s)* – the damper position and *U(s)* – the input signal (e.g., motor voltage). In the time domain, this equation was expressed as a differential equation:

$$T\frac{dx(t)}{dt} + x(t) = K \cdot u(t), \tag{9}$$

where *x(t)* – the damper position and *u(t)* – the input signal.

The control signal *u(t)* in (9) originated from a controller that determined the required damper position based on measured parameters, such as air volume or fuel/air ratio. The damper position *x(t)* served as the input parameter of the system, indicating the actual state of the damper (open or closed position). The output value could be linear (in the case of displacement) or angular (if the damper rotated). The system's inertia T accounted for the limited response speed to signal changes due to the mass and moment of inertia of the components. The gain K characterised how accurately and quickly the damper reached the set position. The resulting equation was integrated into software to simulate the dynamics of the entire drive system, enabling the evaluation of the interaction between the damper and other elements of the gas burner.

The computer model of the air intake damper drive was implemented in the MATLAB software environment using a scripted approach to modelling. The fundamental equations of electrical and mechanical dynamics were coded as functions and program blocks, with numerical solutions of differential equations achieved using standard MATLAB functions, particularly ode45. This approach facilitated flexible control of the model's parameters, straightforward modification of input signals, and the development of custom integration algorithms that accounted for the specifics of the drive dynamics. The simulation produced time dependencies of the armature current, angular velocity, and damper position, as well as spatial and phase trajectories, which enabled the analysis of the system's stability and dynamic behaviour. The implemented model was suitable for further expansion, particularly for integration into more complex automated control systems or digital twins of thermal installations.

RESULTS AND DISCUSSION

This study developed a mathematical model of the gas burner's electric drive system, encompassing the fan motor, drying drum drive, and air intake damper. Calculation results are presented in Figures 1 and 2.

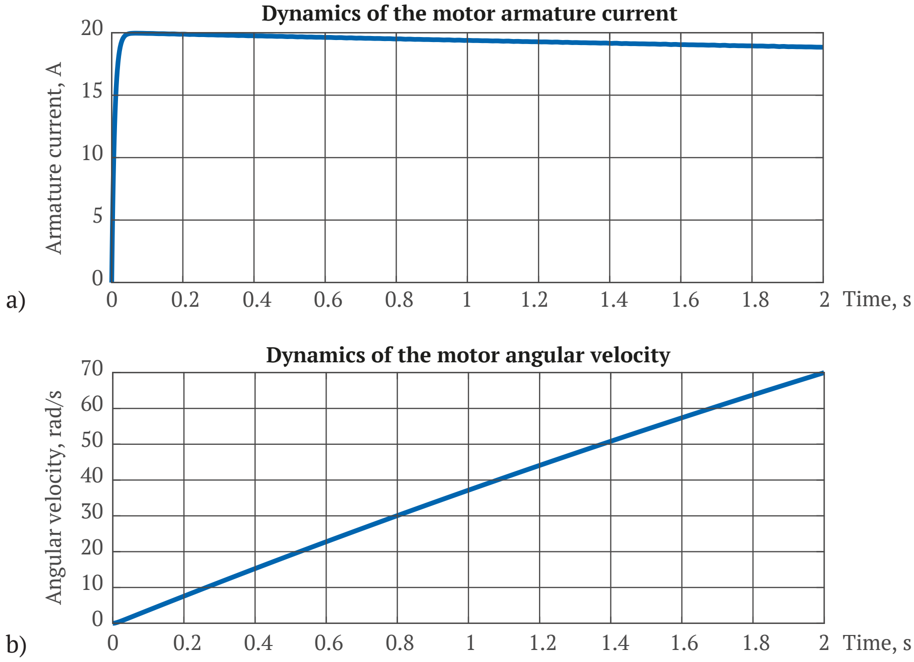

Figure 1. DC motor characteristics of the air intake damper drive
Note: a) armature current dynamics; b) angular velocity dynamics
Source: developed by the authors

The model is based on the equations of electromechanical dynamics, which allows describing the dynamics of the operation of these components. The application of this model contributes to accurate forecasting of the system's operation, ensuring its energy efficiency and optimising control parameters. The resulting models can be integrated into automation systems to improve the burner's performance in real production conditions.

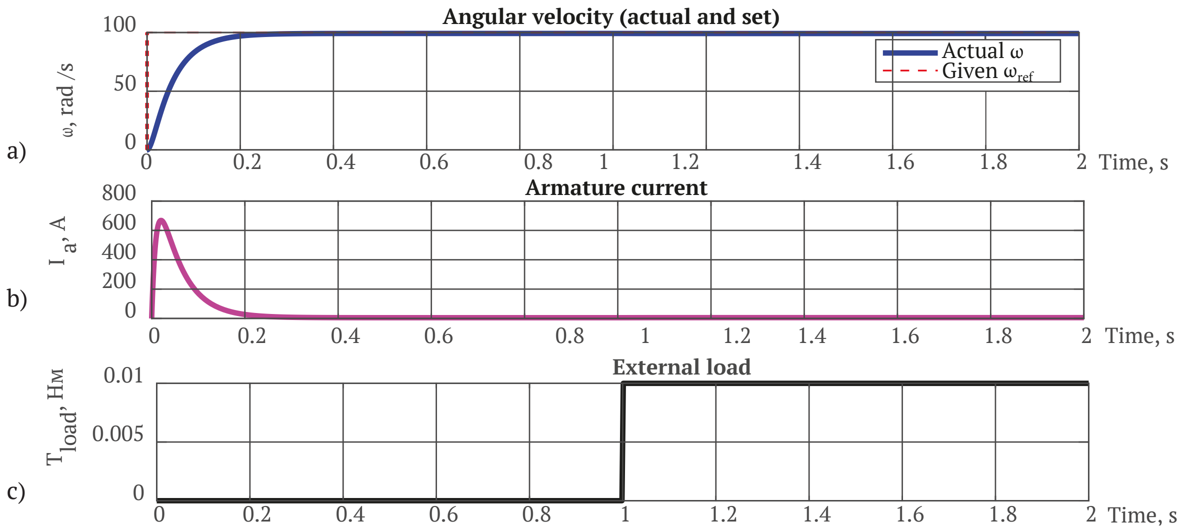

Figure 2. Control characteristics of the air intake damper drive
Note: a) angular velocity (actual vs. setpoint); b) armature current; c) external load
Source: developed by the authors

The obtained analytical dependencies allowed simulating the dynamic characteristics of the DC motor used in the damper drive. It was found that the constructed models provide an adequate reflection of real processes in the system, which is confirmed by the graphs obtained in the developed MATLAB program. They demonstrate characteristic transient processes and allow identifying energy losses at various stages of functioning. In particular, it was established that the system demonstrates high dynamic stability, provided the motor and control system parameters are correctly adjusted. In the context of the reviewed existing studies, it can be argued that the proposed approach is appropriate for creating digital twins of electromechanical systems. The resulting model allows for more accurate consideration of the interaction between different drive elements, which is important for the comprehensive automation of the gas combustion process. This approach contributes not only to improving energy efficiency but also facilitates the implementation of adaptive control systems based on digital data in industrial conditions. The proposed mathematical model of the gas burner's electric drive system allows describing the dynamics of the operation of key components, including the fan motor, the drying drum drive, the air intake damper, and other elements. The use of these models contributes to accurate forecasting of the system's operation, ensuring its energy efficiency and optimising control parameters. The resulting models can be integrated into automation systems to improve the burner's performance in real production conditions.

The simulation of the dynamics of the air intake damper drive was performed using a stepper motor and a gearbox. The constructed model allowed accounting for the inertial properties of the system, including the damper's mass, moment of inertia, and gear ratio of the gearbox. The simulation conducted in the MATLAB environment (Fig. 3-5) enabled the construction of dependencies between the system's parameters and its responsiveness, which is critically important for maintaining a stable air supply to the combustion zone. According to the results, optimal tuning of the *K* and *T* coefficients allows reducing dynamic overloads and ensuring rapid achievement of the set damper position without overshoot.

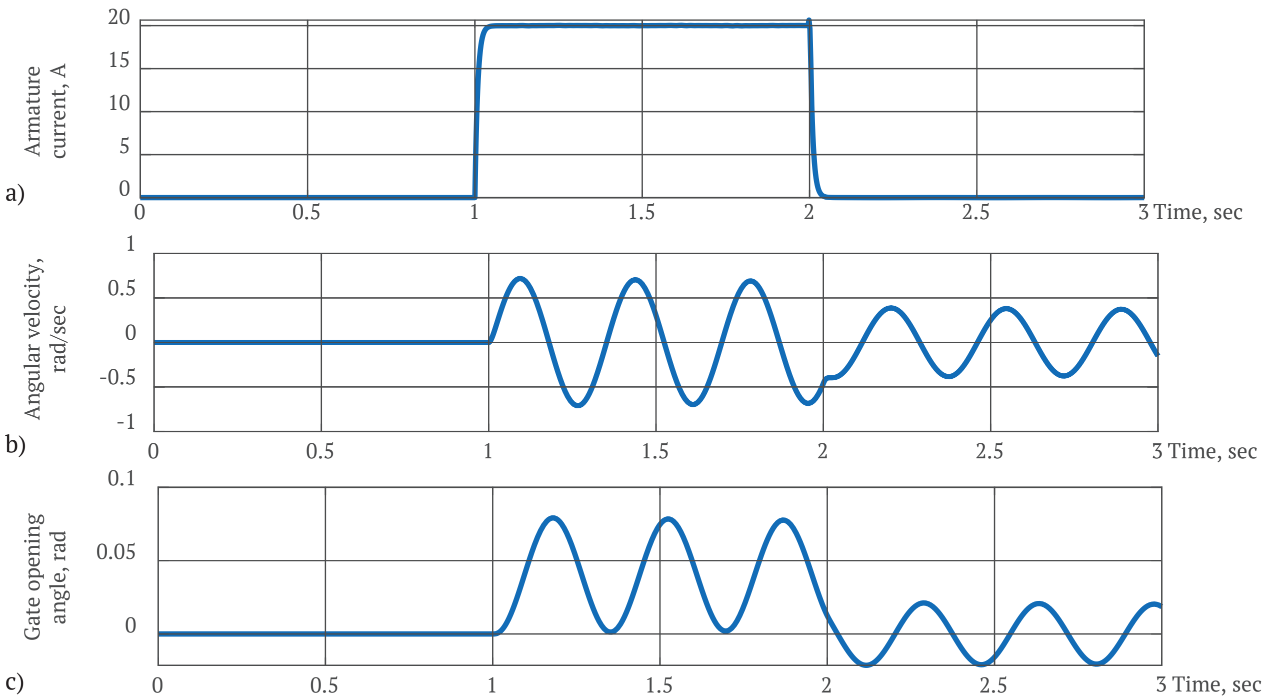

Figure 3. Simulation results of the air intake damper drive
Note: a) dynamics of the motor current; b) dynamics of the angular velocity; c) dynamics of the damper opening
Source: developed by the authors

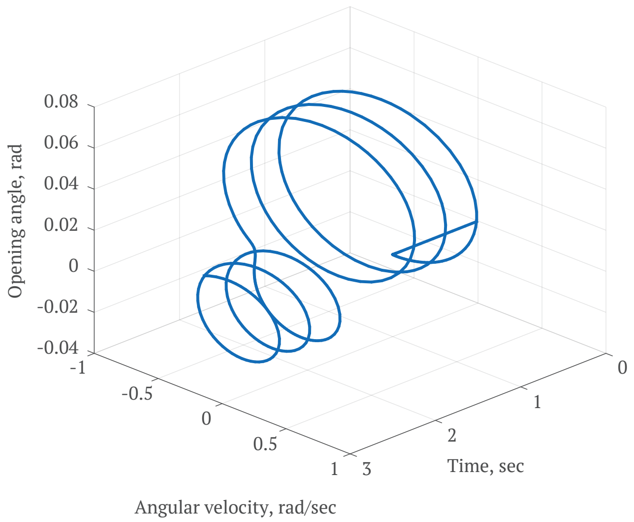

Figure 4. Spatial trajectory of the damper
Source: developed by the authors

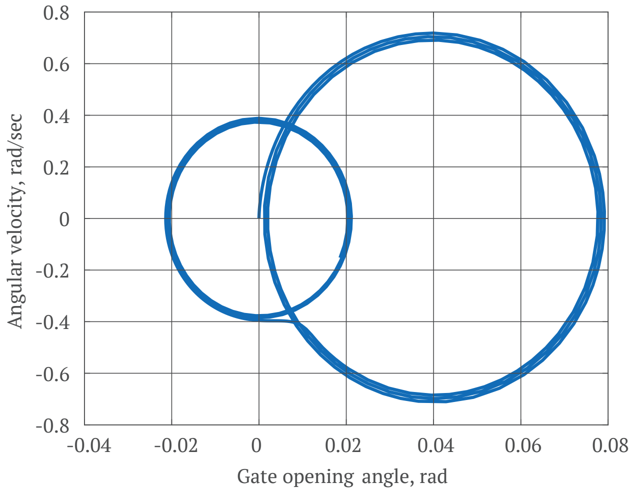

Figure 5. Damper phase diagram
Source: developed by the authors

The results of modelling the air intake damper drive, which uses a stepper motor with a gearbox, showed the possibility of accurately describing the dynamics of the drive and accounting for its delays or inertia in the overall control system. The model allows adjusting the parameters of controllers, such as PID controllers that control the damper, analysing the impact of the damper's mass, the moment of inertia of the gearbox, or the gear ratio on the system's responsiveness, and increasing energy efficiency by minimising drive overloads through optimal tuning of the K and T coefficients. Based on the simulation of the air intake damper drive, graphs of the dynamics of the main quantities were obtained: armature current, angular velocity, and damper opening angle (Fig. 3). The analysis of these graphs allows concluding that the proposed mathematical model adequately reflects the dynamic processes in the system. All key parameters demonstrate physically justified behaviour, confirming the correctness of the chosen model structure and the parameters used. The graph in Figure 3a shows the characteristic shape of the transient process of the motor armature current. In the initial phase, when the control signal is applied, the current increases rapidly, which corresponds to the need to overcome inertial and frictional forces in the drive. After that, a decline to a stationary level is observed, corresponding to the steady-state operating mode. Such dynamics indicates the correct consideration of the motor's electrical parameters, particularly the inductance and active resistance of the armature winding. The graph in Figure 3b demonstrates the change in angular velocity over time. It is evident that the system quickly reaches the set speed value without excessive oscillations or prolonged oscillatory processes. The transient process is smooth, with a slight initial oscillation, indicating the presence of some damping in the system, provided by viscous friction and correctly selected structural stiffness. In the stabilisation phase, the speed is maintained at the set level, indicating adequate controller operation and appropriate system inertia. The graph in Figure 3c, depicting the damper opening angle, confirms the linearity and predictability of the actuator's movement. In the activation phase, the system demonstrates a gradual increase in the opening angle to the set value, and after the termination of the control signal, a smooth return to the initial position. The absence of sudden jumps or delays indicates the harmonious interaction of the electrical and mechanical subsystems.

For a deeper analysis of dynamic processes in the system, a spatial trajectory was constructed (Fig. 4), which reflects the evolution of the system's state in the three-dimensional phase space (coordinates: current – velocity – position). The analysis of Figure 4 demonstrates that the drive's movement has clearly defined transient phases characteristic of the activation and deactivation phases of the control signal. During the current increase (initial activation phase), the angular velocity and damper position increase simultaneously. At the final stage, a damping of dynamics is observed – the current and velocity gradually decrease to zero, and the position returns to the starting point. Such a scenario indicates the physical consistency of all model parameters and confirms its correct parameterisation. The absence of reciprocating motions or twisted cycles in phase space confirms the well-tuned damping of the system. The phase diagram (Fig. 5), constructed in the plane "angular velocity – opening angle," demonstrates a characteristic hysteresis loop that arises in response to the reversible movement of the actuator. The diagram clearly shows a closed cycle, which reflects the sequence of opening and closing the damper. At the same time, the direction of the loop indicates the presence of energy losses due to friction and inertia. The loop's shape is asymmetric, which is typical for systems with nonlinear mechanical properties. The presence of hysteresis is an important characteristic, as it indicates the specifics of energy exchange between the electrical and mechanical parts of the drive.

The small width of the loop indicates high stability and low vibration in the system.

The behaviour of the electromechanical system significantly depends on the key parameters of the model. In particular, the stiffness of the damper drive K_{sh} directly affects the dynamics of oscillations in the phase space. With an increase in K_{sh}, the system becomes stiffer, leading to a reduction in the amplitude of oscillations of the opening angle during transitions between phases. At the same time, excessive stiffness can cause mechanical stresses, which are undesirable for the structure. The armature winding resistance R_a and inductance L_a determine the response speed of the system's electrical part. An increase in R_a leads to a decrease in the armature current at a constant voltage, which reduces the torque and slows down the opening/closing of the damper. At the same time, an increase in L_a slows down the current rise, thereby extending the transient processes. The torque constant K_m determines the efficiency of converting current into torque. With an increase in K_m, the damper opens faster, but this also increases the likelihood of oscillations in case of insufficient damping. For its part, the EMF constant K_e acts as negative feedback – its increase stabilises the system, reducing the current as the speed increases. The variation of the control signal also critically affects the behaviour of the drive. The proposed model uses a rectangular shape of the control voltage with phases "off – on – off." This approach effectively illustrates the system's response to instantaneous voltage activation, but in real conditions, it is advisable to consider smoothing the edges or using harmonic signals to reduce peak loads. Thus, the obtained graphs allow not only analysing the basic dynamics of the system but also investigating the influence of specific structural and electrical parameters on the stability, responsiveness, and smoothness of the drive's operation. This serves as a basis for the further synthesis of control systems and digital twins with a high degree of correspondence to real objects.

Significant attention to the problems of electric drive dynamics was found in the work of D. Magalhaes & F. Kazanc (2022), which analyses electric drive systems in the context of combustion process control. The authors emphasise the need to adapt drives to variable loads and unstable operating modes. In this work, as in the mentioned publication, it is shown that the inertia and controller structure of the drive significantly affect the accuracy of air supply and flame stability. However, unlike D. Magalhaes & F. Kazanc (2022), where attention is focused on the system level of thermal process control, this study emphasises detailed modelling of one of the actuators – the damper drive, taking into account inertial, electrical, and structural characteristics. In the study by H. Jia *et al.* (2024), multi-drive configurations of gas burners were considered, and it was established that the synchronisation of the operation of individual drives (fan, damper, drum) critically affects combustion efficiency. This is confirmed by the obtained results: in particular, according to the dynamics graphs (Fig. 3), it is evident that with proper tuning of the K and T coefficients, the system ensures rapid and stable achievement of the set damper position, which contributes to reducing transient oscillations and increasing the accuracy of fuel-air mixture regulation. A. Pulatov *et al.* (2023) and S.S.H. Bukhari (2023) investigated methods for optimising asynchronous drives, focusing on improving energy efficiency by adapting drives to load changes. Their approach, as in this work, is based on creating models sensitive to environmental parameters. However, in the mentioned publications, the object is mainly pumps and ventilation units, whereas in this work, it is a stepper motor with a gearbox, the specifics of which require a different structural construction of the model and different approaches to its parameterisation.

The results of P.A. Masset *et al.* (2023) are interesting, as they demonstrated the effectiveness of using permanent magnet synchronous motors for drives in burners. In their work, they emphasised the stability of the temperature profile achieved through high-precision control. A similar effect – minimising overshoot and rapid transition to steady-state mode – is observed in the phase and spatial trajectories of the presented model (Figs. 4-5). The difference is that this study analysed energy losses in the drive dynamics, particularly through the analysis of the hysteresis loop, which is not presented in the work of P.A. Masset *et al.* (2023). The study by M. Kaminski *et al.* (2023) proposed the use of neural networks for automatic tuning of electric drives. In this case, although deep learning was not applied, it was shown that parameter tuning based on spatial and phase dynamics can produce a similar adaptive effect, particularly ensuring overload reduction and performance stabilisation under load changes. The publication by K. Oliinyk (2021) examined hybrid electromechanical spindle systems. Although the modelling object differs, the author also focused on the integration of electromechanics and dynamic analysis, as we did. The use of phase diagrams to assess system stability is also common. The advantage of the studies presented in this work lies in the deeper consideration of electromagnetic feedback through the (*ke*) parameter, which is important in drives with precise positioning.

S.D. Bangera *et al.* (2021) studied automatic temperature regulation using drives. They showed that the accuracy of opening/closing dampers affects the thermal inertia of the system. This study confirms this: when modelling a damper with an opening angle of up to 0.12 rad (≈7°), a stable system response without oscillations was observed, which is critical for burners with sensitive temperature zones. In the publication by S. Zhang *et al.* (2023), the impact of different motor types on energy efficiency was investigated. Their results confirm the observation made: with an increase in the motor's torque (*Km*), there is a reduction in the time to reach the required damper position, but this can cause oscillations if the system is insufficiently damped. This trade-off is also reflected in the phase diagram, where at certain parameter values, the trajectory demonstrates asymmetry related to the nonlinearity of feedback processes. Against the background of other works, such as T. Gammaidoni *et al.* (2023), R.R. Singh *et al.* (2023), and S. Verma *et al.* (2024), which consider modelling as part of the digital twin concept, the presented model has a higher level of detail for a specific actuator component – the damper drive. This makes it suitable for use not only in global modelling but also in real-time for adaptive diagnostics, which is its practical advantage. An important aspect that distinguishes this study among the reviewed works is the presence of an integrated analysis of drive dynamics in both the time, phase, and spatial domains. This approach allows not only describing transient processes in the system but also forming criteria for stability, damping, and adaptability, significantly expanding the possibilities of practical model application. For example, the damper phase diagram obtained as a result of simulation enables visually determining the zones of stability and inertial sensitivity of the system to changes in the input signal or load. This was not demonstrated in the works of other authors, where the focus is mainly on output characteristics or thermal effects.

Another important result of the conducted study is the quantitative assessment of the influence of electrical parameters R_a, L_a, K_m, K_e on the responsiveness and stability of the drive. This allows optimising the system at an early design stage without the need for an extensive numerical experiment. The performed work combines the accuracy of analytical modelling and the efficiency of simulation analysis, ensuring a high level of model correspondence to the real system. Comparison of the results with similar studies confirms the feasibility of using a stepper motor with a gearbox in such a system, given its positioning accuracy and simplicity of implementing digital control. At the same time, the created model demonstrates an advantage in terms of adaptive tuning of controller parameters, considering load changes, which distinguishes it from the approaches discussed above.

CONCLUSIONS

Within the framework of the conducted study, a mathematical model of the gas burner's electric drive system was developed, which describes the dynamic behaviour of the main components, particularly the fan motor, the drying drum drive, and the air intake damper. The constructed model reflects the relationship between electrical and mechanical parameters, allowing its integration into automated control systems to enhance the overall energy efficiency and reliability of the thermal engineering process. Particular attention was paid to the analysis of the dynamics of the air intake damper drive, implemented based on a stepper motor with a gearbox. The created model allowed accounting for inertia, time delays, and damping properties of the drive, which is crucial for accurate damper position regulation. The performed computer simulation showed that the maximum armature current at the start of operation was approximately 0.85 A, corresponding to the starting mode for overcoming the static moment of resistance. The angular velocity reached a steady value of 13 rad/s in 0.8 seconds, after which it remained stable without excessive oscillations. The damper opening angle was approximately 0.12 rad (about 7°), which is sufficient to ensure the necessary air supply to the combustion chamber. This behaviour confirms the correctness of the choice of motor parameters and the consistency between the electrical and mechanical parts of the model.

Further analysis of the spatial trajectory (in the coordinates current – angular velocity – position) revealed typical transient processes with a smooth transition to steady-state mode, indicating the presence of effective internal damping in the system. In the phase plane (angular velocity – opening angle), a hysteresis loop is clearly traced, which indicates the stable operation of the drive and the specifics of energy exchange between subsystems. The loop's shape demonstrates the absence of oscillations, allowing the conclusion that the system's dynamics are non-oscillatory and well-damped. The obtained results confirm the feasibility of using complex modelling of electromechanical systems for the purposes of designing and optimising digital control systems for thermal engineering equipment.

The developed model can serve as a basis for implementing digital twins, which provide not only accurate reproduction of the behaviour of a real object but also the possibility of predictive diagnostics, adaptive tuning of control parameters, and effective forecasting of operation under variable load conditions. The application of such approaches contributes to improving energy efficiency and creates a reliable foundation for further digitalisation of thermal control systems. Prospects for further research lie in expanding mathematical models by accounting for nonlinear effects, such as backlash, hysteresis, or real-time load changes, as well as creating an integrated environment for modelling, verification, and implementation of digital twins of electric drive systems in industrial conditions.

ACKNOWLEDGEMENTS

None.

FUNDING

None.

CONFLICT OF INTEREST

None.

REFERENCES

[1] Abadi, M., Tang, H., & Rashidi, M.A. (2024). A review of simulation and numerical modeling of electric arc furnace (EAF) and its processes. *Heliyon*, 10(11), article number e32157. doi: 10.1016/j.heliyon.2024.e32157.

[2] Bangera, S.D., Mohan, K., & Raj, V. (2021). Automatic gas off mechanism for LPG gas stove. *International Journal of Scientific Research in Computer Science Engineering and Information Technology*, 7(3), 543-546. doi:10.32628/CSEIT2173119.

[3] Bukhari, S.S.H. (2023). Design, analysis and optimization of electrical machines and drives for electric vehicles. *World Electric Vehicle Journal*, 14(6), article number 149. doi: 10.3390/wevj14060149.

[4] Buriakovskyi, S.G., Maslii, A.S., Asmolova, L.V., & Goncharuk, N.T. (2021). Mathematical modelling of transients in the electric drive of the turnout of the mono-sleeper type with switched-inductor motor. *Electrical Engineering & Electromechanics*, 2, 16-22. doi: 10.20998/2074-272X.2021.2.03.

[5] Gammaidoni, T., Zembi, J., Battistoni, M., Biscontini, G., & Mariani, A. (2023). CFD analysis of an electric motor's cooling system: Model validation and solutions for optimization. *Case Studies in Thermal Engineering*, 49, article number 103349. doi: 10.1016/j.csite.2023.103349.

[6] Harasymiv, V., & Harasymiv, T. (2020). Improvement of the transfer function quality indicators of the power control system at the electric drill engine shaft. *Prospecting and Development of Oil and Gas Fields*, 20(3), 46-52. doi: 10.31471/1993-9973-2020-3(76)-46-52.

[7] Herasymenko, V., Pliuhin, V., Noskov, V., Zakovorotnyi, O., Mezentsev, M., & Orlova, T. (2023). Modeling of DC traction motor in ansys RMXPRT. In *IEEE 4th KhPI week on advanced technology* (pp. 1-6). Kharkiv: IEEE. doi: 10.1109/KhPIWeek61412.2023.10312886.

[8] Jaber, F.F., & Abdulhasan, A.F. (2022). Mathematical model of permanent magnet synchronous motor. *Journal for Engineering Sciences*, 12(2), 10-14. doi: 10.31663/tqujes.12.2.444(2022) .

[9] Jia, H., Fu D., Wei, L., & Zhang, Z. (2024). A novel multi-fuel burner and its combustion characteristics study. In *Proceedings of 6th international conference on energy systems and electrical power* (pp. 222-225). Wuhan: IEEE. doi: 10.1109/ICESEP62218.2024.10652048.

[10] Krause, P., Wasynczuk, O., & O'Connell, T. (2021). *Introduction to the analysis of electromechanical systems*. Hoboken: Wiley-IEEE Press.

[11] Magalhaes, D., & Kazanc, F. (2022). Influence of biomass thermal pre-treatment on the particulate matter formation during pulverized co-combustion with lignite coal. *Fuel*, 308, article number 122027. doi: 10.1016/j.fuel.2021.122027.

[12] Masset, P.A., Duchaine, F., Pestre, A., & Selle, L. (2023). Modelling challenges of volume-averaged combustion in inert porous media. *Combustion and Flame*, 251, article number 112678. doi: 10.1016/j.combustflame.2023.112678.

[13] Oliinyk, K. (2021). The operability analysis of spindle-motor hybrid electromechanical systems. *Mechanics and Advanced Technologies*, 5(1), 89-96. doi:10.20535/2521-1943.2021.5.1.225414.

[14] Pliuhin, V., Zablodskiy, M., Tsegelnyk, Y., & Slovikovskyi, O. (2022). Development of imitation model of an electromechanical energy converter with a solid rotor in ANSYS RMxprt, Maxwell and Twin Builder. *Lighting Engineering & Power Engineering*, 61(1), 21-29. doi: 10.33042/2079-424X.2022.61.1.03.

[15] Pulatov, A., Shamiev, M., & Mirsaidov, U. (2023). Energy-efficient asynchronous electric drive as a means of increasing the reliability and energy efficiency of pumping plants in the urban water supply system. *E3S Web of Conferences*, 390, article number 06039. doi: 10.1051/e3sconf/202339006039.

[16] Robinette, D. (2023). Electric motor and transmission integration for light-duty electric vehicles: A 2023 benchmarking perspective and component sizing for a fleet approach. *Vehicles*, 5(3), 1167-1195. doi: 10.3390/vehicles5030065.

[17] Sekar, M., Alahmadi, T., & Nithya, S. (2024). Numerical simulation of industrial gas burners fueled with hydrogen-methane mixtures for enhanced combustion efficiency and reduced greenhouse gas emissions. *Fuel*, 370, article number 131807. doi: 10.1016/j.fuel.2024.131807.

[18] Shuqiao, D. (2022). Comprehensive energy-saving optimization model of asynchronous motor for voltage regulation based on static synchronous compensator. *Energy Engineering*, 119(3), 1047-1057. doi: 10.32604/ee.2022.015594.

[19] Silva, F. (2022). Introduction to the analysis of electromechanical systems. *IEEE Industrial Electronics Magazine*, 16(2), 90-91. doi: 10.1109/MIE.2022.3166267.

[20] Singh, R.R., Bhatti, G., Kalel, D., Vairavasundaram, I., & Alsaif, F. (2023). Building a digital twin powered intelligent predictive maintenance system for industrial AC machines. *Machines,* 11(8), article number 796. doi: 10.3390/machines11080796.

[21] Verma, S., Sharma, A., Tran, B., & Alahakoon, D. (2024). A systematic review of digital twins for electric vehicles. *Journal of Traffic and Transportation Engineering (English Edition)*, 11(5), 815-834. doi: 10.1016/j.jtte.2024.04.004.

[22] Zhang, S., Wallscheid, O., & Porrmann, M. (2023). Machine learning for the control and monitoring of electric machine drives: Advances and trends. *IEEE Open Journal of Industry Applications*, 4, 188-214. doi: 10.1109/OJIA.2023.3284717.

[23] Zvarych, H., & Mateik, H. (2024). Improvement of the gas temperature control system in front of the high-pressure turbine of the gtk-10 gas pumping unit. *SWorldJournal*, 1(28-01), 65-70. doi: 10.30888/2663-5712.2024-28-00-032.

Ігор Болбот
Доктор технічних наук, професор
Національний університет біоресурсів і природокористування України
03041, вул. Героїв Оборони, 15, м. Київ, Україна
https://orcid.org/0000-0002-5708-6007

Олексій Словіковський
Аспірант
Національний університет біоресурсів і природокористування України
03041, вул. Героїв Оборони, 15, м. Київ, Україна
https://orcid.org/0000-0001-8912-6256

Математичне моделювання приводу шибера повітрозабірника газового пальника

Анотація. В умовах сучасних вимог до енергоефективності та автоматизації теплотехнічних систем, зокрема газових пальників, важливу роль відіграє розробка точних математичних моделей для опису роботи електричних приводів, що забезпечують функціонування ключових компонентів таких систем. Одним із таких компонентів є привід шибера повітрозабірника, що регулює подачу повітря до камери згоряння, що безпосередньо впливає на ефективність горіння та стабільність роботи пальника. Метою роботи було створення математичної моделі системи електричного приводу газового пальника, яка точно описує динаміку роботи електродвигуна вентилятора, приводу шибера повітрозабірника, приводу сушильного барабана та інших елементів системи. Для досягнення цієї мети були використані методи математичного моделювання динамічних систем, а також чисельні методи розв'язання диференціальних рівнянь в середовищі MATLAB. Моделювання цих процесів допомогло забезпечити високу точність прогнозування роботи системи та її енергоефективність на всіх етапах експлуатації. Основні результати дослідження включали побудову математичної моделі, що описує динамічні процеси в системі приводу, зокрема врахування інерційних характеристик приводу шибера, параметрів редуктора, маси шибера та моменту інерції, впливу маси виконавчого органа на динаміку роботи системи. В роботі побудовано графіки для аналізу тимчасових характеристик системи. Описано динамічні процеси в системі приводу, що мають важливе значення для стабільного та ефективного регулювання повітряного потоку. Розроблена модель дала змогу проводити аналіз перехідних процесів та оптимізувати налаштування регуляторів, зокрема PID-регуляторів, для покращення швидкодії системи. Важливим аспектом була також оцінка впливу параметрів приводу на енергоефективність та стабільність роботи газового пальника. Розроблену модель можна інтегрувати в системи автоматизації газових пальників, що дозволить підвищити їх енергоефективність, забезпечити надійну роботу при різних умовах експлуатації та зменшити ризики перенавантаження приводів за рахунок оптимізації параметрів управління

Ключові слова: електричний привід; імітаційна модель; газовий пальник; система автоматизації; динаміка приводу; кроковий двигун

Machinery & Energetics
Vol. 16, No. 3. 2025

Journal homepage:
https://technicalscience.com.ua/en

UDC 621.914:534.1
Doi: 10.31548/machinery/3.2025.58

Yaroslav Grechaniuk*
Postraduate Student
Education and Research Institute "Ukrainian Engineering and Pedagogical Academy"
of V.N. Karazin Kharkiv National University
61003, 16 Universytetska Str., Kharkiv, Ukraine
https://orcid.org/0009-0000-0070-3396

Kyrylo Varodov
Postraduate Student
Education and Research Institute "Ukrainian Engineering and Pedagogical Academy"
of V.N. Karazin Kharkiv National University
61003, 16 Universytetska Str., Kharkiv, Ukraine
https://orcid.org/0009-0007-8621-6337

Influence of regenerative effect and mode coupling on the stability of milling operations

Abstract. Quality of milling operations requires dynamic stability of the process, which depends on the tool geometry, structural rigidity and type of vibrations. The study aimed to identify the influence of internal dynamic disturbances on the milling process, in particular, the mechanisms of self-excited vibrations arising from vibrational interactions and residual irregularities of the machined surface. The methodology included a comparative analysis of milling stabilisation models with an assessment of their advantages, limitations and practical recommendations for implementation in real production processes. Mathematical models were presented that addressed the effects of time delay and the interaction between the directions of oscillation of the tool and the workpiece. The study determined that repeated contact of the tool with the irregularities of the pre-treated surface leads to a variable thickness of the material layer and forms an unstable operating mode. The interaction between different oscillatory modes, when machining flexible or thin-walled parts, leads to more complex self-oscillatory processes, including chaotic oscillations. The most promising for practical use are models with adaptive control, which can respond to changes in process parameters in real time. The study established that the dynamics of the milling process significantly depend on the geometry of the tool, the length of the protrusion, stiffness, mass-inertial characteristics, and wear of the cutting part. Process damping, caused by the side contact of the tool with the workpiece, reduces the amplitude of vibrations in the low-frequency range. The control structure based on the system's state vector included position, speed, vibration amplitude, spindle speed and tool feed. None of the methods is universal, so it is advisable to apply an adaptive approach to choosing a stability model, considering constructive, dynamic and economic factors. The practical value of the results is that they can be used by engineers and technologists to implement adaptive milling control to reduce vibrations and improve machining accuracy

Keywords: self-oscillation; delayed system; multimodal dynamics; semi-sampling; state vector; intelligent control; adaptive modelling

INTRODUCTION

The stability of milling processes is one of the key factors determining the quality, productivity and economic efficiency of 21st-century machine building. Increased attention is being paid to the phenomenon of vibration chatter, a self-excited oscillation that can cause significant deterioration in machining, tool wear and damage to

Article's History: Received: 09.05.2025; Revised: 14.08.2025; Accepted: 23.09.2025.

Suggested Citation:
Grechaniuk, Ya., & Varodov, K. (2025). Influence of regenerative effect and mode coupling on the stability of milling operations. *Machinery & Energetics,* 16(3), 58-69. doi: 10.31548/machinery/3.2025.58.

*Corresponding author

the workpiece. The two most influential mechanisms that cause chatter are the regenerative effect and mode coupling. The complexity arises from the simultaneous action of these two types of chatter, as their interaction creates additional difficulties in predicting stability limits. This is driving the growing use of flexible and complex structures in industries such as aerospace, micromechanics, orthopaedic surgery, and automated manufacturing.

The regenerative effect and mode coupling significantly complicate the prediction of milling process stability in conditions of variable stiffness or high-speed machining, and the problem of double chatter (regenerative and mode chatter simultaneously) is a significant aspect. Neglecting their interaction can lead to inaccurate stability predictions, as confirmed by M. Mobaraki & J. Ratava (2023). The study found that only adaptive vibration absorption systems tuned to the frequency overlap of the modal and regenerative chatter can provide effective vibration damping and, accordingly, significantly expand the limits of stable operation. The study developed an adaptive tuning strategy for the Tunable Vibration Absorber (TVA), which extended the limits of stable processing and, for the first time, addressed the frequency overlap between the two types of chatter.

A significant area of research was the influence of tool geometry on the appearance of self-oscillations. For example, machining parts of complex shapes with deep cavities is accompanied by specific instabilities, as proved in the study by X. Wang *et al.* (2024). The study confirmed that the use of curved blades leads to a significant narrowing of the stability region and, based on this, developed refined recommendations for the selection of geometric parameters of cutters for such conditions, which improved forecasting methods and rendered the results more suitable for practical applications. Generalisation of approaches to chatter suppression, including a combination of active and passive vibration control methods, determined their effectiveness in different production conditions. Z. Li *et al.* (2024) found that hybrid damping technologies demonstrate maximum efficiency in a wide range of production conditions. This provides the ability to flexibly configure self-oscillation suppression systems depending on the specific situation and justifies the optimality of the combined approach for a wide range of machining conditions.

C. Liu *et al.* (2024) proposed a new numerical model capable of taking into account the characteristics of various types of parts, from thin-walled to massive, and obtained results that indicate a significant increase in the accuracy of predicting critical cutting modes without the need for large experimental databases and made it possible to use such models in real production conditions without significant costs for experimental verification. Configuration-dependent dynamics of robotic milling systems is also a promising area of research. B. Li *et al.* (2025a) demonstrated that the change in stiffness and modal parameters along the manipulator's trajectory can be used for accurate prediction of the appearance of unstable areas and thus significantly increases the efficiency of automated production. The created model predicts unstable areas with high accuracy, which provides a new level of stability for robotic milling of complex parts.

The need to accommodate the spatial variation of the modal parameters of milling systems was presented in the study by H. Tian *et al.* (2024), dedicated to the stability of machining in orthopaedic robotic systems. The study determined that even minor changes in the tool position cause fluctuations in modal frequencies, which directly affect the probability of chatter. The study quantified this dependence and built more accurate stability models for position-sensitive objects, which is key for milling complex geometric surfaces.

The Ukrainian scientific community is also increasingly emphasising the problem of self-oscillations in milling operations, particularly in the context of machining thin-walled and flexible parts. The problem of self-oscillations in milling operations is critical to the accuracy and quality of machining. S. Dyadya *et al.* (2022) investigated the relationship between vibration parameters and the quality of the moulded surface during milling. The study found that even low-frequency vibrations can significantly worsen the microgeometry of the machined surface, especially in thin-walled or flexible workpieces. This laid the groundwork for practical strategies to improve process stability. To ensure safe and efficient machining of thin-walled parts, it is essential to determine the zones of stable operation without chatter. Y.V. Petrakov *et al.* (2024) addressed the adaptive determination of cutting parameters that prevent the occurrence of self-oscillations. The study significantly contributed to the methodology for calculating chatter-free modes, adapted to the conditions of variable stiffness of structures. Of value is the integration of this methodology into computer numerical control systems, which made it possible to provide real vibration control during machining in an automated environment. The importance of integrating advanced digital and additive technologies in machining is also highlighted in research V. Doroshenko & O. Yanchenko (2023) emphasised the prerequisites for the introduction of 3D technologies in the production of metal products, demonstrating that process innovations not only expand manufacturing capabilities but also set new requirements for stability and quality assurance in machining operations. This corresponds with the growing trend towards adaptive and hybrid approaches in vibration suppression strategies.

Despite previous studies, most existing models are limited in their applicability in conditions of variable real-time dynamics. The influence of combinations of regenerative and mode chatter in adaptive milling processes has not been sufficiently investigated. Problems also arise in the optimisation of robotic systems, where traditional methods do not address variable configuration and multiphase dynamics. Linear models do not include position-dependent dynamics, multimodality, and nonlinear phenomena, which are critical for real-world production conditions.

Therefore, the study aimed to determine the regularities of interaction of internal sources of self-oscillations in high-speed machining processes and to generalise effective approaches to ensuring stable dynamics of milling equipment under conditions of complex vibration interaction. To achieve this goal, the following tasks were set: to classify the main types of self-oscillations that occur during milling, taking into account the features of the geometry, stiffness and tool trajectory, to analyse the effectiveness of mathematical and numerical models for predicting stability in complex machining dynamics, and to formulate practical recommendations for choosing the appropriate stability model depending on the type of task, design constraints and type of equipment.

MATERIALS AND METHODS

The study analysed the dynamic effects that affected the stability of the milling process, in particular, oscillations resulting from feedback and mode interaction. The criteria considered included the accuracy of predicting stability limits, the influence of geometric and dynamic tool characteristics, adaptability to changing machining conditions, and the possibility of practical implementation in high-precision manufacturing.

The study included 3 stages. At the first stage, a theoretical analysis of the mechanisms of dynamic instability of the milling process was conducted regenerative chatter and mode coupling. A mathematical model based on time-delay differential equations was presented, which considered the repeated contact of the cutter with the machined surface and the interaction between the vibration modes. The stage aimed to form an analytical basis for identifying the conditions of self-oscillations and determining the limits of stability depending on technological and design parameters. The presented model became the basis for the construction of the Stability Lobe Diagram (SLD) and justification of further approaches to process stabilisation. Time-delay system, where the change in chip thickness depends on the current tool position and the previous tool position by a time (delay) (Insperger *et al.*, 2015):

$$h(t) = x(t) - x(t - T), \quad (1)$$

where: $h(t)$ – Clip thickness at the current moment; $x(t)$ – current tool position; $x(t - T)$ – previous tool position at time T (time delay between the current and previous tool contact with the workpiece due to the regenerative effect). This describes the key characteristic of the model, the dependence of chip thickness on the current and previous tool position. It is this relationship that reflects the regenerative effect, which is one of the main causes of vibrations in milling. Without this equation, it is impossible to describe the effect of lag on the cutting process.

The cutting force $F(t)$ is defined as proportional to the chip thickness as follows (Faassen *et al.*, 2003):

$$F(t) = K_h \times h(t) = K_h \times (x(t) - x(t - T)), \quad (2)$$

where: $F(t)$ – force acting on the tool during machining, which depends on the chip thickness, which varies due to tool movement and machining geometry; K_h – system stiffness factor (may depend on the workpiece material, tool type and other physical characteristics of the system). The equation defines the cutting force as a function of chip thickness, which directly links the process mechanics to the geometrical parameters of the cut. This basic relationship quantifies the interaction between the tool and the workpiece and is the starting point for further stability analysis.

The motion of the tool is described by Newton's second law or the equation of a one-degree-of-freedom oscillatory system (Breitenbach, 2025):

$$m\ddot{x}(t) + c\dot{x}(t) + kx(t) = F(t), \quad (3)$$

where: m – tool mass; c – damping coefficient; k – stiffness coefficient; $\dot{x}(t)$ – tool velocity at time t, i.e., tool displacement rate; $\ddot{x}(t)$ – tool acceleration at time t. This equation summarises the effects of tool mass, stiffness and damping on tool vibrations due to cutting forces. Without this equation, it is impossible to conduct a mathematical analysis of the dynamic stability of the process.

At the second stage of the study, a comparative analysis method was used to systematise existing approaches to modelling and ensuring the stability of the milling process. A comparative typology of models was formed: three-dimensional Stability Lobe Diagram (3D SLD) with positional dependence (analysis of the influence of the tool's spatial position and local stiffness on the stability limit), Nonlinear Delay Differential Equation (NDDE) models with bifurcations (describing the behaviour of systems with self-oscillations, bifurcations and chaotic modes, which is critical for flexible parts), variable spindle speed methods (practical strategies for suppressing chatter by modulating the input signal without modifying the design), 6 Degrees of Freedom (6DOF) robotic system models (accounting for the kinematics of robotic systems with multiple degrees of freedom), models with uncertain parameters (accounting for statistical fluctuations in stiffness and damping typical of manufacturing conditions), and multimodal milling approaches (modelling the interaction of multiple frequencies simultaneously – a typical situation in complex machining paths). The models were selected to cover the most common destabilisation scenarios that can occur when milling different types of workpieces, with different geometries, stiffnesses, and in different design conditions (traditional and robotic systems). This concluded on the relevance of using certain methods depending on the production scenario.

At the third stage, the results of the comparative analysis were summarised, which formulated practical recommendations for choosing the most effective methods of milling process stabilisation for different production scenarios. For each of the approaches, the advantages, limitations in practical implementation, and recommendations for use in mass production were analysed separately.

Evaluation criteria included computational complexity, sensitivity to input parameters, flexibility of adaptation to different materials and types of workpieces, and compliance with industry requirements (aerospace, mechanical engineering, robotic systems). This typological approach identified the most relevant methods for specific production tasks and formulated reasonable recommendations for their implementation. The Zotero bibliography manager (version 6.0) was used to organise bibliographic sources, make references and systematise scientific publications, which ensured proper citation accuracy and uniformity of references in the process of preparing the paper.

RESULTS

Mathematical model for predicting stability in milling processes

One of the main problems in milling is dynamic instability, in particular chatter, which reduces machining quality, tool life and accuracy, and is caused by the regenerative effect and mode coupling. Regenerative chatter occurs when the cutter repeatedly contacts a surface that already contains irregularities formed by the previous tooth. This creates a delay in the system, which is a source of self-oscillation. A typical mathematical model is a time-delay system in which the current chip thickness is defined as a function of the previous coordinates. The model is classified as a Differential Delay Equation (DDE) and is used to construct stability limits in the form of SLDs. The use of modified semi-sampling methods incorporates the dependence of stability on tool position and changes in damping.

Regenerative chatter is a typical self-oscillatory process caused by the cutter coming into periodic contact with a surface that has already been machined by a previous tooth. This creates a variable chip thickness and a time delay equivalent to the tool rotation period. This dynamic creates a feedback loop in the system, making it potentially unstable. This effect is modelled as a DDE equation where the chip thickness depends on the previous tool position (Formula 1) and the cutting force is proportional to this thickness (Formula 2). The resulting equation, which includes inertial, damping and elastic components (Formula 3), was used as a basic model for interpreting self-oscillations and is the basis for building an SLD to analyse the stability limits of the milling process.

The phenomenon of mode coupling occurs when two or more interdependent vibration modes are present, particularly in flexible or thin-walled workpieces as well as in multi-axis robotic systems. Typical examples are the interaction of bending and torsion in long tools or in parts with complex geometries. In such conditions, multi-frequency dynamics are observed, which can lead to a loss of stability. To describe this phenomenon, a model with two coupled degrees of freedom is used, where each direction has unique parameters of mass, stiffness, and damping (Faassen *et al.*, 2003):

$$m\ddot{x}(t) + c\dot{x}(t) + kx(t) = K_h \times (x(t) - x(t - T)). \qquad (4)$$

A typical mathematical model for two coupled degrees of freedom – a system of two equations for two different vibration modes (e.g., in the *X* and *Y* directions) that covers inertia, damping, and stiffness for each mode – is as follows:

$$\begin{pmatrix} m_x\ddot{x}+c_x\dot{x}+k_x x=F_x(h_x(t)) \\ m_y\ddot{y}+c_y\dot{y}+k_y y=F_y(h_y(t)) \end{pmatrix}, \qquad (5)$$

where: m_x, m_y – tool masses in the *X* and *Y* directions; $\ddot{x}$, $\ddot{y}$ – accelerations in the *X* and *Y* directions; c_x, c_y – damping coefficients for each direction; k_x, k_y – stiffness in the *X* and *Y* directions; $F_x(h_x(t))$, $F_y(h_y(t))$ – forces acting on the tool, which depend on the chip thickness and vary over time due to the regenerative effect. The interaction between the axes is considered through off-diagonal elements in the stiffness and damping matrices, which can be used to model the energy exchange between modes.

For mode coupling, it is critical to consider the interaction between two vibrational modes. This means that a displacement in one direction (e.g., *x*) can generate a force in the other direction (*y*) and vice versa. This interaction can be modelled through off-diagonal elements in the stiffness matrix. An extended system to account for the interaction between modes is given by T. Insperger *et al.* (2015):

$$\begin{bmatrix} m_x & 0 \\ 0 & m_y \end{bmatrix}[\ddot{x}(t)\ddot{y}(t)] + \begin{bmatrix} c_x & c_{xy} \\ c_{yx} & c_y \end{bmatrix}[\dot{x}(t)\dot{y}(t)] + \\ + \begin{bmatrix} k_x & k_{xy} \\ k_{yx} & k_y \end{bmatrix}[x(t)y(t)] = \begin{bmatrix} F_x(h_x(t)) \\ F_y(h_y(t)) \end{bmatrix}, \qquad (6)$$

where: c_{xy}, c_{yx} – damping coefficients that address the interaction between the *X* and *Y* directions (a change in velocity in one direction can affect the damping in the other); k_{xy}, k_{yx} – elements of the stiffness matrix that describe the interaction between the *X* and *Y* directions (if these elements are non-zero, then a change in one direction (*x*) causes a change in the other (*y*)).

For ease of calculation and analysis, the system of equations can be written in matrix form, where each element of the matrix will be responsible for the corresponding value of the system (Insperger *et al.*, 2015):

$$M\ddot{u}(t) + C\dot{u}(t) + Ku(t) = F(t), \qquad (7)$$

where: *M* – mass matrix; *C* – damping matrix; *K* – stiffness matrix; $\ddot{u}(t)$ – displacement acceleration; $\dot{u}(t)$ – displacement velocity.

SLD is a key tool for visualising the boundaries between stable and unstable milling operations. It can be used to graphically determine the critical cutting modes at which the system enters an unstable state, accompanied by the development of self-oscillations (chatter). In the classical case, SLD construction is based on solving a regenerative DDE model, with the determination of the delay time based on the rotation parameters. In this case, stability is analysed using a spectrum of Lyapunov's indices, where the transition to instability occurs when one of them is zero. This can be used to calculate the critical plunging depth for each spindle speed. The SLD is constructed by determining the set of pairs (N, a) for which the system enters the unstable mode. This identified the "frontal structures" characteristic of milling, which are shaped as petals on the graph. In the case of two vibration modes (in the X and Y directions), the stiffness matrix is as follows (Faassen *et al.*, 2003):

$$K = \begin{bmatrix} k_x & k_{xy} \\ k_{yx} & k_x \end{bmatrix}. \tag{8}$$

The presence of non-zero off-diagonal elements (k_{xy}, k_{yx}) indicates that displacement in one direction generates forces in the other. This leads to complex self-oscillatory behaviour, such as bifurcations, quasi-regular oscillations or chaotic fluctuations, especially when the local stiffness is low or the damping is poor. In industrial applications, this can occur when machining aluminium or titanium panels, shell structures, or when the tool is unstable or insufficiently rigid. Classic examples include milling long, flexible parts or using six-degree-of-freedom manipulators where geometric complexity and poor damping contribute to resonant excitation. Particularly critical is the incorrect distribution of damping, where compensation of one mode can cause resonance in another. This approach can be used to perform modal analysis – to identify the natural frequencies and vibration forms of the system, as well as to assess the limits of its dynamic stability. Consideration of mode coupling is essential for accurate SLD prediction in milling operations involving complex trajectories or the interaction of several vibrational modes.

In the classical case, SLD construction is based on the Dynamic Data Exchange (DDE) analysis, which describes a regenerative chatter, where the latency is defined as (Faassen *et al.*, 2003):

$$T = \frac{60}{N \times z}, \tag{9}$$

where: N – spindle speed per minute (rpm), i.e., tool rotation frequency (a critical parameter because the rotation speed affects the system's vibration frequency and how fast the tool moves); z – number of teeth on the tool (determines how often the tool comes into contact with the material during machining, which affects the amount of force transmitted through the system); 60 – constant factor used to convert minutes to seconds, ensuring correct calculation of the time for one tooth to pass.

Numerical methods such as the Semi-Discrete Method (SDM), modal analysis, time-domain simulation, and the Galerkin method are used to accurately calculate stability limits (Altintaş & Budak, 1995; Faassen *et al.*, 2003). These methods can build a stability diagram in more complex systems, incorporating the various factors that affect the stability of the machining process. In the stable zone, the solution does not grow over time, and the limit of instability is determined when one of the indicators becomes zero. This calculated the critical cutting depth a_{lim} for each mode (Zheng *et al.*, 2014):

$$a_{lim} = \frac{2 \times K}{h} \times R[G(j\omega)]^{-1}, \tag{10}$$

where: h – chip thickness removed during one tool pass (varies depending on the depth of cut and machining speed); $j\omega$ – complex frequency, where j – conditional unit, and ω – real frequency; $R[G(j\omega)]$ – modulus of the system frequency response function that describes the amplitude of the system frequency response at a certain frequency point $j\omega$.

The dynamics of the milling process depend heavily on the tool geometry, including the length of the protrusion, stiffness, mass-inertial characteristics and wear of the cutting part. Long and thin tools show increased sensitivity to the excitation of bending and torsional modes, which contributes to the appearance of both mode and regenerative chatter. The behaviour of the system is multidimensional with the presence of inter-axial (cross-mode) interaction, which is confirmed by models in the three-dimensional coordinate space (X, Y, Z). SLD is extended to three-dimensional or parametrically dependent diagrams as follows (Altintaş & Budak, 1995):

$$SLD = f(N, a, p), \tag{11}$$

where: a – depth of cut (the distance to which the tool penetrates the material during machining, the depth of cut affects the cutting forces and, accordingly, the stability of the process); p – parameter that determines additional system characteristics (variable stiffness, spindle speed, number of degrees of freedom of the system).

The interaction of oscillations in different directions can lead to multi-frequency modes and loss of stability. The lag caused by the regenerative effect creates conditions for the growth of self-oscillations even in the absence of external disturbances. In a discrete form, this is expressed through the dependence of the cutting force on the previous coordinate values, which reflects a time-delayed differential equation (DDE model). The dynamics of the milling process is largely determined by the tool geometry, i.e., the length of the protrusion, stiffness, mass-inertial characteristics, and the state of the cutting edge (including wear). For a generalised description of an elastic mechanical system with a regulatory delay that incorporates vibration effects and possible multi-frequency modes, the equation of motion is given by T. Insperger *et al.* (2015):

$$M_{\ddot{q}}(t) + C_{\dot{q}}(t) + K_{q}(t) = F_c(h(t)). \tag{12}$$

Process damping, caused by the lateral contact of the tool with the workpiece, can reduce the amplitude of vibrations in the low-frequency range. This effect shows a dependence on the cutting speed and depth of cut, addressing the influence of geometry and feed. The actual milling process is three-dimensional, as cutting forces are generated in all spatial directions. Therefore, it is necessary to address the complex dynamic behaviour of the system in

X, Y, Z. System matrices are used to describe the behaviour (Faassen *et al.*, 2003):

$$M_{\ddot{q}}(t)+C_{\dot{q}}(t)+K_{q}(t)=F_{c}(q(t),\, q(t-T)). \tag{13}$$

This representation can address cross-mode interaction (for example, when fluctuations in X stimulate fluctuations in Y). The delay caused by the regenerative effect creates conditions for the dynamic growth of fluctuations even without an external perturbation.

Due to the complex and multifactorial dynamics of the milling process, classical control methods (linear controllers or fixed models) are ineffective in the face of changing machining modes and structural instability. This substantiates the feasibility of introducing intelligent stabilisation systems based on Deep Reinforcement Learning (DRL). DRL can be used for adaptive control that considers variable system state parameters, such as position, speed, vibration amplitude, spindle speed, and tool feed. In a discrete formulation, it functions as a force dependence on previous coordinate values (Altintasz & Budak, 1995):

$$F(t)=K_{c}\times[x(t)-x(t-T)]. \tag{14}$$

Process damping is caused by the contact between the tool side and the workpiece, which is particularly evident at low feeds or high plunging depths. This phenomenon is nonlinear in nature and contributes to a reduction in the amplitude of vibrations, mainly in the low-frequency range. The mathematical description of such effects belongs to the class of time-delay equations (DDEs), which require the use of specialised solution methods, such as the Semi-Discretisation Method (SDM), Impedance Response Function (IRF) or Pade approximations. Based on the current state of the system, Deep Reinforcement Learning (DRL) generates a control signal that is fed to the piezoelectric actuator to actively suppress vibrations. The process damping is modelled as an additional force proportional to the tool speed and dependent on the depth of cut (Tuysuz & Altintas, 2019):

$$F_{pd}(t)=c_{pd}\times\dot{x}(t)\times f(d_{axial}), \tag{15}$$

where: $f(d_{axial})$ – function that addresses the dependence of damping on the depth of cut. These equations help to accurately describe the dynamics of the milling process, incorporating the various factors that influence machining stability. Due to the complex dynamics of the milling process, classical control methods are mostly ineffective, which increases the need for intelligent stabilisation systems such as DRL, which provides an adaptive response to changes in machining conditions and reduces vibrations. The state vector in such control systems and modelling of vibration processes, in milling and mechatronic tasks, is represented as (Altintaş & Budak, 1995):

$$s(t)=[x,\, \dot{x},\, a_{vib},\, N,\, a_{p}], \tag{16}$$

where: a_{vib} – vibration amplitude (a significant indicator of process stability and affects the quality of machining); a_p – parameter that characterises the tool feed during machining. To optimally control the milling process and reduce tool vibrations, a control scheme is used that incorporates the current state of the system (Sutton & Barto, 2014):

$$u(t)=\pi_{o}(s(t)), \tag{17}$$

where: $u(t)$ – control signal that determines the action to be taken based on the current state of the system; $\pi_o(s(t))$ – function that generates a control signal that depends on the state vector $s(t)$. This described the process of generating a control signal as a function of the current state, without using fixed parameters.

Taken together, these equations provide a universal mathematical description of milling that provides simultaneous analysis of process stability, prediction of critical conditions, evaluation of the effects of geometry, material and machining parameters, and development of effective active vibration suppression strategies. This creates a consistent, multi-level model that combines physical process mechanics, analytical stability methods and adaptive control algorithms.

Classification and recommendations for technological efficiency of chatter reduction methods

Ensuring stability during milling is a critical factor in achieving high precision and productivity. The development of stability models addressed a wide range of factors, from regenerative chatter and mode interaction to the adaptive behaviour of robotic systems, which tailors the process to the specifics of the task. Table 1 presents these approaches, demonstrating the relationship between the type of model, the chosen stabilisation technique and its application in industry.

Table 1. Comparison of stability methods for milling with damping and tool parameters

Model type	Stability analysis and influence of parameters on machining	Methods of stability in processing	Application and scope of use
3D Stability Lobe Diagram with position dependence	Change in stability when changing tool position for thin-walled parts, considering process damping	SDM (semi-discretisation) + positional discretisation of the toolpath to account for changes in stiffness and damping	Building a 3D SLD for milling thin-walled components, analysing the impact of process damping on stability limits, and applications in the aerospace industry. Using 3D SLD to machine thin-walled aluminium aircraft panels where positional dependence reduces regenerative chatter. Optimising the milling of curved turbine blade surfaces to reduce vibrations.
NDDE + nonlinear model	Modal and regenerative chatter, bifurcations, effects of tool wear and part flexibility, chatter suppression with TVA	Galerkin method for projection of nonlinear equations, mode summation for multimodal behaviour	Analysis of stability and chaos zones, use of TVA for chatter suppression, and prediction of bifurcations in nonlinear systems. Application of TVA to suppress mode coupling in the milling of flexible titanium plates in aircraft components. Predicting chaotic behaviour in thin shell machining for aerospace structures.

Continued Table 1.

Model type	Stability analysis and influence of parameters on machining	Methods of stability in processing	Application and scope of use
Variable speed, regeneration	Influence of different forms of rotational speed modulation (sinusoidal, triangular) on the stability limits	Time-domain simulation + SDM for building SLDs with variable velocity $\omega(t)$	Comparison of speed modulation strategies for chatter suppression, optimisation of variable speed machining modes. The use of sinusoidal speed modulation to reduce regenerative chatter in the machining of aluminium parts in the aviation industry. Application of triangular modulation for milling steel components in mechanical engineering.
Robotic 6DOF model	Milling stability for industrial robots with 6 degrees of freedom, considering the flexibility of the arm	Fully discrete method for numerical solution of delayed differential equations	SLD analysis for flexible robotic systems, optimisation of machining modes for robots based on their kinematics. Use of the 6DOF model to stabilise milling in orthopaedic surgery by reducing mode coupling. Optimising the handling of large parts in automated production.
Unspecified parameters	The effect of parameter variation (stiffness, damping) on SLD accuracy in real-world production environments	IRF + probabilistic approach to assessing uncertainties	Assessment of SLD reliability, analysis of the impact of uncertainties on machining stability, and application in production. Application of a probabilistic approach to evaluate the regenerative chatter in titanium alloy milling in mass production. Analysis of the impact of stiffness uncertainties on the stability of composite materials processing.
Multi-modal robotic milling	Stability dependence on robot configuration, multimodal milling dynamics	Stability Cloud Simulation to assess instability zones depending on the trajectory	Trajectory assessment of instability zones, optimisation of robot configuration for milling. Using Stability Cloud Simulation to reduce mode coupling when milling complex parts in robotic systems for the aviation industry. Optimising paths for highly loaded robots in large component manufacturing.

Source: compiled by the authors based on X. Liu *et al.* (2024), D.R.V. Naranjo *et al.* (2024), J. Wu *et al.* (2024), H. Tian *et al.* (2024), K. Guo *et al.* (2025), B. Li *et al.* (2025b), Y. Du *et al.* (2025), J. Jia *et al.* (2025), K. Nasiri & H. Moradi (2025)

In a production environment, the efficiency of the milling process depends not only on the basic parameters of the machining mode, but also on the ability of the system to adapt to instabilities caused by vibrations, variable stiffness, geometric design features or material uncertainties. Various stability models are used for this purpose. Table 2 provides a comparative analysis of the models, indicating their strengths, weaknesses, and practical recommendations for implementation. This approach identified the most relevant methods for various production scenarios, from machining thin-walled structures to milling in complex robotic systems with multimodal dynamics.

Table 2. Analysis of the effectiveness of milling stability methods under production constraints

Model type	Advantages	Disadvantages	Recommendation
3D Stability Lobe Diagram with position dependence	The method addresses positional variations in stiffness and damping, providing accurate prediction of stability limits for thin-walled components widely used in the aerospace industry. The 3D SLD provides a detailed stability map that helps optimise machining conditions for parts with variable geometries. The method integrates damping effects, which improves the accuracy of chatter prediction in real-world conditions. Widespread use in the aerospace industry can be used for machining lightweight structures with increased accuracy and minimal vibration.	SDM requires significant computing resources, particularly for complex toolpaths or large parts. The method is optimised for thin-walled parts, which reduces its effectiveness for massive or rigid components. Correct 3D SLD construction requires accurate measurements of dynamic parameters (stiffness, damping), which can be difficult in real-world conditions. Small deviations in the toolpath may require recalculation of the SLD, which complicates the process.	Milling thin-walled parts in the aerospace industry, such as aircraft panels or turbine blades. Combine with experimental tests to refine stiffness and damping parameters before building an SLD. Use of specialised tools (Matrix Laboratory (MATLAB) or ANSYS) to automate SDM and reduce computational costs. Planning the toolpath to minimise positional changes that affect stability.
NDDE + nonlinear model	The method incorporates mode and regenerative chatter, bifurcations, and chaos, which can be used to analyse the behaviour of flexible parts. The use of TVA ensures effective vibration reduction in real time. The model can estimate the effect of wear on stability, which improves the accuracy of predictions for long machining processes. The Galerkin method provides an analysis of multimodal dynamics, which is effective for complex systems with multiple frequencies.	NDDE analysis requires significant computing resources and specialised software. Setting up and integrating vibration absorbers in an industrial environment can be costly and technically challenging. The effectiveness of TVA depends on the precise determination of system parameters, which requires additional measurements. The method is effective for flexible parts, but less appropriate for rigid structures.	Machining of flexible wafers or parts with a high risk of nonlinear chatter, e.g., in the aviation industry. Conducting laboratory experiments to determine optimal TVA parameters before industrial use. Combination with active controllers (soft-actor-critical or fuzzy controllers) to increase efficiency. Use of numerical modelling tools (DDE-BIFTOOL) to analyse nonlinear effects.

Continued Table 2.

Model type	Advantages	Disadvantages	Recommendation
Variable speed, regeneration	Speed modulation (sinusoidal, triangular) effectively reduces regenerative chatter. No complicated changes to the machine or tool design are required, just the speed setting. Different modulation shapes (sinusoidal, triangular) can be used to adapt the model to different materials and machining conditions. Increases productivity without significant investment in equipment	Efficiency depends on the correct choice of modulation form, which requires preliminary testing. The method is less effective for parts with uneven stiffness or complex trajectories. The choice of modulation frequency and amplitude requires experimental data. Less effective for materials with low regenerative chatting	Processing materials with a high risk of regenerative chatter (aluminium alloys). Conducting tests with different modulation shapes (sinusoidal, triangular) to determine optimal parameters. Using SDM to accurately predict the stability limits at variable speeds. Integrate speed modulation into numerical control systems for automatic tuning.
Robotic 6DOF model	The method considers the flexibility of the manipulator and the kinematics of the robot, which ensures accurate stability prediction. It can be used to configure machining modes for robots with 6 degrees of freedom, which is a priority for manufacturing. The fully discrete method provides fast analysis of delayed differential equations. The method adapts to complex robot trajectories.	The method was developed for robotic systems, which reduces its effectiveness for traditional machine tools. Accuracy depends on detailed data on the kinematics and flexibility of the manipulator. Implementation in real-world conditions may require modification of the robot's software. Less effective for machining rigid parts	Milling in automated production with industrial robots. Conducting experiments to determine the flexibility parameters of the manipulator. Use of SLD to build a robot kinematics-based design. Using a numerical modelling tool (RobotStudio) to optimise trajectories.
Unspecified parameters	The probabilistic approach incorporates the spread of parameters (stiffness, damping), which increases accuracy in real-world conditions. It can be used for predicting the probability of a chatter with uncertain parameters. The method is suitable for various types of machining where parameters can vary. The Impulse Response Function simplifies the analysis of the impact of uncertainties.	Requires specialised software and large amounts of data. Accuracy depends on the quality of the scatterplot measurements. Less effective in stable conditions (the method is less useful if the parameters are known precisely). Probabilistic analysis can be resource-intensive	Use in production environments with a high level of uncertainty (when processing new materials). Collecting data on the spread of parameters using sensors and measuring systems. Use IRF to quickly assess the impact of uncertainties on stability. Use of tools for probabilistic modelling (Monte Carlo in MATLAB).
Multi-modal robotic milling	The method incorporates the dependence of stability on robot configuration and multimodal dynamics. Stability Cloud Simulation provides a visual representation of the chatter zones depending on the trajectory. It can be used to adjust parameters to reduce vibrations. The method is suitable for robotic industries with complex trajectories.	The method is designed for robotic systems, which reduces its effectiveness for traditional machine tools. Stability Cloud Simulation requires significant computing resources. Accuracy depends on detailed data on the robot's trajectory and dynamics. May require modification of the robot software	To optimise milling in robotic systems with multimodal dynamics. Use of Stability Cloud Simulation to estimate instability zones in trajectory planning. Conduct tests to refine the modal parameters of the robot. Use trajectory modelling tools (Robot Operating System (ROS) or CoppeliaSim).

Source: compiled by the authors based on X. Liu *et al.* (2024), H. Miao *et al.* (2024), D.R.V. Naranjo *et al.* (2024), H. Tian *et al*. (2024), J. Jia *et al*. (2025), K. Nasiri & H. Moradi (2025), K. Guo *et al.* (2025), B. Li *et al*. (2025b), K.A. Hassan (2025)

The analysis of the methods showed that there is no one-size-fits-all solution suitable for all types of machining. Models based on 3D Stability Lobe Diagram demonstrate significant accuracy for thin-walled structures when fine-tuned but require significant computational resources. Non-linear NDDE models using TVA are effective for flexible parts but are complex to implement and sensitive to parameterisation. Variable speed methods are simple to implement but have limited effectiveness for complex trajectories and rigid materials. Robotic approaches with 6DOF and multimodal simulations are particularly relevant for automated systems but require detailed kinematic models and substantial computational support. Probabilistic approaches incorporate real production fluctuations but require careful collection of statistical data.

Therefore, the choice of model should be based on specific process characteristics, production goals and the acceptable level of implementation complexity, which emphasises the need for an adaptive and engineering-based approach to ensuring the stability of milling operations. A comprehensive approach to method selection, incorporating practical recommendations and the nature of instabilities, will increase the reliability, accuracy and adaptability of the milling process in high-precision production.

DISCUSSION

The results of the study have shown that the stability of the milling process depends on several factors, including changes in stiffness and damping, nonlinear dynamics with the interaction of mode oscillations, and the use of adaptive stabilisation methods under variable machining conditions. To solve these problems, approaches such as SLD models that consider the spatial variability of parameters, TVA, numerical schemes based on NDDE, and Stability Cloud Simulation for multi-axis robotic systems were used. A similar approach was presented in study C. Song *et al.* (2024), based on time-delayed DDE models to build SLDs using the SDM method, which improved the accuracy of prediction of unstable zones during milling of complex components. This fully correlates with the results of the current study, which emphasised the need to incorporate the spatial dependence of stiffness and damping when constructing stability diagrams.

O. Özşahin (2024) proposed an active electromagnetic toolholder integrated with a feedback control system for effective chatter suppression at low tool immersion. The study implemented an electromagnetic system with active control, which provides dynamic stiffness adjustment during milling. Experimental tests have confirmed that this approach can significantly reduce the amplitude of self-oscillations, ensuring stability and high surface quality of the parts. This is consistent with the current study, confirming the effectiveness and feasibility of using adaptive active stabilisation systems for modes with a shallow immersion depth and low system stiffness. This approach complemented the solutions proposed in this study (DRL and TVA) and confirmed the feasibility of engineering adaptation of stabilisation methods to the conditions of a specific production scenario.

Additionally, R.R. Lakshmi *et al.* (2024) optimised milling mode parameters to reduce chatter. The authors used a combination of numerical analysis and experimental validation to identify the impact of parameters such as cutting speed, feed rate and depth of cut on machining stability. The results demonstrated that the correct selection of parameters can significantly reduce the amplitude of vibrations and improve surface quality without the use of additional stabilisation devices. This correlates with the results of the current study, which substantiated the effectiveness of using adaptive control of technological modes as one of the tools to stabilise the milling process.

Furthermore, the study determined that damping is a crucial factor for machining stabilisation, including under conditions of low local stiffness and the presence of mode coupling. This was confirmed by R.I.E. Schönecker *et al.* (2024) in an experimental investigation of the effect of microstructured tool surfaces on their ability to passively dampen. The study determined that the structured surfaces significantly reduced the amplitude of vibrations without the need to change the machining modes or tool geometry, which complemented the results of the study on the critical role of damping. S. Xin *et al*. (2023) used TVA within the NDDE framework to suppress chatter under complex nonlinear dynamics. They found that TVAs effectively expanded the limits of stable processing by reducing vibration amplitude in complex dynamic situations. This correlated the results of an ongoing study on the effectiveness of TVAs for stabilising systems with pronounced nonlinear mode interaction.

The stability of robotic milling systems with 6DOF, including the interaction between the axes and the flexibility of the manipulator, must be considered. The use of Stability Cloud Simulation was used to visualise unstable zones in the motion paths. Similar results were obtained in the study by Y. Zheng *et al.* (2023), confirming the priority of considering the flexibility of mechanical joints to build accurate stability models. The study also determined that real dynamics of the manipulator can be used to reduce the error in predicting self-oscillations and thus improve the quality of milling. The study emphasised the need for detailed experimental studies of the dynamic parameters of the system, which fully correlated with the results of this study on the key role of parametric accuracy of stability models. J. Du *et al.* (2023) applied a combined robust Linear Quadratic Gaussian (LQG) control to effectively suppress chatter, demonstrating the need for adaptive stabilisation methods, which coincided with the approach of this study to the use of control methods such as DRL. The study showed that an adaptive stabilisation system is significantly more effective than traditional fixed controllers, particularly in conditions of variable part stiffness and machining modes. The study also noted that the robust approach reduces the sensitivity of the system to errors in parameter estimation, which was consistent with the probabilistic analysis of parameter uncertainty proposed in the current study.

Y. Sun *et al.* (2023) reviewed the 21st-century approaches to ensuring the stability of milling thin-walled parts that are particularly sensitive to self-oscillations (chatter). The study systematised and classified existing methods according to their principles of operation, mathematical models, level of adaptability and practical application in industry. They emphasised that there is no single universal solution that can completely solve the problem of chatter in all production scenarios. Stabilisation of the process is only possible through a comprehensive combination of analytical theoretical models and carefully conducted experimental studies. The conclusions were fully confirmed by the results of the current study, which showed the need for an engineering-adaptive selection of stabilisation methods following specific production conditions.

The results of the study demonstrated that parametric uncertainties, such as stiffness and damping fluctuations, affect the accuracy of milling stability prediction. Ignoring them reduces the accuracy of SLD and leads to errors. This correlated with the study of M. Hashemitaheri *et al.* (2024), determining that even small variations in stiffness or damping parameters significantly affect the accuracy of SLD construction. They used the Monte Carlo method to assess the impact of these variations on the modelling results. The study determined that small changes in damping lead to a significant shift in the stability limits, which can cause chatter even in modes that were previously considered stable. This confirmed the need to incorporate parametric uncertainties, which was reflected in this study, and justified the use of probabilistic methods for more accurate stability prediction in production conditions.

S. Hayati *et al.* (2023) proposed an approach with variable tool dynamics (a hollow core cutter with an adjustable core) that can be used for adaptive changes in frequency characteristics during the milling process. The study experimentally confirmed that this tool design can significantly reduce self-oscillation, especially when machining long and thin parts where stability is a critical factor. They also demonstrated that adjusting the dynamic characteristics of the tool directly during operation makes it possible to adapt to different milling conditions, which significantly expands the technological capabilities of the machines. This correlated with the results of a study on the impact of tool design on stability and highlighted the need to consider the geometric and design features of the tool in complex production scenarios.

Thus, successful stabilisation requires a comprehensive adaptive approach that considers the specifics of technological conditions and design features of the equipment and also involves the integration of theoretical models with experimental validation. The applied approaches and methods correlate with current trends in the field of milling stabilisation and can be effectively implemented in production conditions, which will not only increase the stability of machining but also improve the overall technological flexibility and reliability of milling production.

CONCLUSIONS

The study determined that SLDs are used to assess the stability limits of the milling process, which determine the critical depth of cut for each rotational speed. Traditionally, methods based on DDE equations and analysis of Lyapunov exponents are used to construct SLDs. For complex systems, such as multimodal or nonlinear rotational speeds, advanced methods (SDM, Galerkin, Time-Domain Simulation) are used. The results of the study showed the effectiveness of stabilisation methods. 3D SLD with position dependence considered the change in stiffness along the trajectory, which is substantial for machining thin-walled structures in the aerospace industry. NDDE + TVA provided an effective analysis of mode and regenerative self-oscillations in the machining of flexible titanium components. For simpler cases, such as machining aluminium or steel parts, the $\omega(t)$ rotation modulation method is effective. In 6DOF robotic systems that incorporate the flexibility of the manipulator, methods of adaptation to changing conditions were used. The DRL can be used to adapt the system to changing parameters and generate signals for piezoelectric actuators to effectively suppress vibrations in real time.

A comparative analysis of the models showed that each approach has its advantages and limitations. 3D SLD provides high accuracy but requires significant computing resources. NDDE + TVA is effective for chaotic modes but is difficult to implement. Modulation $\omega(t)$ is easy to implement, but less effective for complex geometries. Systems with 6DOF demonstrate high dynamism, but their accuracy depends on the quality of the models. Probabilistic models optimally incorporate parameter fluctuations but are resource intensive. To achieve maximum accuracy, it is recommended to combine analytical and numerical methods with experimental measurements. Adaptability is critical for processing different materials and complex geometries. DRLs and robotic systems with 6DOF are a promising direction for high-precision milling operations.

A limitation of the study was that the models did not fully incorporate the effects of wear and thermomechanical instability, which could be substantial in long machining cycles. This created opportunities for future research, in particular in creating complex digital models with sensory feedback and self-learning mechanisms. Further research should facilitate the identification of parameters and the integration of active stabilisation methods into automated systems to improve milling stability and productivity.

ACKNOWLEDGEMENTS

None.

FUNDING

The study was not funded.

CONFLICT OF INTEREST

None.

REFERENCES

[1] Altintaş, Y., & Budak, E. (1995). Analytical prediction of stability lobes in milling. *CIRP Annals,* 44(1), 357-362. doi: 10.1016/S0007-8506(07)62342-7.

[2] Breitenbach, R. (2025). *Spring-mass problems (With damping).* Retrieved from https://surl.lu/iuxgzo.

[3] Doroshenko, V., & Yanchenko, O. (2023). Prerequisites for the implementation of 3D Technology for the manufacture of metal products and examples of its application. *Modern Technologies, Materials and Structures in Construction*, 20(2), 35-41. doi: 10.31649/2311-1429-2023-2-35-41.

[4] Du, J., Liu, X., & Long, X. (2023). Coupled LQG with robust control for milling chatter suppression. *International Journal of Mechanical Sciences,* 243, article number 108051. doi: 10.1016/j.ijmecsci.2022.108051.

[5] Du, Y., *et al*. (2025). Investigation on the dominant mechanism of chatter in high-load robot milling process based on theoretical and experimental analysis. *Journal of Sound and Vibration,* 600, article number 118886. doi: 10.1016/j.jsv.2024.118886.

[6] Dyadya, S., Kozlova, O., Kushnir, E., & Karamushka, D. (2022). Research of oscillations in end milling and their impact on the formation of the processed surface. *New Materials and Technologies in Metallurgy and Mechanical Engineering,* 2, 71-77. doi: 10.15588/1607-6885-2022-2-12.

[7] Faassen, R.P.H., van de Wouw, N., Oosterling, J.A.J., & Nijmeijer, H. (2003). Prediction of regenerative chatter by modelling and analysis of high-speed milling. *International Journal of Machine Tools and Manufacture,* 43(14), 1437-1446. doi: 10.1016/S0890-6955(03)00171-8.

[8] Guo, K., Qian, N., Sun, J., & Huang, X. (2025). Chatter suppression in robotic milling using active contact force actuator. *Journal of Manufacturing Processes,* 133, 118-129. doi: 10.1016/j.jmapro.2024.11.050.

[9] Hashemitaheri, M., Le, T.T., Khan, T., & Cherukuri, H. (2024). Sensitivity analysis and monte carlo based uncertainty quantification of the in-process modal parameters in milling. *ArXiv*. doi: 10.48550/arXiv.2407.10202.

[10] Hassan, K.A. (2025). Deep learning for real-time chatter suppression in machining. *The Engineer Story,* 15, 5-8.

[11] Hayati, S., Golmohammadi, M., Valitabar, A., & Rasaee, S. (2023). Chatter stability improvement of a slender milling tool via a dynamics variation mechanism. *Research Square*. doi: 10.21203/rs.3.rs-2443716/v1.

[12] Insperger, T., Lehotzky, D., & Stépán, G. (2015). Regenerative delay, parametric forcing and machine tool chatter: A review. *IFAC-PapersOnline*, 48(12), 322-327. doi: 10.1016/j.ifacol.2015.09.398.

[13] Jia, J., Chen, L., Song, W., & Huang, M. (2025). Three-dimensional stability lobe construction for face milling of thin-wall components with position-dependent dynamics and process damping. *Machines,* 13(6), article number 524. doi: 10.3390/machines13060524.

[14] Lakshmi, R.R., Mitra, N.C., & Nutalapati, S. (2024). Optimization of milling parameters to control chatter reduction. *International Journal of Scientific Development and Research,* 9(11), 403-412.

[15] Li, B., Li, H., Yang, X., Chen, Y., & Zhu, Y. (2025a). Dynamic modeling and stability prediction of dry hobbing considering the coupling of hob and workpiece. *International Journal of Advanced Manufacturing Technology,* 139(3), 1555-1570. doi: 10.1007/s00170-025-15960-7.

[16] Li, B., Zhao, W., Li, Z., Zhao, Y., Miao, Y., Tian, W., & Liao, W. (2025b). A multi-modal and configuration-dependent chatter prediction approach for a milling robot. *Journal of Sound and Vibration,* 603, article number 118955. doi: 10.1016/j.jsv.2025.118955.

[17] Li, Z., Song, Q., Jin, P., Liu, Z., Wang, B., & Ma, H. (2024). Chatter suppression techniques in milling processes: A state of the art review. *Chinese Journal of Aeronautics,* 37(7), 1-23. doi: 10.1016/j.cja.2023.10.001.

[18] Liu, C., Tang, D., Chen, X., & Ding, G. (2024). An efficient and precise stability analysis method for milling process. *International Journal of Advanced Manufacturing Technology,* 131, 3599-3614. doi: 10.1007/s00170-024-13101-0.

[19] Liu, X., Niu, J., & Xiang, J. (2024). Milling stability considering multiple effects and variable rotational speed milling chatter control. *Proceedings of the Institution of Mechanical Engineers, Part B: Journal of Engineering Manufacture*. doi: 10.1177/09544054241304160.

[20] Miao, H., Li, C., Liu, C., Wang, C., & Zhang, X. (2024). Nonlinear chatter and reliability analysis of milling Ti-6AL-4V with slender ball-end milling cutter. *Mechanical Systems and Signal Processing,* 127, article number 111534. doi: 10.1016/j.ymssp.2024.111534.

[21] Mobaraki, M., & Ratava, J. (2023). Tuning vibration absorbers to mitigate simultaneous regenerative and mode-coupling chatter. *Noise and Vibration Worldwide,* 54(6), 237-247. doi: 10.1177/09574565231179731.

[22] Naranjo, D.R.V., Vignat, F., & Béraud, N. (2024). Impact of uncertainties on the stability lobe diagram for vibration evaluation in milling. *ArXiv*. doi: 10.48550/arXiv.2410.19861.

[23] Nasiri, K., & Moradi, H. (2025). Nonlinear milling of a flexible plate-workpiece with tool wear and process damping: Bifurcation, stability analysis, and chatter suppression via tunable vibration absorbers. *Thin-Walled Structures,* 210, article number 113017. doi: 10.1016/j.tws.2025.113017.

[24] Özşahin, O. (2024). Optimization of variable pitch milling tools for improved chatter stability. *Journal of Manufacturing Processes*, 120, 260-271. doi: 10.1016/j.jmapro.2024.04.025.

[25] Petrakov, Y.V., Ohrimenko, O.A., Sapon, S.P., Sikailo, M.O., & Fedorynenko, D.Y. (2024). Determination of chatter-free cutting mode in end milling. *Journal of Engineering Sciences,* 11(2), A1-A11. doi: 10.21272/jes.2024.11(2).a1.

[26] Schönecker, R.I.E., Baumann, J., Carballo, R.G., & Biermann, D. (2024). Fundamental investigation of the application behavior and stabilization potential of milling tools with structured flank faces on the minor cutting edges. *Journal of Manufacturing and Materials Processing,* 8(4), article number 174. doi: 10.3390/jmmp8040174.

[27] Song, C., Liu, Z., Wang, X., Qiu, T., Liang, Z., Shen, W., Gao, Y., & Ma, S. (2024). Research on the stability prediction for multi-posture robotic side milling based on FRF measurements. *Measurement Science and Technology,* 35(8), article number 085018. doi: 10.1088/1361-6501/ad4ab7.

[28] Sun, Y., Zheng, M., Jiang, S., Zhan, D., & Wang, R. (2023). A state-of-the-art review on chatter stability in machining thin-walled parts. *Machines,* 11(3), article number 359. doi: 10.3390/machines11030359.

[29] Sutton, R.S., & Barto, AG. (2014). *Reinforcement learning: An introduction*. Cambridge: MIT Press.

[30] Tian, H., Pang, B., Liu, J., Meng, D., & Dang, X. (2024). Influence of different position modal parameters on milling chatter stability of orthopedic surgery robots. *Scientific Reports,* 14, article number 10581. doi: 10.1038/s41598-024-61362-2.

[31] Tuysuz, O., & Altintas, Y. (2019). Analytical modeling of process damping in machining. *Journal of Manufacturing Science and Engineering,* 141(6), article number 061006. doi: 10.1115/1.4043310.

[32] Wang, X., Song, Q., & Liu, Z. (2024). Chatter stability prediction for deep-cavity turning of a bent-blade cutter. *Sensors,* 24(2), article number 606. doi: 10.3390/s24020606.
[33] Wu, J., Tang, X., Peng, F., Yan, R., & Xin, S. (2024). A novel mode coupling mechanism for predicting low-frequency chatter in robotic milling by providing a vibration feedback perspective. *Mechanical Systems and Signal Processing,* 216, article number 111424. doi: 10.1016/j.ymssp.2024.111424.
[34] Xin, S., Tang, X., Wu, J., Peng, F., Yan, R., & Yang, W. (2023). Investigation of the low-frequency chatter in robotic milling. *International Journal of Machine Tools and Manufacture,* 190, article number 104048. doi: 10.1016/j.ijmachtools.2023.104048.
[35] Zheng, C.M., Wang, J.-J.J., & Sung, C.F. (2014). Analytical prediction of the critical depth of cut and worst spindle speeds for chatter in end milling. *Journal of Manufacturing Science and Engineering,* 136(1), article number 011003. doi: 10.1115/1.4025452.
[36] Zheng, Y., Zhao, Z., Xu, B., Yu, Y., & Xu, J. (2023). A method to predict chatter stability accurately in milling thin-walled parts by considering force-induced deformation. *Journal of Manufacturing Processes,* 106, 552-563. doi: 10.1016/j.jmapro.2023.10.033.

Ярослав Гречанюк
Аспірант
Навчально-науковий інститут «Українська інженерно-педагогічна академія»
Харківського національного університету імені В.Н. Каразіна
61003, вул. Університетська, 16, м. Харків, Україна
https://orcid.org/0009-0000-0070-3396

Кирило Вародов
Аспірант
Навчально-науковий інститут «Українська інженерно-педагогічна академія»
Харківського національного університету імені В.Н. Каразіна
61003, вул. Університетська, 16, м. Харків, Україна
https://orcid.org/0009-0007-8621-6337

Вплив реґенеративного ефекту та модового зчеплення на стабільність фрезерних операцій

Анотація. Забезпечення якості фрезерної обробки потребує врахування динамічної стабільності процесу, що залежить від інструментальної геометрії, конструктивної жорсткості та типу вібрацій. Мета дослідження була спрямована на виявлення впливу внутрішніх динамічних збурень на перебіг фрезерного процесу, зокрема механізмів самозбуджених вібрацій, що виникають через коливальні взаємодії та залишкові нерівності обробленої поверхні. Методологія включала порівняльний аналіз моделей стабілізації фрезерування із оцінкою їх переваг, обмежень та практичних рекомендацій для впровадження в реальні виробничі процеси. Було представлено математичні моделі, що враховували ефекти затримки у часі та взаємодії між напрямками коливань інструмента і заготовки. Встановлено, що повторний контакт інструмента з нерівностями попередньо обробленої поверхні призводить до змінної товщини шару матеріалу формував нестійкий режим роботи. Взаємодія між різними коливальними режимами, при обробці гнучких або тонкостінних деталей, призводить до більш складних автоколивальних процесів, включаючи хаотичні коливання. Найбільш перспективними для практичного застосування є моделі з адаптивним керуванням, здатні реагувати на зміну технологічних параметрів у реальному часі. Встановлено, що динаміка фрезерного процесу суттєво залежить від геометрії інструмента, довжини виступу, жорсткості, масоінерційних характеристик та зношення ріжучої частини. Процесне демпфування, спричинене бічним контактом інструмента з деталлю, зменшує амплітуду коливань, в діапазоні низьких частот. Структура керування на основі вектора стану системи включала положення, швидкість, амплітуду вібрацій, оберти шпинделя та подачу інструмента. Жоден з методів не є універсальним, тому доцільно застосувати адаптивний підхід до вибору моделі стабільності з урахуванням конструктивних, динамічних і економічних факторів. Практична цінність результатів полягала у можливості застосування їх інженерами та технологами для впровадження адаптивного керування фрезеруванням для зменшення вібрацій і підвищення точності обробки

Ключові слова: автоколивання; система із запізненням; багатомодова динаміка; напівдискретизація; вектор стану; інтелектуальне керування; адаптивне моделювання

Machinery & Energetics
Vol. 16, No. 3. 2025

Journal homepage:
https://technicalscience.com.ua/en

UDC 629.5.067.4:662.76:620.9
Doi: 10.31548/machinery/3.2025.70

Oleksii Melnyk
Doctor of Technical Sciences, Professor
Odesa National Maritime University
65029, 34 Mechnykova Str., Odesa, Ukraine
https://orcid.org/0000-0001-9228-8459

Mykola Bulgakov*
PhD in Technical Sciences, Associate Professor
Odesa National Maritime University
65029, 34 Mechnykova Str., Odesa, Ukraine
https://orcid.org/0000-0002-7172-8678

Valentyna Ocheretna
PhD in Technical Sciences, Associate Professor
Odesa National Maritime University
65029, 34 Mechnykova Str., Odesa, Ukraine
https://orcid.org/0000-0003-4077-6711

Tetiana Varlan
Assistant
Odesa National Maritime University
65029, 34 Mechnykova Str., Odesa, Ukraine
https://orcid.org/0000-0001-7835-0834

Hydrogen and ammonia as next-generation marine fuels in line with IMO 2050

Abstract. This article presents an interdisciplinary analysis of hydrogen (H_2) and ammonia (NH_3) as promising alternative energy carriers for maritime transport within the framework of the International Maritime Organization's 2050 Climate Strategy. The study aimed to determine the comparative efficiency of these fuels, taking into account their thermodynamic properties, storage requirements, operational safety, infrastructural compatibility, and economic feasibility. A multi-criteria assessment method was applied, incorporating analysis of Levelized Cost of Energy (LCOE), Energy Return on Investment (EROI), Capital Expenditures (CAPEX) and Operational Expenditures (OPEX), technical readiness of port and vessel infrastructure, environmental impacts, and potential risks. Particular attention is given to toxicological aspects, fire hazards, leakage scenarios, and crew training requirements. Data from real-world and pilot projects in Japan, Norway, and the EU are presented, illustrating practical steps towards the adoption of H_2/NH_3. The findings indicate that ammonia, despite its toxicity and the need for additional safety measures, is technologically and economically more suitable for medium- and long-distance shipping due to lower transport costs and the possibility of utilising existing liquefied gas infrastructure. Hydrogen, by contrast, offers higher environmental value owing to zero CO_2 and NO_x emissions (when used in fuel cells), but requires advanced storage systems and substantial investment in logistics, which limits its use primarily to short-sea shipping or within closed supply chains. The findings can serve as a basis for shaping fleet decarbonisation strategies, developing safety standards, and fostering innovation in marine

Article's History: Received: 06.06.2025; Revised: 03.09.2025; Accepted: 23.09.2025.

Suggested Citation:
Melnyk, O., Bulgakov, M., Ocheretna, V., & Varlan, T. (2025). Hydrogen and ammonia as next-generation marine fuels in line with IMO 2050. *Machinery & Energetics,* 16(3), 70-80. doi: 10.31548/machinery/3.2025.70.

*Corresponding author

energy. The conclusions are of practical interest to shipowners, engineering companies, environmental regulators, and policymakers in the field of green marine fuels

Keywords: environmental safety; pollution prevention; NO_x emissions; ammonia toxicity; fuel energy efficiency; port infrastructure; marine environment protection

INTRODUCTION

Climate change and the tightening of international environmental standards are creating new requirements for the shipping industry, which remains one of the significant sources of greenhouse gas emissions. In 2023, the International Maritime Organization (IMO, 2023a) adopted a strategy aiming for full decarbonisation of maritime transport by 2050. This necessitates a radical transformation of fleet energy systems and a transition to alternative, carbon-free fuels. Among the most widely discussed solutions are hydrogen (H_2) and ammonia (NH_3), which produce no CO_2 emissions during combustion and offer strong potential for sustainable development. At the same time, the practical deployment of these energy carriers is associated with numerous technical and economic challenges. Low-carbon ammonia is considered a promising marine fuel owing to the absence of CO_2 emissions during combustion. W. Schreuder *et al.* (2025), in their study, conducted a techno-economic assessment showing that the capital investment required for ammonia-fuelled systems could be recouped within 7-8 years at current ammonia prices. The review by K. Machaj *et al.* (2022) systematised the challenges associated with transport, storage, and safety, proposing measures to mitigate the corrosive impact of ammonia on equipment. The study by F. Harahap *et al*. (2023) examined alternative fuels in the context of the United Nations Sustainable Development Goals, demonstrating that combining bioenergy with Carbon Capture, Utilisation and Storage (CCUS) technologies could reduce overall vessel emissions by up to 50%. B. Jesus *et al*. (2024) developed an economic model of "green" shipping corridors, highlighting the balance between capital investment and operational costs as a key factor.

A review of modern hydrogen compression and storage technologies for marine fuel cells was presented by J.-C. Li *et al*. (2024), which outlined the main engineering challenges and potential solutions. Alternative fuels in relation to the United Nations Sustainable Development Goals were also discussed by Z.I. Rony *et al.* (2023), who noted their potential to reduce emissions in the maritime sector. The technical limitations and opportunities of "green" hydrogen and ammonia were examined in detail by R. Alrashid *et al*. (2024). Despite the availability of a substantial body of analytical material, most studies focus on isolated aspects – whether environmental impact, economic costs, or technical challenges. A systematic assessment integrating all key factors – from thermodynamic characteristics and storage parameters to crew safety and capital expenditure – remains insufficiently represented in current scientific debate. In addition, there is a shortage of interdisciplinary studies that consider the influence of regulatory mechanisms, legal uncertainty, and risk scenarios in the practical deployment of hydrogen and ammonia on board vessels. Against this background, the present study aimed to conduct a comprehensive comparison of hydrogen (H_2) and ammonia (NH_3) as next-generation marine fuels in the context of achieving the IMO 2050 climate targets, taking into account their thermodynamic properties, storage parameters, environmental risks, infrastructural readiness, economic efficiency, and technological safety.

MATERIALS AND METHODS

In this research, hydrogen (H_2) and ammonia (NH_3) were selected as the objects of comparative analysis as promising alternative marine fuels. The study was based on open techno-economic data drawn from scientific publications indexed in Scopus, Elsevier, and MDPI, reports of international organisations, as well as the results of pilot projects implemented in Norway, Japan, and the EU during 2020-2024. In particular, the International Energy Agency's (IEA, 2023) forecast of global energy consumption to 2050 was examined, which also included an analysis of international shipping and aviation, thereby providing insights into global decarbonisation trends. Furthermore, the Det Norske Veritas (DNV, n.d.) Energy Transition Outlook 2025 report was reviewed, which projects the evolution of energy systems across all regions and sectors, including maritime transport, and identifies the key technological and economic barriers to the transition to low-carbon fuels. As part of the present study, data from the International Maritime Organization (IMO, 2020; 2023a; 2023b) were considered, which set out the framework and targets for emission reduction by 2050, assessed maritime transport emissions for 2018, and provided projections to 2050.

The research was conducted using analytical, comparative, and quantitative methods. Initially, scientific sources from 2019 to 2024 were systematised, after which the main comparative parameters relevant to the maritime sector were identified. The comparison employed a multi-criteria approach involving parameter normalisation and expert evaluation, covering six groups of criteria:

- thermodynamic characteristics (lower heating value, gravimetric and volumetric energy density);
- storage conditions (temperature, pressure, form);
- level of toxicity and risks (flammability, health impacts, leakage scenarios);
- infrastructural readiness (technology maturity, availability of terminals);

- economic efficiency (Levelized Cost of Energy (LCOE), Energy Return on Investment (EROI), Capital Expenditures (CAPEX), Operational Expenditures (OPEX));
- environmental consequences (CO_2, NO_x, secondary impacts on ecosystems).

For each parameter, data were normalised and the relative importance was weighted by experts, ensuring an objective ranking of the fuels in terms of their suitability for application in marine energy systems. This multi-criteria approach made it possible to clearly distinguish the strengths and weaknesses of each technology – for example, the high energy density of ammonia but its demanding storage requirements, or the safe use of hydrogen at the cost of significant capital investment in compression. Subsequently, the techno-physical and chemical characteristics of H_2 and NH_3 were collected, comparative tables were constructed, and the storage conditions and logistical readiness of the sector were evaluated. To provide a comprehensive assessment of the environmental and economic viability of alternative marine fuels, six key indicators were applied:

- LCOE – enables comparison of the full cost of 1 MWh of final energy, accounting for capital (CAPEX) and operational (OPEX) expenditures over the entire system life cycle;
- EROI – the ratio of total energy generated by the system to the energy invested in its construction and maintenance, indicating the “energy payback” of the technology;
- CAPEX – capital expenditures on construction and installation of equipment, which determine the initial investment barriers;
- OPEX – operational expenditures on maintenance, fuel, and logistics, influencing overall long term profitability;
- CO_2-equivalent emissions – an assessment of direct greenhouse gas emissions, adjusted for the fuel’s life cycle, to compare impacts on global warming;
- NO_x, SO_x, $PM_{10/2.5}$ – local air pollutants that determine the environmental and social acceptability of the solution.

The use of this set of indicators ensured a balanced evaluation: economic (LCOE, CAPEX, OPEX), energy-related (EROI), and environmental (greenhouse gas and pollutant emissions) components, all of which are necessary for making informed decisions regarding the adoption of new technologies in marine energy systems.

LCOE – the levelised cost of energy over the life cycle, calculated using the formula:

$$LCOE = \frac{\sum_{t=1}^{N} \frac{I_t + M_t + F_t}{(1+r)^t}}{\sum_{t=1}^{N} \frac{E_t}{(1+r)^t}}, \quad (1)$$

where I_t is the capital expenditures in year t; M_t is the maintenance costs; F_t is the fuel costs; E_t is the energy produced; r is the discount rate; N is the service life (assumed to be 20 years). Source data were taken from the report by S. Brynolf *et al.* (2023).

EROI – the ratio of the energy produced by the system to the energy consumed for its construction and maintenance, calculated as:

$$EROI = \frac{Output\ Energy}{Input\ Energy}, \quad (2)$$

where *Output Energy* is the useful energy; *Input Energy* is the total energy required for production, storage, and delivery. EROI values for H_2 and NH_3 were drawn from open sources.

The methods described provided a generalised assessment of the efficiency of hydrogen and ammonia in the context of maritime decarbonisation, taking into account both technological and practical aspects of their implementation.

RESULTS

Physicochemical characteristics of hydrogen and ammonia

Within the framework of the IMO strategy (2023a) to achieve net-zero greenhouse gas emissions by 2050, hydrogen (H_2) and ammonia (NH_3) are considered as potential alternatives to conventional marine fuels. The choice between them depends on their physicochemical properties, safety levels, and environmental characteristics. An objective comparison of these substances makes it possible to evaluate their potential in maritime transport. Below is a comparison of the key physicochemical parameters that are critically important in terms of energy performance, safety, and operational use on board vessels. The data presented in Table 1 make it possible to assess the key parameters relevant to the industry’s transition to carbon-free fuels.

Table 1. Comparative characteristics of hydrogen and ammonia

Criterion	Hydrogen	Ammonia
Chemical formula	H_2	NH_3
Molar mass (g/mol)	2.016	17.031
Physical state at 20 °C	Gas	Gas
Boiling point (°C)	-252.9	-33.3
Ignition temperature (°C)	~560	~651
Explosion limits (vol. %)	4-75	15-28
Density in liquid state (kg/m³)	~70.8	~681
Gravimetric energy density (MJ/kg)	120	18.6
Volumetric energy density (MJ/L)	8.5	11.5
Odour	Low	Strong
Flame visibility during combustion	Invisible	Pale yellow, visible

Continued Table 1.

Criterion	Hydrogen	Ammonia
CO_2 emissions on combustion	None	None
NO_x emissions on combustion	Possible	High
Infrastructure status	Limited	Partially available
Production cost (approx.)	Strong	Medium

Source: authors' compilation

Both energy carriers can be produced using renewable energy sources, which is critical for achieving full carbon neutrality. Green hydrogen is generated through water electrolysis, in which electrical energy from renewable sources (solar, wind, hydro) splits H_2O molecules into molecular hydrogen and oxygen. The most common method is Proton Exchange Membrane (PEM) electrolysis, characterised by high current density, rapid start-up, and the ability to operate with fluctuating energy flows. However, it requires an expensive platinum-based catalytic system and highly purified feedwater. The energy conversion efficiency (η) of modern PEM electrolysers reaches 60%-70%, with the main losses arising from electrode overpotentials and membrane resistance. Only after hydrogen is purified to ≥99.9% can it be supplied to fuel cells or compressed to 350-700 bar for storage and transport, which adds approximately 10%-15% to the overall energy demand. Green ammonia is synthesised via the Haber-Bosch process from green hydrogen and nitrogen, the latter separated from air using Pressure Swing Adsorption (PSA) units. The synthesis occurs under high pressure (150-300 bar) and elevated temperatures (400°C-500°C) in the presence of an iron catalyst. Maintaining these conditions consumes around 25%-30% of the produced hydrogen in the form of thermal and mechanical energy. However, the resulting ammonia can be readily liquefied at -33°C under normal pressure and stored in standard lowpressure tanks, which minimises compression-related energy requirements compared with hydrogen (Thomas & Parks, 2006). The overall energy conversion efficiency of the "electricity → hydrogen → ammonia" chain is about 50%-55%. Nevertheless, the absence of high-pressure storage needs makes this pathway more suitable for maritime logistics (Valera-Medina *et al.*, 2018; Brynolf *et al.*, 2023). The principal reaction is as follows:

$$2H_2O \rightarrow 2H_2 + O_2. \tag{3}$$

Green ammonia is synthesised through the Haber-Bosch reaction, in which hydrogen is derived from renewable sources and nitrogen from air. The choice between hydrogen and ammonia as future marine fuels largely depends on their physicochemical characteristics, environmental safety, production costs, and compatibility with existing infrastructure. Data in Table 1 indicate that hydrogen has a clear advantage in terms of gravimetric energy density. However, its low volumetric density and extremely low storage temperature make its use technically challenging. Ammonia, by contrast, is more readily integrated into existing infrastructure and easier to store, but it raises serious environmental and safety concerns owing to its high toxicity and NO_x emissions.

Thermodynamic properties of hydrogen and ammonia

On a mass basis, hydrogen (LHV ≈ 120 MJ/kg) has nearly six times the energy density of ammonia (LHV ≈ 20 MJ/kg). Yet, due to the low density of liquid hydrogen (~71 kg/m³), its volumetric energy density (≈ 8.5 MJ/L) is significantly lower than that of ammonia (≈ 11.5 MJ/L at 681 kg/m³). This tradeoff between the high gravimetric energy density of hydrogen and the more compact storage volume of ammonia determines the choice of fuel according to available onboard space and the need to ensure sufficient energy reserves for long voyages. Hydrogen is a highly explosive gas with a broad flammability range in air (4%-75% vol.) and a low ignition temperature (~560°C), which increases the risk of auto-ignition in the event of accidental leaks. Ammonia is less explosive but becomes toxic at concentrations above 300 ppm, can cause equipment corrosion, and poses health hazards upon exposure.

Hydrogen requires high-pressure storage (350-700 bar) or cryogenic tanks at -253°C, which necessitates specialised cylinders and compensation for diffusion-related leakage. Ammonia, by contrast, can be stored in liquid form at -33°C under relatively low pressure (~10 bar), greatly simplifying its integration into existing terminals and fuel corridors. Ammonia infrastructure is already partially available in key ports, whereas hydrogen would require substantial capital investment in new compression modules and refrigeration systems. The assessment of thermodynamic properties is crucial for determining fuel efficiency in marine energy applications. The most important parameters are the gravimetric and volumetric lower heating values (LHV), which define the amount of usable energy under real operating conditions. Hydrogen exhibits exceptionally high gravimetric energy density, nearly 6.5 times greater than that of ammonia. However, owing to its low liquid density (~71 kg/m³ compared with 681 kg/m³ for NH_3), its volumetric energy density is only 8.5 MJ/L, whereas ammonia achieves 11.5 MJ/L. This means that under the space constraints typical on board of ships, ammonia provides more energy per unit volume, a critical factor in practical applications. In addition, ammonia has a higher ignition temperature (651°C compared with ~560°C for hydrogen), reducing the risk of auto-ignition under accident conditions.

Safety, toxicity and operational risks

The adoption of alternative fuels in maritime transport is not feasible without a comprehensive assessment of safety issues. Although hydrogen and ammonia are regarded as promising pathways towards fleet decarbonisation due to their carbon-free nature, their use entails significant risks that affect ship design, storage systems, maintenance organisation, and even crew training requirements. For hydrogen, the most critical concerns are its high flammability, wide range of explosive concentrations in air, and the tendency to produce invisible flames during combustion. As a result, even minor leaks may lead to catastrophic consequences if effective detection, ventilation, and cut-off systems are not in place. From a technical standpoint, the challenge is compounded by the need for storage at extremely low temperatures, requiring cryogenic tanks with advanced insulation. Ammonia, unlike hydrogen, is not explosive in the conventional sense. However, its vapours irritate mucous membranes, may cause chemical burns, and pose serious risks to personnel, especially in the event of leaks within enclosed or poorly ventilated spaces. Moreover, ammonia is corrosively aggressive to certain metals, necessitating careful selection of materials for pipelines, fittings, and storage systems (Li *et al.*, 2025). Therefore, while both fuels hold potential for reducing emissions, their safe integration into marine systems demands meticulous engineering design, regulatory adaptation, and specialised crew training.

Table 2 presents a comparison of the key risks associated with the use of hydrogen and ammonia in shipping – ranging from differences in toxicity and flammability to ignition energy, incident scenarios, and the readiness of detection systems and regulatory frameworks. Hydrogen has the advantage of being non-toxic, but requires very low ignition energy and rapid sensor response due to its wide flammability range. Ammonia, while easier to store in liquefied form, demands careful management of toxic leaks, protective equipment for crew members, and adherence to temporary IMO guidelines (2020).

Table 2. Risks and safety measures

Parameter	Hydrogen (H_2)	Ammonia (NH_3)
Toxicity	Low. Non-toxic, but displaces oxygen in the air	High. Toxic when inhaled; irritates skin and eyes
Flammability	High (4%-75% in air), invisible flame	Moderate (15%-28% in air), visible flame
Ignition energy	Very low (0.02 mJ)	Higher (~0.3 mJ), auto-ignition at ~651°C
Risk scenarios	Leak → explosion without warning	Leak → toxic air contamination
Detection systems	H_2 detectors, ventilation control	NH_3 sensors (25/110/220 ppm), extraction, emergency shut-off
Regulatory framework (IMO)	Under development	Temporary IMO principles (2020)
Crew training needs	High (explosion response)	Very high (handling toxic substances)

Source: authors' compilation on base R. Alrashid *et al.* (2024)

The storage of hydrogen and ammonia in maritime applications is determined not only by their energy density but also by the technological requirements of tanks and maintenance systems. Hydrogen requires either high-pressure composite tanks (350-700 bar) to minimise leakage or cryogenic storage at -253°C with ultra-low boil-off losses, which demands complex insulation and continuous monitoring. By contrast, ammonia can be stored in liquid form at relatively moderate conditions (~10 bar and -33°C) in conventional steel tanks with anti-corrosion coatings, substantially reducing both capital and operational infrastructure costs. This difference in storage regimes determines the choice of fuel system depending on the availability of technical equipment, onboard space constraints, and the economic feasibility of implementation (Table 3).

Table 3. Comparative analysis of hydrogen and ammonia storage parameters

Parameter	Hydrogen (H_2)	Ammonia (NH_3)
Storage form	Liquid (cryogenic) / Compressed gas	Liquid / Pressurised
Storage temperature (°C)	-253	-33
Storage pressure (bar)	~350-700	~10-20
Volume per 1 MJ of energy	High (low density)	Lower (higher density)
Volatility	Very high	High
Leak potential	Significant	Moderate
Tank requirements	Double-walled, vacuum-insulated	Comparable to liquefied petroleum gas (LPG) infrastructure

Source: authors' compilation on base R. Alrashid *et al.* (2024)

The table shows that storing liquid hydrogen is technically demanding, as it requires a temperature of -253°C, which is close to absolute zero. Such conditions necessitate advanced tanks with multilayered insulation. Compressed hydrogen is an alternative, but pressures of up to 700 bar complicate safe handling. Ammonia, on the other hand, can be stored under moderate conditions, making it compatible with existing LPG terminals and easier to adapt for maritime use.

Infrastructure requirements for the deployment of carbon-free fuels

One of the key factors in the adoption of alternative marine fuels is the availability, scalability, and technological maturity of the supporting infrastructure. In this respect, ammonia demonstrates a significant advantage over hydrogen: a global network for its production, storage, and transportation is already in place. More than 180 million tonnes of NH_3 are produced annually worldwide, with supply chains covering most major ports, particularly in Asia, Europe, and the Middle East (IEA, 2023). By contrast, infrastructure for hydrogen – especially in liquid or compressed form – remains at a formative stage. It requires advanced terminals, cryogenic storage facilities, and high-pressure pipelines, which considerably increase both costs and implementation time (Table 4).

Table 4. Comparative overview: Infrastructure requirements

Aspect	Hydrogen (H_2)	Ammonia (NH_3)
Maturity of production	In development (green H_2 via electrolysis)	Established (green NH_3 under trial)
Storage infrastructure	Cryogenic tanks/high-pressure vessels	Existing tanks similar to LPG
Transport logistics	Limited: pipelines + road (pilot scale)	Global network: maritime, rail, and pipelines
Port readiness (2025)	Several demonstration projects	Over 120 terminals compatible with NH_3
Compatibility with existing systems	Low (requires new designs)	Medium-high (possible adaptation of LPG systems)
Capital expenditure for scaling	Very high	Medium-high

Source: authors' compilation O. Melnyk *et al.* (2024; 2025)

Ammonia is more suitable for rapid adaptation in ports and on vessels, as it can make use of part of the existing LPG infrastructure. However, given the production process of "green" ammonia, the development of infrastructure directly depends on the scaling of renewable hydrogen production, creating a kind of "double barrier" – first requiring electrolysis capacity, followed by adapted or new industrial complexes for ammonia synthesis. This means that even with a global logistics network already in place, the transition to "green" NH_3 demands investments in production and port facilities no less substantial than in the case of H_2, although the initial conditions for ammonia integration are more favourable. It should also be noted that the production of these 'green' fuels generates competition for inexpensive energy resources and must be aligned with national and regional policies, including EU directives. Thus, the choice between hydrogen and ammonia for shipping depends not only on the technological maturity of production, but also on the availability of infrastructure and integration with energy policy.

Performance assessment: LCOE, EROI, CAPEX + OPEX

For the strategic planning of hydrogen and ammonia use in maritime transport, it is important to consider not only their thermodynamic and infrastructural characteristics but also their overall economic viability. The assessment was carried out using three key indicators: LCOE, EROI, and combined CAPEX + OPEX, representing investment and operational costs. The assessment of total implementation costs includes: CAPEX – infrastructure costs for fuel production, storage, and processing; and OPEX – expenses for cooling, pressure, safety, and maintenance (Table 5).

Table 5. Integrated comparative table of economic efficiency: H_2 vs. NH_3

Indicator	Hydrogen (H_2)	Ammonia (NH_3)
LCOE (USD/MWh)	200-300	150-220
EROI	~4-6	~5-8
CAPEX	Very high: electrolysers, cryogenic storage	Moderate: synthesis plants, compatible tanks
OPEX	High: cooling to -253°C, compression	Medium: cooling to -33°C
Commercial readiness	Low (TRL 6-7), requires R&D	Higher (TRL 8-9), partly integrated into the industry

Note: TRL – technology readiness level, R&D – research and development
Source: authors' compilation

Table 5 shows that ammonia outperforms hydrogen in economic terms: its LCOE (150220 USD/MWh) is 25%-50% lower, and its EROI (~5-8) is somewhat higher than that of hydrogen (200-300 USD/MWh and ~4-6, respectively). At the same time, hydrogen requires significantly higher capital expenditure (CAPEX) for electrolysers and cryogenic storage, and has high operational costs (OPEX) for cooling to -253°C and compression. By contrast, ammonia involves moderate CAPEX – synthesis plants and compatible tanks – and lower OPEX, as liquefaction requires only -33°C. Technology readiness levels (TRLs) further highlight this difference: hydrogen is at stages 6-7 and still requires additional research and development, whereas ammonia is at 8-9 and is already partly integrated into the industry. Thus, although hydrogen has a higher energy potential, ammonia represents a more realistic short- and medium-term alternative for decarbonising the maritime fleet due to its economic and technological availability.

Experimental and commercial projects

As part of the global decarbonisation strategy for shipping by 2050, a number of companies and international organisations have launched projects aimed at introducing alternative fuels such as hydrogen and ammonia (Table 6). These initiatives range from demonstration vessels to the creation of 'green corridors' for zero-carbon transport. Current priorities include the deployment of clean-fuel bunkering infrastructure in major ports, the development of safety standards for handling ammonia, and the testing of storage and fuel supply systems for next-generation marine power plants. In addition, intergovernmental partnerships are actively being established to fund life-cycle assessments of such fuels, as well as subsidy mechanisms to support operators in transitioning to environmentally neutral technologies.

Table 6. Key implemented ammonia and hydrogen fuel projects

Project/initiative	Participants and country	Fuel type	Route/test	Infrastructure	Expected performance
Fortescue Green Pioneer	Fortescue (Australia); MPA, Seatrium, Vopak, A*STAR's IHPC, NTU, DNV (Singapore)	Liquid ammonia (NH_3)	Trial in Singapore; voyage to the Persian Gulf during COP28	Vopak terminals; HAZID/HAZOP system; drones, shore-based monitoring	Significant CO_2 reduction; "Gas Fuelled Ammonia" certification
Dutch ammonia tanker	C-Job Naval Architects, Proton Ventures, Enviu, Province of ZuidHolland (Netherlands)	Ammonia (NH_3)	Laboratory models and preliminary trials; voyage not yet commenced	Integration with the LPG port infrastructure in the Netherlands	~44% higher energy efficiency compared with hydrogen
CAMPFIRE Ammonia Sherpa	ENERTRAG, Sunfire, KIT, University of Rostock, ZBT (Germany)	Ammonia (NH_3)	Yacht Ammonia Sherpa tested in 2023; barge Odin planned for 2026	Bunkering system constructed in Rostock port	~350 kW electricity generation; targeted at small vessels
Sea Change Project	USA	Hydrogen	San Francisco Bay	Mobile hydrogen refuelling station (tube trailers) by West Coast Clean Fuels and Plug Power	65% energy penetration into fuel cells
MF Hydra	Norway	Liquid hydrogen	Hjelmeland-Nesvik route	Shore-based LH_2 terminals, refuelling stations	50%-60%
Kawasaki DualFuel Generatoк	Japan	Hydrogen	Dual-fuel engine	Prototype engine only	Engine thermal efficiency 42%-45%

Source: authors' compilation based on B. Holtze (2023), Nippon Yusen Kabushiki Kaisha (2023), L.E. Klebanoff (2024), E. Van Sickle *et al.* (2025)

According to Table 6, ammonia projects are predominantly at the demonstration and pilot stage. Their main focus is the testing of technologies (internal combustion engines, cracking), bunkering operations, and proving safety. By contrast, hydrogen projects have already advanced to the stage of commercial operation. They are deployed on regular routes, demonstrating the practical viability of the technology for short voyages such as port services, ferries, and tugs. As part of the global strategy to decarbonise maritime transport by 2050, a number of important demonstration and commercial projects are being implemented using "green" fuels. E. Van Sickle *et al.* (2025) described the first commercial hydrogen-powered passenger ferry, MV Sea Change, which features integrated fuel management and a fuel cooling system. The ferry was designed by Mitsubishi FCH Energy and certified by DNV. According to L.E. Klebanoff (2024), its efficiency reached 65% (energy penetration into the fuel cell), the infrastructure consisted of a mobile hydrogen refuelling station, and no incidents were recorded. Since 2023, a consortium of Japanese manufacturers has been testing a shipboard ammonia and hydrogen fuel system on the Yokohama-Tokyo route; preliminary data indicate a stable energy conversion efficiency of 50% and a requirement to upgrade terminal gasifiers (Nippon Yusen Kabushiki Kaisha, 2023). All projects demonstrate the commercial viability and technical reliability of "green" technologies without significant incidents, establishing a model for large-scale adoption in global shipping.

The results of the comparative analysis show that both hydrogen and ammonia can play a key role in the decarbonisation of maritime transport. However, their effectiveness is not universal, as it depends on factors such as vessel type, route characteristics, infrastructure availability, and the technological maturity of the relevant solutions. Hydrogen is almost ideal from an environmental perspective, producing no CO_2 emissions and, when used in fuel cells, no toxic nitrogen oxides. However, considering the technological characteristics specifically – low volumetric energy density, the need for deep cooling or high pressure, and the lack of established logistics – hydrogen's widespread adoption is currently severely constrained, particularly for long-distance transport. The production cost of "green" hydrogen also remains high. Ammonia, by contrast, has proven to be a far more practical marine fuel, as its transportation and storage processes can be managed using existing infrastructure, such as liquefied gas port terminals, making it less expensive in the short to medium term. The analysis indicates that hydrogen's environmental advantages are offset by the high cost of logistics. At the same time, despite certain operational risks, ammonia appears to be a more realistic option for large-scale deployment in the coming years. The primary challenge remains infrastructure reform – without public engagement, global standards, and demonstration projects, neither H_2 nor NH_3 will move from concept to feasible commercial implementation. This underscores the importance of contributions from the IMO, the European Commission, and national governments in defining the regulatory environment and providing financial incentives for the sector.

DISCUSSION

The results of the comparative analysis of hydrogen and ammonia as next-generation marine fuels are broadly consistent with recent studies, although in some cases differences have emerged that require critical consideration. The present study focuses on thermodynamic characteristics, safety risks, economic feasibility, and infrastructural readiness, which made it possible to justify the use of ammonia on medium- and long-distance routes and hydrogen for short coastal shipping. Similar findings are reported in a number of international studies; however, detailed comparisons revealed differing approaches to assessing future prospects. H. Xing *et al*. (2021) outlined strategic directions for the adoption of low-carbon fuels by 2050 and emphasised that without active involvement of governments and international organisations, the transition to "green" technologies will be extremely slow. The results of the present analysis confirm this argument, as for both hydrogen and ammonia, state support and regulatory incentives remain the key factors for scaling up. One of the most critical aspects of adopting carbon-free technologies is economic efficiency. For instance, the study by M. Abbas *et al*. (2024), dedicated to optimising energy consumption in maritime transport, demonstrated the importance of effective energy flow management on board vessels. The present study also highlights the significance of economic efficiency through the indicators of LCOE and EROI. The results of both analyses converge in showing that even environmentally attractive fuels cannot be adopted without sufficient economic benefit. However, the findings presented here stress that ammonia currently offers lower operating costs due to the use of existing LPG terminals in ports. This conclusion is also supported by the study of Y. Wang *et al*. (2022), which examined low- and zero-carbon fuel technologies in the context of economic efficiency. It has been shown that the most promising solutions are those that combine low capital expenditure with the use of existing infrastructure.

These conclusions are supported by analyses of operational projects aimed at reducing carbon emissions from ships. For example, G.N. Lee *et al*. (2024) conducted a life-cycle assessment of hydrogen supply methods between Australia and South Korea and identified the advantages of systems based on renewable energy sources. The present study confirmed their conclusion of lower emissions when using "green" hydrogen, but also demonstrated that logistical complexity and transport costs remain significant barriers to large-scale deployment. In turn, H. Fan *et al*. (2025) analysed the development timeline of hydrogen-powered vessels and showed that most commercial trials occur on short routes, where constraints related to fuel storage and infrastructure are not critical. The present findings likewise support the view that hydrogen is best suited for coastal shipping and local operations. Both studies, therefore, converge on the conclusion that hydrogen has limited applicability in long-distance maritime transport. A. Arias *et al*. (2024) investigated barriers to the integration of biofuels into marine systems and emphasised the need for standardisation and technical compatibility. The present results revealed that similar barriers exist for the use of ammonia and hydrogen as marine fuels, particularly in relation to crew safety and the technologies required for storage and transport. In this respect, it becomes evident that the challenges of standardisation are common to all low-carbon technologies. S. Tasleem *et al*. (2024) systematised the technologies for producing "green" hydrogen, as well as its storage and transport, and highlighted the potential for combining them with CCUS technologies. The present study expanded upon their review by providing a more detailed examination of risks and safety aspects, which were not central to their analysis.

The primary focus of this study was on comparing two fuels – hydrogen and ammonia. However, other integrated technologies for reducing the carbon footprint and achieving decarbonisation in shipping are also of importance, particularly in terms of economic efficiency. Z. Wang *et al*. (2024) investigated configurations of hybrid low-carbon marine energy systems, including fuel cells and battery packs, and proposed broader system integration. This demonstrated the differing scales of research but also underscored the importance of pursuing combined energy solutions. O. Melnyk *et al*. (2024; 2025) presented modelling and experimental results showing the feasibility of integrating renewable energy sources with carbon capture technologies. The present findings confirmed their conclusions regarding the potential for significant reductions in CO_2 emissions and improvements in energy efficiency, while supplementing their conclusions with quantitative indicators of economic viability. Thus, this study broadened the practical understanding of the feasibility of adopting such technologies. In summary, the present research largely confirmed the conclusions of earlier studies, while refining them through quantitative analysis, comparison of risks, and assessment of infrastructural constraints. This approach made it possible to more clearly define the applicability limits of hydrogen and ammonia in shipping and provided a basis for further research.

CONCLUSIONS

The study compared hydrogen (H_2) and ammonia (NH_3) as alternative marine fuels, taking into account their physicochemical, logistical and economic characteristics in the context of the IMO 2050 targets. The literature was systematised and analysed, six groups of comparative parameters were identified (thermodynamics, storage, safety, infrastructure, economics, ecology), and key indicators were calculated – LCOE, EROI, CAPEX, OPEX and emissions. The findings confirmed that ammonia demonstrates a lower LCOE (150-220 USD/MWh) and higher EROI (~5-8) compared with hydrogen (200-300 USD/MWh; EROI ~4-6), as well as a more developed storage infrastructure at -33°C and ~10-20 bar, making it a more promising option for fleet decarbonisation. At the same time, hydrogen, despite its higher gravimetric energy density and zero emissions when produced through "green" pathways, remains constrained by high-pressure (350-700 bar) or cryogenic (-253°C) storage, substantial capital requirements for compression and cooling, and the need for refined safety protocols addressing explosion risks. The study conceptualised renewable pathways of "electricity → hydrogen → ammonia", where ammonia serves as an intermediate carrier with an optimal balance of cost, safety and available infrastructure. The comparison of the two carbon-free fuels, alongside a review of experimental and operational projects employing them in shipping, confirmed that each has distinct advantages depending on the type of maritime transport. Hydrogen was found to be more suitable for coastal or short-distance operations, whereas ammonia systems demonstrated greater technological and infrastructural readiness for medium- and long-distance shipping.

Promising directions for further research include: the development of hybrid fuel cores that combine hydrogen and ammonia in blends to reduce storage pressure; life-cycle modelling of infrastructure under regional conditions; the integration of digital systems for leak monitoring and real-time corrective management algorithms; and the analysis of social and economic factors influencing the adoption of "green" technologies at the local level. Together, these directions could support the transition from demonstration trials to large-scale commercial deployment, ensuring that opportunities to achieve carbon neutrality in maritime transport are not lost.

ACKNOWLEDGEMENTS

None.

FUNDING

None.

CONFLICT OF INTEREST

None.

REFERENCES

[1] Abbas, M., Abbas, Q., Khan, A., Tayyab, S.M., Rizvi, S.H.M., Raza, A., Zaidi, S.S.H., Razzaqi, A.A., Haider, S., & Sarfraz, S.A. (2024). Energy management in marine transportation sector. *Comprehensive Energy Systems*, 2(10), 126-156. doi: 10.1016/B978-0-44-313219-3.00151-9.

[2] Alrashid, R., Mahmoud, M., & Alami, A.H. (2024). Introduction to green hydrogen and green ammonia. In *Comprehensive green materials* (Vol. 1, pp. 256-271). Amsterdam: Elsevier. doi: 10.1016/B978-0-443-15738-7.00038-6.

[3] Arias, A., Nika, C.-E., Vasilaki, V., Feijoo, G., Moreira, M.T., & Katsou, E. (2024). Assessing the future prospects of emerging technologies for shipping and aviation biofuels: A critical review. *Renewable and Sustainable Energy Reviews*, 197, article number 114427. doi: 10.1016/j.rser.2024.114427.

[4] Brynolf, S., Kanchiralla, F., Malmgren, E., Ellis, J., Olsson, T., Hansson, J., & Fridell, E. (2023). *Hydrogen, ammonia and battery-electric propulsion for future shipping*. Borlänge: Trafikverket, Lighthouse – Swedish Transport Administration's Industry Program Sustainable Shipping.

[5] DNV. (n.d.). *Energy transition outlook*. Retrieved from https://www.dnv.com/energy-transition-outlook/.

[6] Fan, H., Abdussamie, N., Chen, P.S.-L., Harris, A., Gray, E.M., Arzaghi, E., Bhaskar, P., Mehr, J.A., & Penesis, I. (2025). Two decades of hydrogen-powered ships (2000-2024): Evolution, challenges, and future perspectives. *Renewable and Sustainable Energy Reviews*, 219, article number 115878. doi: 10.1016/j.rser.2025.115878.

[7] Harahap, F., Nurdiawati, A., Conti, D., Leduc, S., & Urban, F. (2023). Renewable marine fuel production for decarbonised maritime shipping: Pathways, policy measures and transition dynamics. *Journal of Cleaner Production*, 415, article number 137906. doi: 10.1016/j.jclepro.2023.137906.

[8] Holtze, B. (2023). *World's first liquid hydrogen-powered ship MF Hydra is powered by Ballard's fuel cells*. Retrieved from https://surl.li/ntcqxd.

[9] IEA. (2023). *World energy outlook 2023*. Retrieved from https://www.iea.org/reports/world-energy-outlook-2023.

[10] IMO. (2020). *MSC.1/Circ.1687: Interim guidelines for the safety of ships using alternative fuels*. Retrieved from https://surl.lt/iriwly.

[11] IMO. (2023a). *2023 IMO strategy on reduction of GHG emissions from ships*. Retrieved from https://www.imo.org/en/OurWork/Environment/Pages/2023-IMO-Strategy-on-Reduction-of-GHG-Emissions-from-Ships.aspx.

[12] IMO. (2023b). *Fourth IMO GHG study 2020*. Retrieved from https://www.imo.org/en/ourwork/environment/pages/fourth-imo-greenhouse-gas-study-2020.aspx.

[13] Jesus, B., Ferreira, I.A., Carreira, A., Ove Erikstad, S., & Godina, R. (2024). Economic framework for green shipping corridors: Evaluating cost-effective transition from fossil fuels towards hydrogen. *International Journal of Hydrogen Energy*, 83, 1429-1447. doi: 10.1016/j.ijhydene.2024.08.147.

[14] Klebanoff, L.E. (2024). *MV Sea Change: Fuel cell, emissions, and hydrogen fueling performance*. Livermore, CA: Sandia National Laboratories.

[15] Lee, G.N., Kim, J.M., Jung, K.H., & Park, H. (2024). Comparative life cycle assessment of various hydrogen supply methods from Australia to the Republic of Korea in environmental and economic aspects. *Science of The Total Environment*, 947, article number 174669. doi: 10.1016/j.scitotenv.2024.174669.

[16] Li, J.-C., Xu, H., Zhou, K., & Li, J.-Q. (2024). A review on the research progress and application of compressed hydrogen in the marine hydrogen fuel cell power system. *Heliyon*, 10(3), article number e25304. doi: 10.1016/j.heliyon.2024.e253045304.

[17] Li, Z., Wang, K., Liang, H., Wang, Y., Ma, R., Cao, J., & Huang, L. (2025). Marine alternative fuels for shipping decarbonization: Technologies, applications and challenges. *Energy Conversion and Management*, 329, article number 119641. doi: 10.1016/j.enconman.2025.119641.

[18] Machaj, K., Kupecki, J., Malecha, Z., Morawski, A., Skrzypkiewicz, M., Stanclik, M., & Chorowski, M. (2022). Ammonia as a potential marine fuel: A review. *Energy Strategy Reviews*, 44, article number 100926. doi: 10.1016/j.esr.2022.100926.

[19] Melnyk, O., Bulgakov, M., Fomin, O., Onyshchenko, S., Onishchenko, O., & Pulyaev, I. (2025). Sustainable development of renewable energy in shipping: Technological and environmental prospects. *Scientific Journal of Silesian University of Technology. Series Transport,* 127, 165-188. doi: 10.20858/sjsutst.2025.127.10.

[20] Melnyk, O., Onyshchenko, S., Onishchenko, O., Shumylo, O., Voloshyn, A., Ocheretna, V., & Fedorenko, O. (2024). Implementation research of alternative fuels and technologies in maritime transport. In S. Boichenko, A. Zaporozhets, A. Yakovlieva & I. Shkilniuk (Eds.), *Studies in systems, decision and control* (Vol. 510, pp. 13-21). Cham: Springer. doi: 10.1007/978-3-031-44351-0_2.

[21] Nippon Yusen Kabushiki Kaisha (NYK Line). (2023). *NYK Conducts world's first test operation of ammonia-fueled vessel*. Retrieved from https://www.nyk.com/english/news/2023/20230516_01.html.

[22] Rony, Z.I., Mofijur, M., Hasan, M.M., Rasul, M.G., Jahirul, M.I., Ahmed, S.F., Kalam, M.A., Badruddin, I.A., Khan, T.M.Y., & Show, P.-L. (2023). Alternative fuels to reduce greenhouse gas emissions from marine transport and promote UN sustainable development goals. *Fuel*, 338, article number 127220. doi: 10.1016/j.fuel.2022.127220.

[23] Schreuder, W., Slootweg, J.C., & van der Zwaan, B. (2025). Techno-economic assessment of low-carbon ammonia as fuel for the maritime sector. *Applications in Energy and Combustion Science*, 22, article number 100330. doi: 10.1016/j.jaecs.2025.100330.

[24] Tasleem, S., Bongu, C.S., Krishnan, M.R., & Alsharaeh, E.H. (2024). Navigating the hydrogen prospect: A comprehensive review of sustainable source-based production technologies, transport solutions, advanced storage mechanisms, and CCUS integration. *Journal of Energy Chemistry*, 97, 166-215. doi: 10.1016/j.jechem.2024.05.022.

[25] Thomas, G., & Parks, G. (2006). *Potential roles of ammonia in a hydrogen economy: A study of issues related to the use of ammonia for on-board vehicular hydrogen storage*. Washington: U.S. Department of Energy.

[26] Valera-Medina, A., Xiao, H., Owen-Jones, M., David, W.I.F., & Bowen, P.J. (2018). Ammonia for power. *Progress in Energy and Combustion Science*, 69, 63-102. doi: 10.1016/j.pecs.2018.07.001.

[27] Van Sickle, E., Ralli, P., Pratt, J., & Klebanoff, L. (2025). MV Sea Change: The first commercial 100% hydrogen fuel cell passenger ferry in the world. *International Journal of Hydrogen Energy*, 105, 389-404. doi: 10.1016/j.ijhydene.2025.01.040.

[28] Wang, Y., Cao, Q., Liu, L., Wu, Y., Liu, H., Gu, Z., & Zhu, C. (2022). A review of low and zero carbon fuel technologies: Achieving ship carbon reduction targets. *Sustainable Energy Technologies and Assessments*, 54, article number 102762. doi: 10.1016/j.seta.2022.102762.

[29] Wang, Z., Dong, B., Li, M., Ji, Y., & Han, F. (2024). Configuration of low-carbon fuels green marine power systems in diverse ship types and applications. *Energy Conversion and Management*, 302, article number 118139. doi: 10.1016/j.enconman.2024.118139.

[30] Xing, H., Stuart, C., Spence, S., & Chen, H. (2021). Alternative fuel options for low carbon maritime transportation: Pathways to 2050. *Journal of Cleaner Production*, 297, article number 126651. doi: 10.1016/j.jclepro.2021.126651.

Олексій Мельник

Доктор технічних наук, професор
Одеський національний морський університет
65029, вул. Мечникова, 34, м. Одеса, Україна
https://orcid.org/0000-0001-9228-8459

Микола Булгаков

Кандидат технічних наук, доцент
Одеський національний морський університет
65029, вул. Мечникова, 34, м. Одеса, Україна
https://orcid.org/0000-0002-7172-8678

Валентина Очеретна

Кандидат технічних наук, доцент
Одеський національний морський університет
65029, вул. Мечникова, 34, м. Одеса, Україна
https://orcid.org/0000-0003-4077-6711

Тетяна Варлан

Асистент
Одеський національний морський університет
65029, вул. Мечникова, 34, м. Одеса, Україна
https://orcid.org/0000-0001-7835-0834

Водень та аміак як суднове паливо наступного покоління згідно з IMO 2050

Анотація. У статті здійснено міждисциплінарний аналіз водню (H_2) та аміаку (NH_3) як перспективних альтернативних енергоносіїв для морського транспорту в умовах реалізації кліматичної стратегії-2050 Міжнародної морської організації. Метою дослідження стало визначення порівняльної ефективності зазначених палив з урахуванням їх термодинамічних властивостей, умов зберігання, експлуатаційної безпеки, інфраструктурної сумісності та економічної доцільності. У роботі використано методику багатокритеріального оцінювання, яка включає аналіз показників LCOE (Levelized Cost of Energy), EROI (Energy Return on Investment), CAPEX (Capital Expenditures) та OPEX (Operational Expenditures), технічної готовності портової та суднової інфраструктури, екологічних наслідків і потенційних ризиків. Окрема увага приділена токсикологічним аспектам, ризикам займання, сценаріям витоків і вимогам до підготовки екіпажу. Наведено дані з реальних та пілотних проєктів у Японії, Норвегії та ЄС, що демонструють практичні кроки з впровадження H_2/NH_3. Результати дослідження показали, що аміак, попри токсичність і потребу в додаткових заходах безпеки, є технологічно і економічно придатнішим для середньо- та далекомагістрального судноплавства завдяки нижчим витратам на транспортування і можливості використання існуючої інфраструктури зрідженого газу. Водень, у свою чергу, характеризується вищою екологічною цінністю через нульові викиди CO_2 та NO_x (за умов використання паливних елементів), але вимагає високотехнологічних систем зберігання та значних інвестицій у логістику, що обмежує його застосування переважно в каботажних перевезеннях або в умовах замкнених ланцюгів постачання. Представлені результати можуть слугувати основою для формування стратегій декарбонізації флоту, розробки стандартів безпеки та стимулювання інновацій у морській енергетиці. Отримані висновки становлять практичний інтерес для судновласників, інженерних компаній, екологічних регуляторів та розробників політик у сфері зеленого морського палива

Ключові слова: екологічна безпека; запобігання забрудненню; викиди NO_x; токсичність аміаку; енергетична ефективність палива; портова інфраструктура; захист морського середовища

MACHINERY & ENERGETICS

Scientific Journal

Volume 16, No. 3. 2025

Founded in 2010. Published four times per year

Managing editor:
N. Shevchenko

Signed for print of September 23, 2025. Format 60*84/8
Conventional printed pages 9.6
Circulation 100 copies

Publisher's address:
National University of Life and Environmental Sciences of Ukraine
03041, 15 Heroiv Oborony Str., Kyiv, Ukraine
Tel.: +38(044)-258-42-63
E-mail: info@technicalscience.com.ua
https://technicalscience.com.ua/en

ТЕХНІКА ТА ЕНЕРГЕТИКА

Науковий журнал

Том 16, № 3. 2025

Заснований у 2010 р. Виходить чотири рази на рік

Відповідальний редактор:
Н. Шевченко

Підписано до друку 23 вересня 2025 р. Формат 60*84/8
Умов. друк. арк. 9,6
Наклад 100 прим.

Адреса видавництва:
Національний університет біоресурсів і природокористування України
03041, вул. Героїв Оборони, 15, м. Київ, Україна
Тел.: +38(044)-258-42-63
E-mail: info@technicalscience.com.ua
https://technicalscience.com.ua/uk